ENHANCING DISTRIBUTION PLANNING METHODS USING STATE OF THE ART MODELING TECHNIQUES TO FACILITATE HIGH GROWTH DISTRIBUTED ENERGY RESOURCES

by

Wesley O. Davis

A dissertation submitted to the faculty of
The University of North Carolina at Charlotte
in partial fulfillment of the requirements
for the degree of Doctor of Philosophy in
Electrical Engineering

Charlotte

2020

Approved by:

Dr. Sukumar Kamasaladan

Dr. Valentina Cecchi

Dr. Yogendra Kakad

Dr. Maciej Noras

ABSTRACT

WESLEY O. DAVIS. Enhancing Distribution Planning Methods Using State of the Art Modeling Techniques to Facilitate High Growth Distributed Energy Resources . (Under the direction of DR. SUKUMAR KAMASALADAN)

Climate change is one of the most pivotal issues for the world in which we live today. The power grid transformation to become, smarter sustainable and carbon-free, has been a primary emphasis in recent times. This includes the integration of Distributed Energy Sources (DERs). In this work, innovative and novel techniques are presented to facilitate and expedite the engineering, planning, and deployment of high penetration levels of renewable and distributed energy resources to aggressively attack climate change and move the industry to a new paradigm. Towards this end, both traditional and non-traditional techniques and methodologies are leveraged to enhance distribution planning methods such that more electric distribution feeders can be analyzed more dynamically. Tried and true iterative mathematical techniques and convergence algorithms are used to adhere to the Laws of Physics for the flow of electricity.

Findings in the area of Control Theory and System Identification are used to develop dynamic and predictive models of the electric distribution system that analyze the impact of interconnecting high levels of renewable generation. These predictive models are represented by parametric models or transfer functions developed from the Laplace Transform technique, leveraging proven powerful tools of time domain and frequency domain analysis to evaluate system stability. Critical to this work is both the validation of realized models wherein these models can accurately predict system response at varying load levels, renewable energy penetration levels, all-around necessary sensitivities. Such a dynamical model development process can be used and applied to any electric distribution feeder to better optimize penetration levels and provide the planning engineer with smart models to optimize system planning.

DEDICATION

This dissertation and the contributions thereof is dedicated to those that toiled and strove before me. To my ancestors that endured the Middle Passage and worked for generations to help build the economic power that we know as the United States of America from sun up to sun down without a wage or compensation and in the shadows of fear and intimidation, thank you for the ultimate sacrifice. To my great-great grandfather Jimmy Bellamy, born a slave, to my great-grandfather James Bellamy, my grandmother and grandfather Mary and Roscoe Gore, and my mother Carrie Dale Gore Davis, thank you for the unwavering determination that you all instilled in me to never give up in spite of the challenge. Lastly, to the late Dr. Gary Lebby and North Carolina Agricultural and Technical State University, and to Dr. Anil Pahwa and Kansas State University, along with the multiple electric utilities that I was fortunate to work for as a practicing engineer over the years, I want to thank all for the opportunity to learn about one of the most intricate and complex control systems known to man, the design and operation of the generation, transmission and electric distribution systems that define modern society. Thank you.

ACKNOWLEDGEMENTS

I would like to acknowledge those that toiled and strove before me. Thank You.

TABLE OF CONTENTS

LIST OF TABLES

LIST OF FIGURES

LIST OF ABBREVIATIONS

ANSI - American National Standards Institute

ARX - Auto-regressive with eXogenous input

CI - Commercial and Industrial Customer

CHP - Combined Heat and Power

DER - Distributed Energy Resource.

DR - Demand Response

dV/dP - Change in voltage with respect to change in active power

dV/dP - Change in voltage with respect to change in reactive power

ECE - An acronym for Electrical and Computer Engineering.

EIA - US Energy Information Agency

EPRI - Electric Power Research Institute

EV - Plug In Electric Vehicle

FERC - Federal Energy Regulatory Commission

GW - Giga-watt

IEEE - Institute of Electrical and Electronic Engineers

IOU - Investor Owned Utility

kV - Kilo-volt

kVA - Kilo-volt Ampere

kW - Kilo-watt

LTI Linear Time Invariant

MIMO - Multiple Input Multiple Output Model

MISO - Multiple Input Single Output Model

MW - Mega-watt

PF - Power Factor

PV - Photovoltaic

SAIDI - System Average Interruption Duration

SAIFI - System Average Interruption Frequency

SI - System Identification

SISO - Single Input Single Output Model

TF - Transfer Function

PREFACE

This dissertation is original, unpublished, independent work by the author, W. O. Davis.

CHAPTER 1: INTRODUCTION

The electric distribution systems that serve the nations urban, suburban and rural communities are undergoing unprecedented change driven by the growth in Distributed Energy Resources (DER), regulatory policy, aging infrastructure and economic challenges related to capital investments and rate recovery[1][2][3][4]. On top of the increased request to deploy DERs, the need to address climate change is one of the most pivotal issues for the world today. Electric utilities, customers and energy policy makers must collectively facilitate these changes to ensure that the future grid is both reliable and sustainable, as well as meeting the needs of a changing world and a more educated consumer. Today DERs consist of customer owned or behind the meter generation such as rooftop solar, combined heat and power plants (CHP), or Plug-in Electric vehicles (EV), wind, energy efficiency and demand response. Over 50 GW of wind [5] has been added to the grid within the last 10 years. PV is growing rapidly, the U.S. Solar industry data indicates that PV capacity grew more than 34 percent alone from 2013 to 2019 by adding over 10 GW of additional capacity. The residential market has grown by a more than 51 percent bringing solar capacity in the US to over 23 GW of installed capacity [3].

To provide a broader view of DERâs and their importance one need only understand that the calls for climate change is perhaps the most pivotal issue for the world in which we live today. Numerous research studies, publications, books, and regulations support the need to address climate change. Reducing Carbon emissions thus transitioning from reliance on fossil fuels to a clean energy economy unlock exponential value for the global economy as well as the United States. Addressing climate change effectively will redirect the certain path of unknown and costly aftereffects âa

Carbon Free future is necessary to avert the impacts of global warming.

Undeniably, there is problem and knowledge gap how the distribution system is planned. To make the transformative change necessary to achieving a carbon free future, critical research and innovation directed at the 55,000 substations and 185,000 feeders that exist today. Today the substation and feeders that serve 331 million populations are not designed and operated to accommodate the amount of renewable energy resources necessary to achieve significant reductions in Carbon emissions. The current way in which this infrastructure is deployed by its planning, design and operation is antiquated and incapable of helping achieve a clean energy economy.

The aim of the instant work is to develop innovative and novel techniques to facilitate and expedite the changes necessary in engineering, planning and deployment of high penetration levels of renewable and distributed energy resources to across the 55,000 substations and 185,000 feeder. The hypothesis her is that if there were a way to develop models of the distribution systems such that perturbations such as solar power injections can be accurately modeled and thus predicted, the process of bringing renewables online would be cut significantly helping the industry meet the more aggressive goals by 2050. Having a tool to expedite the transition represent an unprecedented technology to counter climate change and more quickly move the industry to a new paradigm. Electric planning engineers, line crew personnel, utility executives, regulators, policy makers and investors will need to think differently, and use modern toll and innovation analyzing how the distribution grid is planned, designed, operated, used and afforded.

A synopsis of research design and methods in the instant work, provides both traditional and non-traditional mathematical techniques and methodologies are leveraged to enhance outdated distribution planning methods such that more electric distribution feeders can be analyzed in a more dynamic way. Tried and true iterative mathematical techniques and convergence algorithms will be used to adhere to the

physics of the flow of electricity and classic circuit analysis bounded by Ohms Law and Kirchhoffâs Current and Voltage Laws. For example, the Newton Raphson Powerflow iterative technique will be applied to solve for voltage, active power, reactive power, node currents, angle, and power factor to begin the modeling process. Under normal steady-state conditions a power system requires four key componentsâ 1. Generation supplies residential, commercial and industrial loads, in addition to system losses, 2. Bus or nodal voltage magnitudes must be held close to rated values, 3. Generators operate within specified real and reactive power limits, and 4. Transmission lines and transformers are not overloaded. The power flow will derive iterative solutions to a set of nonlinear algebraic equations.

Married to the power flow equations necessary to adhere to the physics of the electric circuit is the vast work and findings in Control Systems Theory. Classic Control System Theory will be used to develop dynamic and predictive models of the electric distribution system. To use control theory in application a bridge must be constructed between the real world, mathematical theory, and application. The bridge to be constructed is the process of system modeling. The challenge is modeling a power system, similar to modeling any complex system such as aircraft, motor controls, cars or what have you, is the clear fact that few systems are linear over the full ranges of expected operating conditions. Thus, to address nonlinearity and continuous time type systems, LaPlace Transform techniques can be used to evaluate system response. Algebraic equations using the LaPlace variable will be used rather than the differential or difference equations.

These dynamical models will be used to analyze the system response and the impact of injecting high levels of renewable generation into the grid at any point. These informative models will be represented by traditional transfer functions developed from the LaPlace Transform technique leveraging the powerful tools of time and frequency domain analysis to evaluate system stability at higher levels of penetrations.

Critical to this work is both the validation of the realized models wherein these models can accurately predict system response at varying load levels, renewable energy penetration levels, weather, and necessary sensitivities.

Significance and Value of the Instant Research - Such a dynamical model development process can be used and applied to any electric distribution feeder to better optimize penetration levels with pinpoint locations. The models to be developed will go a long way to help meet the energy needs of 331 million Americans served by electric utilities that own, operate and maintain over 55,000 electric substations, 195,500 distribution feeders, and over 600,000 miles of high voltage transmission lines. When leveraged, the models developed can be leveraged by the distribution planner to effectively minimize the tedious and time-consuming equipment modeling that is currently used in the planning cycle. When using the models developed here, the planner can quickly look at system response for load additions or solar power interconnection requests. The major contribution and real values is a tool that helps utilities expedite the move to higher DER penetrations at the system level, where PV systems will definitively be interconnected either at the larger utility mega-watt scale or at the smaller customer kilo-watt scale. It is quiet conceivable that the time and resources or engineering skill to perform necessary engineering studies to evaluate each and every DER interconnection request is not currently available nor in the pipeline of graduate schools, thus having a method to develop robust dynamical models to evaluate a large percentage of the 195,000 feeders is a valuable resource in moving towards a clean energy economy.

To accommodate the evolution of the electric distribution system critical to realizing a carbon free futures and a clean energy economy, significant changes must be undertaken to enhance the planning of the system. In chapter 2, this dissertation endeavors to present a comprehensive literature review to provides an initial step into research focusing on four primary concerns: the classic distribution planning process,

DER technology, the integration and interconnection of DERs into the grid, reliability of the grid, and regulatory policy. Beginning with the identification of these topics, the literature review establishes a guide for subsequent research in enhancing the planning of the distribution system thereby providing utilities with solutions to planning the modern grid, and developing a credible framework for other research concerned with the changing power system. Chapter 3 develops a dynamic impedance modeling and validation framework it is shown that we can calculate the aggregated or Thevinin equivalent impedance from field measurements. Building on chapter 3, chapter 4 performs a sensitivity analyses of the power grid based on the classic power flow Jacobian. Chapter 5 presents an implementation methodology wherein the researcher designs a power grid sensitivity transfer function using system identification techniques. Chapter 6 applies the transfer function design methodology developed in chapter 5 to both a random feeder and a real world power system. Chapter 6 delves into the model order reduction for liner and non-linear systems using Bodeplot, magnitude and frequency diagrams to analyze model performance as well tuning or the models for efficiency. Chapter 6 also analyzes the step and impulse response of the models through simulation. Validation of the models are presented in chapter 6 using the real world system data for a normal sunny day and variable cloudy day to test models under real conditions. Lastly, chapter 7 conclude this work with an overview of the the problem, reinforcing the contributions to enhanced distribution planning, a framework for; validating power system models, developing aggregated transfer functions using system identification, and a framework to understand the effects of DERs on power system voltage.

The specific contributions of this work are the development of framework to develop and validate models from power networks for use in every day planning at the utility. Secondly, this work established a framework for developing aggregated transfer function parametric models based on System Identification. Last an thirdly this

work create a framework to understand the effects of DERs on power system voltage at varied DER penetrations levels and under different system operating conditions.

CHAPTER 2: LITERATURE REVIEW

Planning of the medium and low voltage electric distribution system in the 21st Century faces both technical and regulatory challenges. Future distribution planning of the grid presents electric power companies with difficult engineering problems that are dynamic and complex when compared to the traditional methods of distribution planning in the 20th Century. The National Academy of Sciences has stated that the most pivotal invention of the 20th Century was the evolution of the electric power grid. Now industry must find innovative solutions in this Third Industrial Revolution that is required for modernizing the grid. The networks and feeders that make up the current grid are being confronted with an exponential growth in Distributed Energy Resources (DERs). The past challenges confronted by utility engineers primarily consisted of simply meeting customer demand, and supplying a regulatory required Root Mean Square (RMS) voltage with adequate power quality to the end use customer. Today the planning problem is multi-faceted in meeting capacity shortfalls, ever increasing reliability performance requirements, minimal funding for traditional capital projects given trends in rate recovery, and the proliferation of DERs behind the customer meter.

2.1 INTRODUCTION

The electric distribution systems that serve the nation's urban, suburban and rural communities are undergoing unprecedented change driven by the growth in Distributed Energy Resources (DER), regulatory policy, aging infrastructure and economic challenges related to capital investments and rate recovery [4, 5, 1]. Electric utilities, customers and energy policy makers must collectively facilitate these changes

to ensure that the future grid is both reliable and sustainable, as well as meeting the needs of a changing world and a more educated consumer.

One of the major changes facing electric US utilities is the growth and penetration on the systems of DERs. DERs consist of customer owned or behind the meter generation such as rooftop solar, combined heat and power plants (CHP), or Plug-in Electric vehicles (EV), wind, energy efficiency and demand response. Over 50 GW of wind [1] has been added to the grid within the last 10 years. PV is growing rapidly, the U.S. Solar industry data indicates that PV capacity grew more than 34% alone from 2013 to 2014 by adding 7 GW of additional capacity. The residential market grew by a reported 51% bringing solar capacity in the US to approximately 20 GW [3].

In addition to PV growth, both aging infrastructure and the recent EPA Clean Power Imitative further exacerbates the problem. Post WWII, the US economy saw a period of significant growth. As a result, the utility industry also saw unprecedented capital intensive infrastructure investments necessary to meet consumer demand in the 1950-60's era. The majority of the 1950-60 improvements are over 50 years old. The aged equipment includes critical power system components such as substation transformers, circuit breakers, buses and bays within the substation, vintage copper conductors, wood poles and cross arms, porcelain insulators, downed guy wires, voltage regulators, and customer service transformers. The aforementioned equipment is critical to the delivery of electric power to the end user [6] and pose a risk to system reliably and the creating a modern grid.

To accommodate the evolution of the electric distribution system, significant changes must be undertaken to enhance the planning of the system. This literature review provides an initial step into research focusing on four primary concerns: the classic distribution planning process, DER technology, the integration and interconnection of DER's into the grid, reliability of the grid, and regulatory policy. Beginning with the

identification of these topics, the literature review establishes a guide for subsequent research in enhancing the planning of the distribution system thereby providing utilities with solutions to planning the modern grid, and developing a credible framework for other research concerned with the changing power system.

2.2 Base of Knowledge in IEEE Xplore: Power System Planning

Due diligence is necessary when conducting research on the electric power system. Critically looking at and studying the prevalent knowledge in the relevant research community, from the electric utility industry, within the governing regulatory bodies, and other stakeholders in a comprehensive manner is necessary. In this literature review, IEEE eXplore was used to examine the base of knowledge on the subject primarily from conference publications, journals and magazines, and relevant industry books. Different research rules were used to identify materials to begin the effort. Table 1 lists the artifacts identified in the base search categories.

Table 2.1: Results From IEEE eXplore Using Different Phrases

Research Phrase	Conference Publication	Journal or Magazine	Books	Total
"Power System Planning"	15187	6063	108	21358
"Integrating Renewables Into the Grid"	59	8	4	63
"Power System Planning" AND "Integrating Renewables Into the Grid"	32	9	1	42
"Power System Planning" AND "Reliability"	3225	1458	20	4703
"Power System Planning" AND "Regulatory Policy"	39	20	0	59

Using the search phrase **"power system planning"** uncovered 21, 358 documents

on the instant topic. Such a large volume of information suggests a mature base of knowledge and understanding of power system planning. Of the 21,358 research artifacts, over 15,000 have been published since 2001, and only slightly over 6,000 publications recorded by IEEE Journal or Magazine publications in the 93 years between 1907 and 2000. Again, demonstrating a base of mature knowledge and a growing interest in the research area. However, in contrast, when appending **"integrating renewables into the grid", "reliability"** and **"regulatory policy"** to **"power system planning"**, the aggregate volume of research material falls drastically as is depicted in Table 2.1. While a decent amount of material exists on Reliability, *limited research information as related to power system planning exists in the areas of Integrating Renewables into the Grid, and Regulatory Policy. Integrating renewables into the grid, reliability and regulatory policy as inter-related to power system planning is exponentially ripe for further research and innovation.* The reality is that the electric distribution system is a single complex control system, however, modern stakeholders tend to analyze and plan the system in silo's of; capacity, reliability, or DERs, omitting the interdependencies of the single system. Given the overdue need for research in this area, the dominate references found through IEEE eXplore are critically investigated in the following sections.

2.2.1 Power System Planning and the Integration of Renewables into the Grid

The significant changes and transformation that the distribution system is undergoing critically impact the reliability performance of the grid in terms of system capacity, customer peak demand, load profiles and the way that generation, transmission and distribution systems are planned and operated. Specifically, DERs impact system voltage, capacitor optimization, and voltage regulator set points. Not only are utility customers installing DERs at their homes and businesses, but also state, federal and local governments are promulgating policy and regulations that require that utility companies accommodate the integration of renewables. For example, the District

of Columbia Government in its **Vision for A Sustainable DC** has set the goal to reduce energy consumption by 50% and increase the use of renewable energy by 50%. Most telling of the pressure on electric utilities is the recent proposed takeover of Pepco Holdings, Inc. by Exelon Utilities. In the conditions of the settlement agreement, in an effort of gain approval by the District of Columbia Public Service Commission and community stakeholders, the merging companies were required to agree to the following stipulations related to DERs:

- Develop or assist in the development of 10 MW of solar generation in the District of Columbia by 2018
- Purchase 100 MW of renewable energy, capacity and ancillary services
- Be an "enthusiastic partner" of the DC Public Services Commission for the promotion of renewable and distributed generation in the
- District. . . expediting, and streamlining the process for interconnecting customer-owned, behind-the-meter distributed generation Ref. [7].

Other stipulations involved *changing distribution planning process*. However, most utility companies are not readily prepared to accommodate the increase in renewable generation in the traditional distribution planning process as DERs create complex engineering technical issues when connected to the grid.

Addressing some of the technical issues that renewable energy resources create is covered in [8]. In Ref. [8] researchers capture the fundamental difference in central generation and DERs noting that DERs unlike central generation is located close to the load and can be considered "*virtual power plants*" via aggregation of decentralized DERsunits. IEEE standards place a cap of 10MW on individual or aggregate installations in order to be classified as distributed generation. One of the critical issues facing the integration of DERs is the level of penetration and the rate of growth. The

size, location, type of DER and its intended uses are all characteristics that affect the impact that DERs can have on the distribution system. Also, the amount or aggregate penetration levels of DERs impacts the system in terms of the DG's percent of peak load for both the feeder and the substation transformer. DER penetration levels have an effect on the fault current contribution relative to the utility's available fault current and changes dynamically based on variable MW production, making it difficult to coordinate substation circuit breakers, reclosers, sectionalizers, and fuses. Additionally, DERs can have a "**voltage rise**" affect when located near the substation or at the head of the feeder. Voltage rise causes the load tap changer (LTC) at the substation to see a lower line current and thus causes the LTC to lower the taps resulting in an un desirable increase in voltage along the feeder. Other operational areas where DERs impact the distribution system is the power quality related to voltage flicker and harmonic distortion of system voltages. The results from Ref. [8] are that engineering challenges exist in accommodating DERs and the need for utility companies to improve their planning processes and tools to accommodate the high penetration of DERs and simultaneously improve reliability performance.

In Ref. [9] a brief overview of the classic planning process is given along with support for the notion that the traditional planning process is not adequate for pending industry changes. In its critical assessment of the outdated distribution planning process, the author highlights that currently utility company planners do not consider DERs or demand side management as serious alternatives to solving system problems. A reference is made to the complex optimization problems that distribution system planners are faced with and goes on to state that the traditional planning of the system is the process to determine " where, when and which new equipment should be installed . . . ' that minimizes . . . operational costs . . . ". Additionally, Ref. [9] informs the reader of the critical need for "design criteria" when planning the distribution systems and how design criteria uses fundamental load flow tools to validate system

design alternatives in both "....'normal operation and emergency conditions....'" Furthermore, Ref. [9] recommends that the future planning process be improved to include alternative planning solutions such as energy storage, taking advantage of load shifting capability. Lastly, Ref. [9] discusses the reality that the aggregate peak loads of customers is changing unsymmetrically due to more DERs being operated in parallel with increased loading caused by Plug In Electric Vehicles (PHEVs), along with strip heating in heat pumps. Succinctly, Ref. [9] captures the fact that classic power system planning determines which alternatives increase system capacity and that future system modelling should account for the changing load profiles caused by the interaction between DER's and loads.

In 1997 Ref [10] predicted that the planning function would change in several different ways. First the planning function would need to incorporate more stochastic forecasting methods as opposed to single deterministic load forecasting. Secondly, Ref. [10] predicted that system reliability would increase in value to the customer and regulator, creating a need for the utility company to include the degree of reliability when making planning decisions. Thirdly, [10] noted the need for ***"optimized integrated planning"*** where more modern system planning alternatives would need to be implemented into the planning process. New alternatives such as distribution automation, DERs, demand-side management and load control should be considered in efforts to bypass traditional, costly and large capital investments.

The classic distribution planning process for today is captured in Figure 2.1 [11]. In Figure 2.1, the short-range planning process receives inputs from the load forecast, the existing system configuration and any already planned system additions. During the short range planning process, capacity short falls or other criteria violations are identified. The output from the short-range planning process as described in Ref. [11] are solutions, projects or system additions necessary to relieve any capacity overloads or other criteria violations, such as low voltage or poor power factor. The output is

a detailed construction recommendation. While Figure 2.1 gives an overview of the traditional short-term planning process, it should be noted that the major difference between short-term planning and long-term planning in the traditional way is the fact that long term planning tries to ensure that short-term planned additions have a "...low present worth cost..."[11].

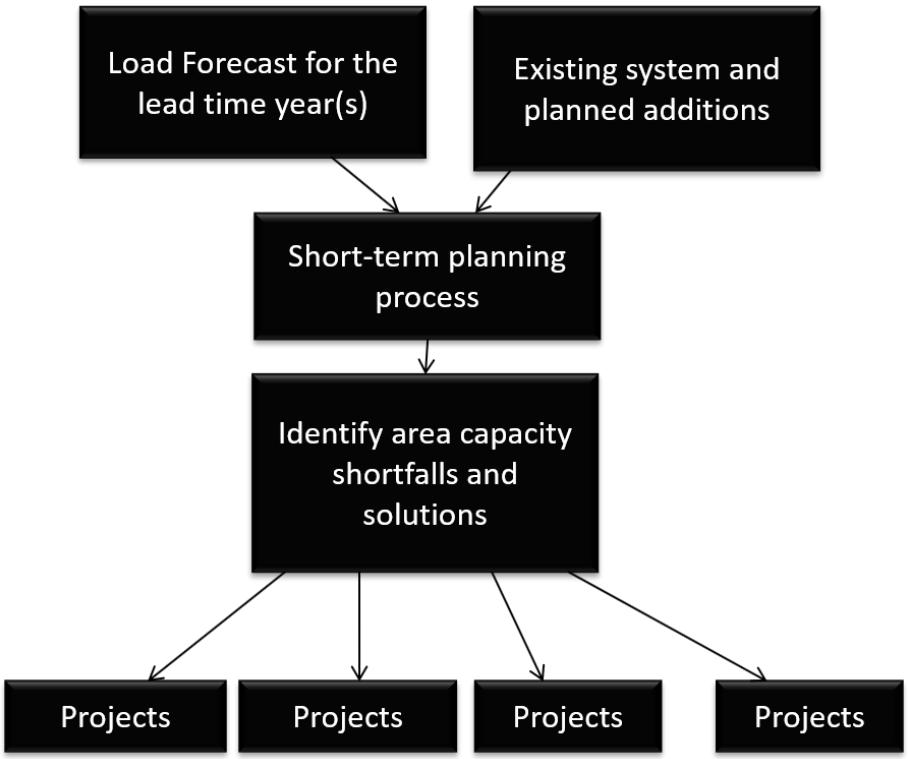

Figure 2.1: Source - H. Lee Willis, Power Distribution Planning Reference Book [1]

2.2.2 Reliability and Power Systems Planning

As captured in Ref. [10], integrating reliability improvements and DERs, along with capacity expansion into existing and proven distribution planning process will be critical in the future planning of the power system. In [12], the writers suggest that improving reliability will require that reclosers and cross connections or feeder ties, be used as a solution in DER based planning when system load is growing.

In Ref. [13] the authors further iterate the pressure on utility companies to reduce capital expenditures while simultaneously improving SAIDI and SAIFI reliabil-

ity performance. SAIDI and SAIFI are defined as **"...continuously supplying electricity to customers without interruptions..."** [13] supports optimizing reliability using several conditional constraints. The first constraint is budgetary where capital and operational and maintenance costs are not to exceed predefined spending limits. Secondly, SAIDI and SAIFI improvements are set as annual reliability targets that must be met to avoid regulatory penalties and sanctions. Ref. [13] goes on to recommend accumulating cost and benefits of each project or reliability program and developing a cost efficiency curve. The curve is used to forecast expected improvements in SAIFI and SAIDI. Some of the reliability programs included in the analysis include: fusing laterals, reclosers, installing sectionalizers, feeder automation, tree trimming, line inspection and fault indicators. The planning process can be improved by using optimization techniques to identify specific projects to invest in to improve reliability towards stated SAIFI and SAIDI reliability targets. Meeting the regulatory reliability targets, serving customer demand and facilitating the increase in DERs is placing undue pressure on the planning function within electric utilities. This pressure will require that utilities make enhancements to the existing distribution planning process.

2.2.3 System Identification, Distribution System Planning, and Renewables

Alone, System Identification returns over 97,000 conference papers, journals, magazine articles, standards, books and courses. This indicates that System Identification by it self is a mature topic. System Identification is a way developing mathematical models of real-life systems and has been broadly useful in areas such as automatic control, aviation, spaceflight, astronomy, medicine, biology, marine ecology and society, economics and many other fields.â [The Research Survey of System Identification Method, IEEE]. In [The Research Survey of System Identification Method, IEEE] several modern methods for identifying and modeling real systems is presented. For example, an overview of techniques such as neural networks, fuzzy logic, swarm in-

telligence optimization algorithms, auxiliary model identification algorithm, genetic algorithm, multi-innovation identification algorithm and hierarchical identification algorithm are presented wherein these techniques have been used to model nonlinear systems. However, when System Identification is combined with Distribution System AND Renewable, the number of articles is limited to twenty-one. These twenty-one artifacts are made up of mostly conference papers and journal articles. In [A Network Planning Perspective for Grid Integration of Renewable Distributed Generation in South Africa, IEEE] the author discusses the many accepted utility guidelines used to aid in the integration of renewables. While the paper does a good job of highlighting the need to integrate more distributed generations resources. The author also identifies the need for voltage stability, and optimal allocation or location of PV, validating that voltage instability happens takes place via the progressive increase and decrease of voltage at certain buses. However, the authors apply rudimentary tools such as solar irradiance maps over-layered on to the distribution system, and do not pose a realizable solution to managing the voltage rise phenomenon or a way of modeling the system to address the some of the issues preventing higher penetration levels of DERs.

2.2.4 Regulatory Policy

Adding even more complexity to the fray is the fact the regulatory landscape for electric utilities has changed very little if any over the last 60 years. Electric utilities have been around for more than 140 years and spread rapidly across the US in the 1900s. Most utilities operate under a "regulatory compact" wherein the regulatory body sets rates to fully compensate the utility for the costs it incurs to meet the obligation to serve [14]. Around 1965, the industry began to change as the post WWII annual growth rates of seven percent were on a steady decline. " The traditional rate formula which encouraged capital expansion put utilities in the position of continuing to dump money into the rate base, thus increasing costs." Also, in the 1960's and

early 1970's the US faced an energy crisis. The 1970's Energy Crisis was the catalyst for the Public Utility Regulatory Policy Act (PURPA) which moved the industry towards promoting energy conservation through competition in the generation sector. However, PURPA was in reality the first step towards reform in both generation and transmission. The Federal Energy Regulatory Commission issued several other major orders between 1980 and 2015, mostly reforming how the generation and transmission networks operated. The problem here is that regulatory reform has primarily impacted and improved generation markets and transmission access [15] and not the distribution system.

2.3 Types of Distributed Resources

There are several resources that are considered to be DERs. DERs either require a fuel to generate power or do not require a fuel. Both types of DERS mentioned above can be classified as distributed generation (DG). However, those DERs that do not require a fuel can be further classified as renewable energy resources. Another set of resources widely considered DERs that do not require a fuel supply and are not considered renewable, are energy efficiency and Demand Response (DR).

2.3.1 Combined Heat and Power Plants

DERs that require a fuel consist of combined heat and power plants (CHP) and micro-turbines. CHPs capture waste heat such as steam or hot water and use it for building space heating and cooling hot water. By capturing the waste heat CHPs can be 30 percent more efficient than a typical coal fired power plant. The engine or turbine is usually supplied with natural gas or fuel oil to generate electricity. The heat recovery unit captures the hot exhaust gases for building steam, hot water or cooling and heating purposes. Figure 2.2 below provides a holistic view of the power system from the generation, transmission and distribution to the enduser at the home. Many of the DERs for the modern grid and moving forwards will be co-located and located

near loads.

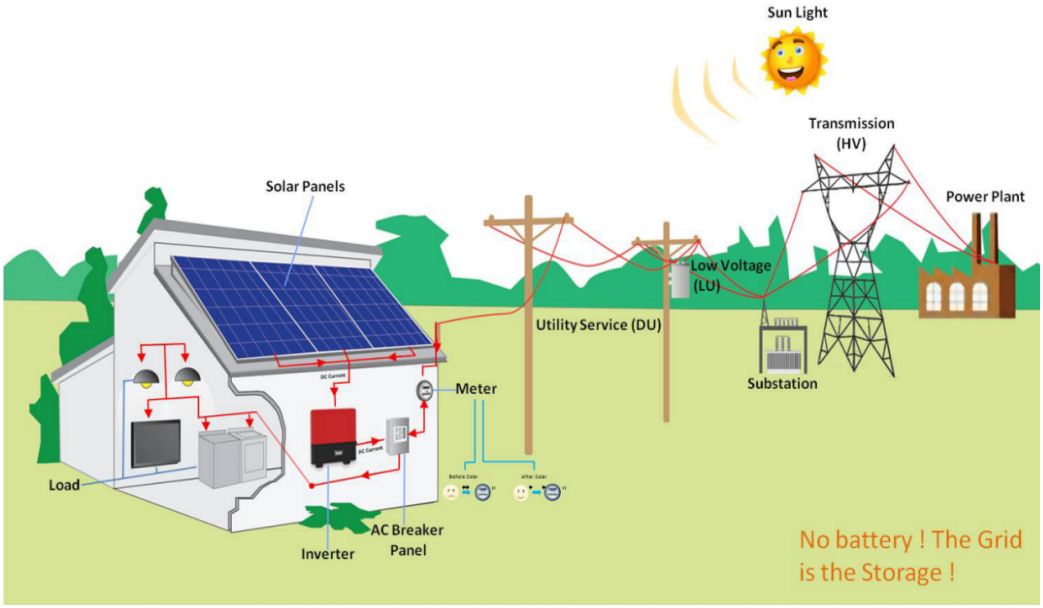

Figure 2.2: Combined Heat and Power (CHP), source: EPA.gov

CHP's are used in commercial buildings, apartment communities, schools, colleges and universities, municipal water treatment facilities and in large manufacturing applications. CHP systems can produce $500 - 3000$ MW and are designed to operate daily and unlike other DER's, CHP's are not intermittent resources and provide operating flexibility and grid resiliency as they can be called upon during grid outages.

2.3.2 Micro-turbines

Micro-turbines are about the size of a refrigerator and can produce 25 kW to 1MW. Micro-turbine technology grew out of automotive turbochargers and small jet engine designs. The typical micro-turbine consists of a compressor, combustor, turbine, alternator, recuperator, and generator. The key components of the microturbine design is the compressor-turbine or turbocompressor. The turocompresson is mounted on a common shaft along with a typical electric generator. The recuperator is similar to the heat recovery of a CHP in that the opportunity to recover waste heat is provided in the design [16].

CHPs and microturbines are well suited for DG and microgrid applications due to their ability to be dispatched when called upon. Both CHP and microturbines offer the flexibility to support intermittent resources such as wind and solar [16].

2.3.3 Battery Storage

Battery storage uses electrochemical technologies to store energy for later utilization. While battery technology has been in use since the early 1900's, grid scale use is not used widely due to challenges in energy density, power performance, lifetime, charging capabilities, safety, and cost. Battery storage technologies most commonly used include lithium-ion (Li-ion), sodium sulfur (NaS), and lead acid batteries [17].

Various battery technologies have different discharge rates. The higher the discharge rate, the lower the available capacity for storage and the lower the output voltage. For example, a battery is rated in amp-hour (Ah) and this serves the ability of the battery to store energy. A 550 Ah battery has the capability to deliver 50 amps for 11 hours. Figure 2.3 provides an overview of how a battery and PV are connected to charge and discharge in a grid connected system. The key to connecting the battery is the DC/DC buck/boost converter and the DC/AC inverter. The buck-/boost converter is necessary to booth charge the battery (buck) and to discharge the battery (boost) onto the DC bus. The DC bus supplies the DC/AC inverter to create a 60 Hz AC voltage source to serve the load and synchronize with the utility. The battery can be charged from the PV system during the day and discharged at night. Also, the battery can be charged via the AC Bus at anytime.

The advantage of battery storage is the ability to store energy when it is inexpensive and discharge under peak load conditions when the cost generate power is generally higher. Another benefit of storage is utility companies can use storage to defer costly capital projects such as substations given that peak load conditions only occur a few hours per year. Along the same lines, battery storage can be used to provide voltage support.

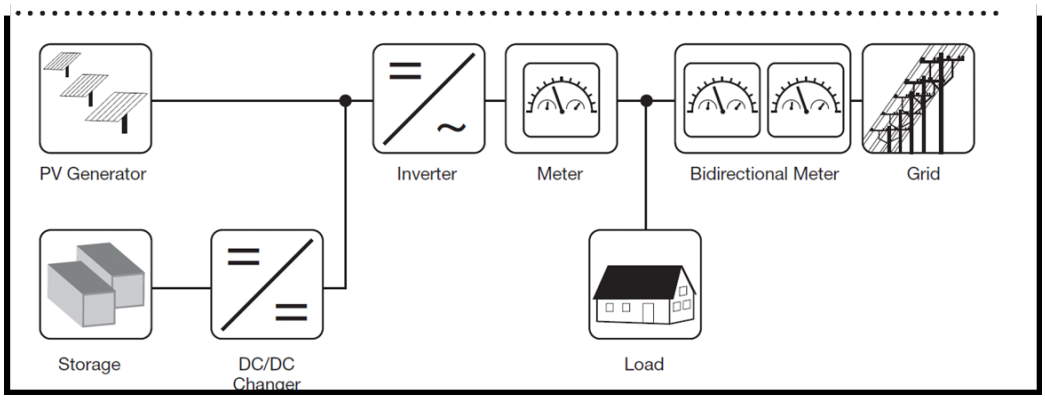

Figure 2.3: PV Systems with Battery Storage, source U.S. Department of Energy

2.3.4 Fuel Cells

A fuel cell operates similar to a battery, however, it is considered an electromechanical engine. Unlike a battery, the fuel cell does not charge or discharge. It harnesses the energy released when hydrogen and oxygen combine. Fuel cells consist of a negative electrode or anode, and a positive electrode or cathode. The electrodes are layered near an electrolyte. Hydrogen is supplied to anode, and the cathode is supplied by air. Hydrogen molecules separate into protons and electrons, and flow through an external circuit, creating a flow of electricity [18].

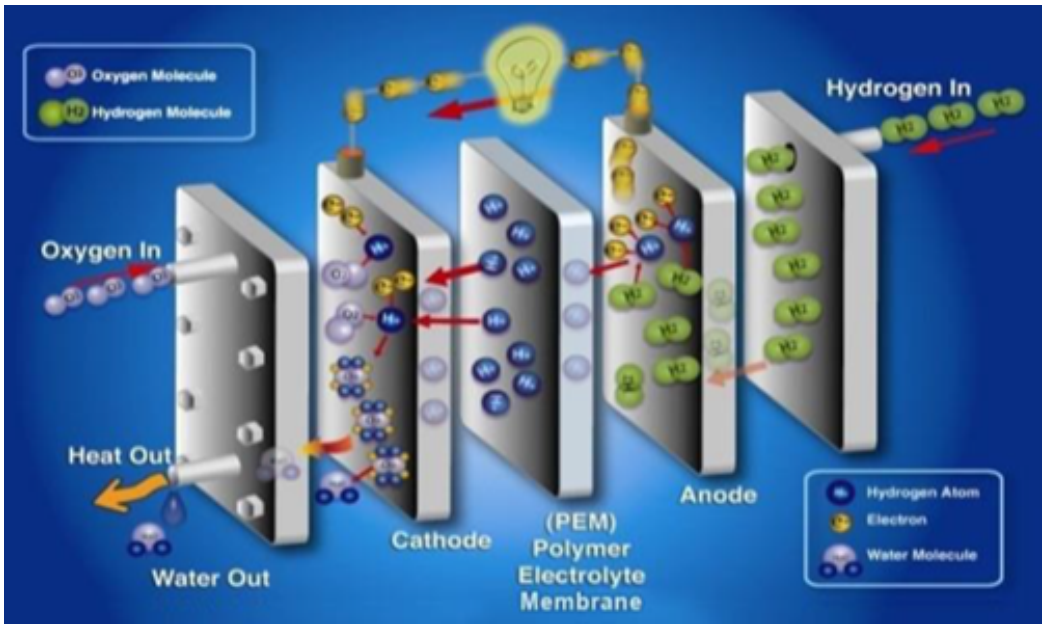

Figure 2.4: Fuel Cell's Generate Electricity, source - fuelcellenergy.com

Fuel cells have been used on a small scale as backup power for telecom towers in the U.S. They typically range in size from $1-200$ kW. Fuel cells generate a significant amount of heat in its reaction An inherent characteristic of carbonate fuel cells is that they generate a good deal of heat in the chemical process and this makes them useful in situations where electricity and heat are utilized by end- supplied to customers.

2.3.5 Wind

Wind like solar is an abundant and renewable source or energy. Wind turbines generate electric power when the wind blows and turns two or three fiberglass blades attached to an induction generator. The generator is typically wound rotor or squirrel cage induction. The rotor is connected to the main shaft, which spins a generator to create electricity. The amount of power generated depends on the size of the generator and the air volume, velocity of the air and air density. Power generated by a wind generator is determined by the following equation:

$$P = \frac{1}{2} C A \rho v^3 \tag{2.1}$$

Where C is the Power Coefficient and depends on the design, of the induction machine. A is the area of the wind captured by the rotor blades. ρ is the density of the air (averaging $1.225 Kg/m^3$ at sea level), and v is the wind velocity. To operate as a generator, the induction machine must produce a counter torque that opposes the driving torque of the prime mover. This action causes the induction machine to operate above synchronous speed and act as a generator delivering power to the system.

2.3.6 Solar

A typical silicon Photovoltaic V cell is made up of thin wafer that includes an ultra-thin layer of phosphorus-doped (N-type) silicon on top of a thicker layer of boron-doped (P-type) silicon. The arrangement creates an electric field at the top of

the surface of the cell where these two materials are in contact. This is called a P-N junction. When light rays hits the surface, the electrons are stimulated causing current to flow when an electrical load is connected [2]. A normal silicon PV cell produces about $0.5 - 0.6$ volt DC under open-circuit and no-load conditions. The current and voltage (I-V) produced by the cell is dependent on the following characteristic equation:

$$I = I_l - I_o(e^{qV/kT} - 1) \tag{2.2}$$

Where I_l is cell current due to photons and $q = 1.6x10^{-19}C, k = 1.38x10^{-23}J/K$, a cell temperature in Kelvin. Figure B.5 below captures the basic I-V curves of a PV cell when exposed to different angles of the sun. While the voltage of the PV cell is limited by the cell technology, the max power output of the cell is dependent upon the angle of the sun and the intensity of the light rays. Thus if I represents the cell current and V represents the voltage at maximum power, the maximum power output of the cell is:

$$P_{max} = I * V \tag{2.3}$$

Photovoltaics (PV) can be used to charge batteries, operate motors, and to power any number of electrical loads. PV systems require power conversion equipment such as an inverter to produce alternating current (AC) for use with conventional appliances, and for paralleling with the utility grid [2].

2.4 Inverter Technology and IEEE 1547

Several different types of inverters are available in the market place. There are both high frequency and low-frequency transformers used by the inverter. The is necessary for a grid connection in order to isolate the PV system from the utility to minimize the impact of failures [22]. IEEE USA standards requires that inverters connected to the grid employ a transformer. A typical inverter can be either single phase for

residential or small commercial, or three phase for large commercial or industrial interconnections

2.4.1 Volt/VAr Control of PV Systems

Volt/VAr Control of PV Systems is an important part of an inverters capabilities when a PV system is tied to the grid. Controlling reactive power can be accomplished by controlling either the voltage or the current. In voltage control, pulse width modulation (PWM) only affects the frequency of the output voltage and does not but impact the RMS values of the voltage and current. In most cases a DC/DC converter is installed between PV system and inverter to control the output voltage and current [22].

2.4.2 Smart Inverter Functions

Smart Inverter Functions - As PV installation continue to grow, more and more feeders will experience high penetration levels. Higher penetration levels will require a smarter grid and smart inverters. With the growth of PV in California, the California Public Utilities Commission created the Smart Inverter Working Group. The working group has been tasked with identifying new inverter capabilities that will facilitate high penetration levels of PV[23]. This most recent findings of the group identified the functions that are needed to facility the growth of PV at the distribution level.

- Generation and storage, including storage as a load
- Functionalities of DER and modern grid equipment
- Distribution-transmission impacts
- DER supplying adequate inertia for the grid
- Microgrids
- High penetration of renewables and other DERs

- Intermittency and uncertainty of renewable generation
- Two-way communications, controls, and dispatchability
- Interoperability and intelligent devices integration
- Demand response and load effects
- Interactive effects among advanced requirements and specifications
- Evaluation and testing modeling and simulation requirements
- Acceptance of power hardware and control hardware
- Reliability and resiliency of DER-grid interconnections.

2.4.3 Overview of IEEE Standard 1547

IEEE Standard 1547 is designed to prove the industry with interconnection standards and protocols for distributed energy resource (DER) interconnection and interoperability. The current work of the standard addresses issues such as: Generation and storage, impact of PV on distribution-transmission, high penetration of renewables and other DERs, Intermittency and variability of renewable generation, two-way communications, controls, and dispatchability, demand response and load effects, requirements and specifications for considering evaluations of reliability and resiliency of DER-grid interconnections.

IEEE Standard 1547 has been a work in progress since 2007. The standard creates requirements for system performance, operation, testing, safety considerations, and maintenance of interconnected DER systems. The current standards also address general requirements such as, responding to abnormal conditions, power quality, islanding, test specifications, design requirements, installation, maintenance and commissioning [21].

2.5 Summary

This chapter reviewed literature on power system planning, the different types of DERs, regulatory policy and relevant IEEE standards concerning interconnecting DERS to the distribution system. Given the dynamic changes and the available technology, enhancements to the traditional distribution planning processes is necessary and ripe to facilitate grid modernization. Enhancements to the distribution planning process need to be researched in order to address some of the technical issues created by the exponential growth of DERs. The proliferation of DERs will require non-traditional solutions meet the engineering, reliability and economical pressures currently faced by electric utilities. Chapter 2 lays the foundation for the specific contributions of this work for the development of framework to develop and validate models from power networks for use in every day planning at the utility. Secondly, this work established a framework for developing aggregated transfer function parametric models based on System Identification. Last an thirdly this work create a framework to understand the effects of DERs on power system voltage at varied DER penetrations levels and under different system operating conditions.

CHAPTER 3: DYNAMIC IMPEDANCE MODELING and VALIDATION of A POWER NETWORK

3.1 Introduction

Determining the impedance of an actual distribution feeder can be challenging. This is the case primarily due to the many number of impedance combination and segments of the feeder in the field. In order to adequately analyze a distribution feeder for purposes of studying the impact of high penetration of DERs, a valid impedance model must be developed and appropriately validated by comparing measured impedance versus impedance calculated from network characteristics. The equivalent circuit must be valid for all load levels that a feeder could possibly experience. Other challenges that a distribution feeder presents is that the R/X ratios for radial distribution systems are relatively high as compared to high voltage transmission systems. As a result classic power flow equations for networked systems and traditional numerical algorithm such as New Raphson and Gauss Siedel are challenged to converge due to the radial nature of power distribution networks Hence a novel procedure is developed to for dynamic impedance modeling and validation of a power network. Chapter 3 is critical to formulating the basic principle for this work related to dynamic impedance modeling. System impedance does not change and thus critical to building validating parametric model's for this work. The specific contributions of this work are the development of framework to develop and validate models from power networks for use in every day planning at the utility. Secondly, this work established a framework for developing aggregated transfer function parametric models based on System Identification. Last an thirdly this work create a framework to understand the effects of DERs on power system voltage at varied DER

penetrations levels and under different system operating conditions.

In [19] the authors developed a modified Newton Raphson method for radial distribution systems. The work clearly articulates the problem in the "... Newton method works well for transmission systems, however, it's convergence is poor for ...distribution systems due to the high r/x ratio which deteriorates the diagonal dominance of the Jacobian matrix." The methodology developed in [19] orders the laterals instead of the busses. The goal in [19] is to analyze the system without reducing the size of the system. In the instant work a different approach will be taken to determine feeder impedance's wherein a classic circuit analysis approach will be taken. This methodology begins by calculating the impedance's for bus sections and then determining an equivalent feeder impedance and circuit. Any methodology used to determine feeder impedance's must hold for all load levels for both complex and simple circuits typical of a distribution feeder.

3.2 Dynamic Impedance Modeling and Validation

To accomplish dynamic impedance modeling and validation of a power network a six step procedure was developed and applied to power network. The first step was to perform an iterative Newton Raphson power flow on the circuit and then determine the demand and voltage at each bus. Secondly, after logging the complex demand, voltages and angle at each bus, an analysis was made to determine the amount of power absorbed in each line section due to system demand. Next the new procedure required the development of the Thevinin equivalent circuit using measured values for active power, reactive power, voltage and angle. The goal here is to determine the Thevinin equivalent impedance of the power network. Now that the power absorbed in each line section is determined as measured by powerflow, a simple equivalent circuit can be constructed and thus analyzed. Using complex powers at each node, the measured impedance's can then be calculated using Kirchoffâs Voltage and Current Lawâs. The next step is to validation the measured impedance's by calculating them

manually. To evaluate load level sensitivities and accomplish the task of validating the feeder impedance, network load was varied at all conceivable load levels from 0â 110%. Lastly error between measured and calculated impedance's were defined by the error of epsilon, where epsilon is the resulting quotient of the calculated impedance divided by the measured impedance.

Table 3.1 gives the characteristics of the test feeder and Figure B.7 in the appendix will be used to validate a distribution feeder impedance. Figure 3.1 below is a simple one line diagram of the feeder and will be used for our analysis.

Table 3.1: Feeder RC103 Characteristics

System Characteristic	Feeder Detail
System Voltage	4.16kV lint to line wye, 2.4kV line to neutral
Nodes	372
Line Sections	371
Shunt Capacitors	1200 kVar (4 units at 300 kvar each)
Line Fuses	51
Line Switches	76
Spot Loads	184
Connected Load	5853
Demand at Peak Load	S = $1949 - j15$kVA
DER Generation	0

Step 1: Run the power flow and determine the demand and voltage at each bus identified in Figure 3.1.

$$\text{S1} = 864 - j231 \text{ kVA} \tag{3.1}$$

$$\text{S2} = 342 - j162 \text{ kVA} \tag{3.2}$$

$$\text{S3} = 120 + j55 \text{ kVA} \tag{3.3}$$

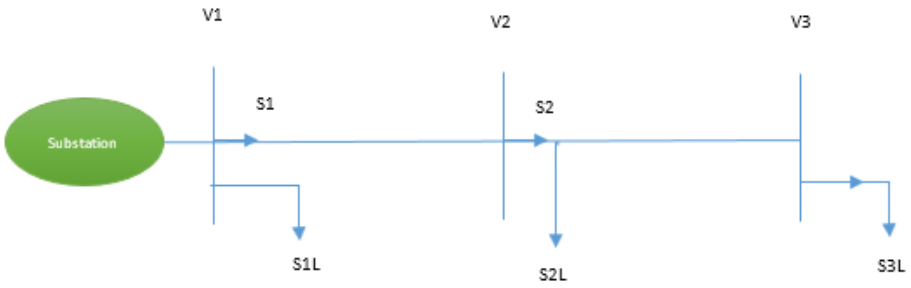

Figure 3.1: Power Flow One Line Diagram of Feeder RC103 in Figure B.7 above

$$V1 = 4.4 \times 10^3 \angle 0.41°\text{v} \tag{3.4}$$

$$V2 = 4.3 \times 10^3 \angle 0.41°\text{v} \tag{3.5}$$

$$V3 = 4.3 \times 10^3 \angle 0.41°\text{v} \tag{3.6}$$

Step 2: Determine the power absorbed in each line section.

S1 is the total feeder power flowing through the line and S12 is the amount of power absorbed in the line section between Bus 1 and Bus 2. All bus section powers are calculated below:

$$\text{S12} = \text{S1} - \text{S2} \tag{3.7}$$

$$\text{S23} = \text{S2} - \text{S3} \tag{3.8}$$

$$\text{S13} = \text{S1} - \text{S3} \tag{3.9}$$

Thus,

$$\text{S12} = (864 - 342) + j(-231 + 162) = 522 - j51 \text{ kVA} \tag{3.10}$$

Similarly, for S23 and S13,

$$\text{S23} = 222 - j217 \text{ kVA} \tag{3.11}$$

$$\text{S13} = 744 - j268 \text{ kVA} \tag{3.12}$$

Step 3 & 4: Develop an equivalent circuit using measured values and impedance's from power flow results and determine the system impedance Z13. Now that the power absorbed in each line section is determined as measured by power flow, a simple equivalent circuit can be constructed and thus analyzed from Figure 3.2.

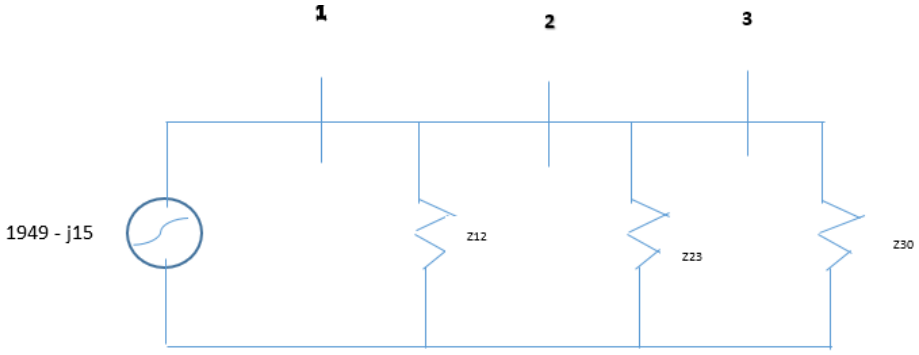

Figure 3.2: Construction equivalent electrical from Power Flow power flow one-line diagram

Using S12, S13 and S23 complex powers, the measured impedances can be calculated as follows:

$$Z12 = \frac{V1^2}{S12} = 36.6 + j3.05\,\Omega \tag{3.13}$$

$$Z23 = \frac{V2^2}{S23} = 48.026 + j35.26\,\Omega \tag{3.14}$$

$$Z13 = \frac{V1^2}{S13} = 23.03 + j7.93\,\Omega \qquad \text{(measured system impedance)} \tag{3.15}$$

Step 4: Calculate the percent error between the measured and calculated system impedance values:

The purpose of the above exercise is to determine the equivalent impedance between Bus 1 and Bus 2. Thus, the parallel combination of Z12 and Z23 should give an equivalent impedance and closely match the measured value of Z13 above.

$$Z13(\text{calculated}) = Z12||Z23 = 22.56 + 6.77\,\Omega \tag{3.16}$$

Table 3.2: Load flow data form power flow iterations at varying load levels

Load Level	P1	P2	P3	Q1	Q2	Q3 w/o Cap	V1	V2	V3	∠ V_1	∠ V_2	∠ V_3	% error Epsilon
0%	24	5	0	704	369	0	4400	4600	4700	0.04	1.54	2.33	1.0184
20%	186	73	24	616	329	11	4400	4500	4500	0.09	2.01	3.06	1.6962
40%	352	140	48	522	288	21	4400	4500	4500	0.14	2.5	3.81	2.6104
50%	426	174	60	299	268	27	4400	4400	4400	0.17	2.67	4.2	2.8048
75%	650	259	90	343	215	41	4400	4400	4400	0.25	2.75	5.23	2.8216
100%	869	345	120	200	160	55	4400	4300	4300	0.32	3.41	6.3	1.9946
105%	914	363	126	171	149	57	4400	4200	4200	0.33	4.04	6.53	1.8114
110%	959	380	132	140	138	60	4400	4200	4200	0.35	4.37	6.76	1.634

The difference or error between the measured and calculated system impedance we will call epsilon:

$$\epsilon = 1 - \frac{Z13\text{-calculated}}{Z13\text{-measured}} = 1.9946 \text{ or } 2.0\% \tag{3.17}$$

There is a 1.9946% error at 100% of the feeder peak load. To further test the impedance validation technique the feeder is evaluated at varying load levels 0% through 110% of peak load of the base case.

Step 6: Validate feeder impudence's at varying load levels $0 - 110\%$:

A Matlab program was developed to analyze the impedance from light load conditions through overloading situations at Bus 1, Bus2 and Bus 3. Power Flow studies were conducted at 0%, 20%, 40%, 50%, 75%, 100%, 105% and 110% load levels. Active power, reactive power, voltage and angles were evaluated at each load level.

The active power for the circuit ranged from 24 kW at 0% load level to 959kW at 110% load. At no load, Bus 3 did not have any active power flowing through it that was measurable by Power Flow. The 24 kW measured at Bus 1 is the no-load losses of the feeder when engergized at 4 kV. Figure 3.3 below provides an oaverview of the active load at all load

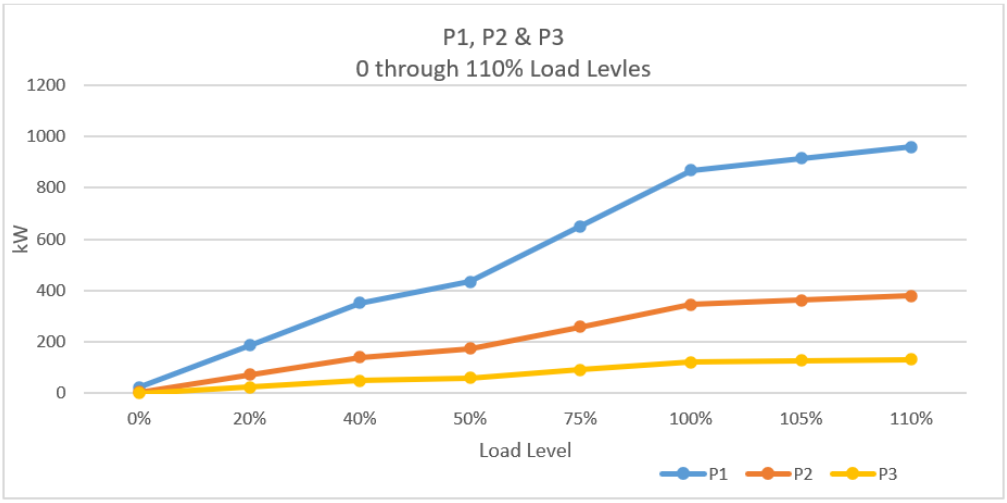

Figure 3.3: Active power at different load levels

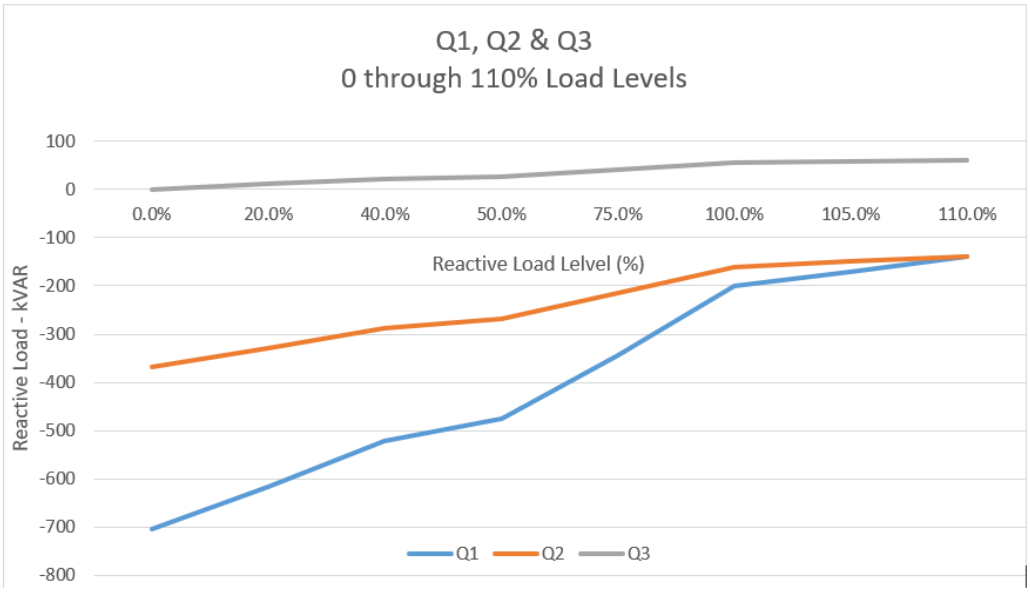

Figure 3.4: Reactive power from power flow at different load levels for three bus system

Figure 3.4 captures the reactive characteristics of the feeder. Reactive power ranged from a lagging 704 kVars at no load at Bus 1 down to a lagging 138 and 140 kVars at Bus 2 and Bus 3 respectively. Throughout all load levels Bus 2 and Bus 3 recorded lagging reactive power. However, Bus 3, located near the end of the line operates at leading power factor. Bus 3 recorded leading kVars from 0 at no-load to 60 kVars at

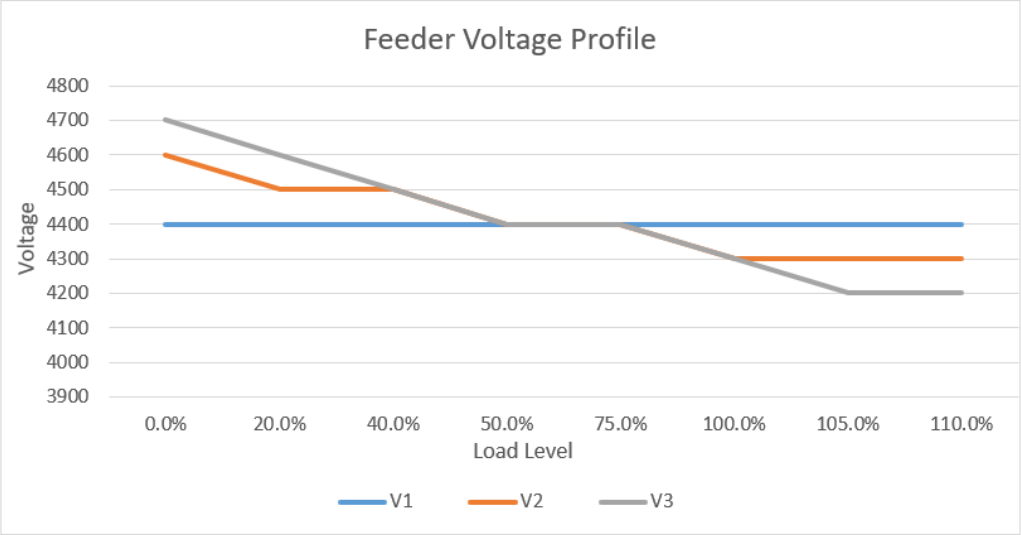

Figure 3.5: Feeder voltage profile

light load. Bus 3 has a three phase 300 kVar bank of capacitors tied to it to support the voltage in normal operation. The effects of the capacitors banks can be seen in the voltage profile of Figure 6. Bus 3 has a voltage of 4.7 kV at no-load and 4.2 kV when the feeder is heavily loaded at 110%. As the load increased, inductive reactive power at Bus 2 and Bus 3 continued to decline, however, due to the 300 kVar capacitor bank at Bus 3, the capacitve reactive power at Bus 3 continued to rise slightly from 0 to 60 kVar to provide much needed voltage support.

Figures 3.5 and 3.6 below capture the characteristics of the feeder voltage and angle respectively. The voltage at the source bus, Bus 1, remained flat at 4.4 kV through all load levels. However, the voltage at Bus 2 and Bus 3 ranged from $4.6 - 4.7$ kV under no-load conditions and $4.2 - 4.3$ kV at 110% load. Between 40 and 100% load levels all three busses operates with 100 volts or 2% of the nominal 4.4kV.

The angle at each bus decreased as more power was placed on the feeder. While the angle at Bus 1 generally was steady between -0.04 through -0.35 degrees, the difference in the angles at Bus 2 and Bus 3 continued to decrease to almost 7 degrees. The more critical issue when analyzing the voltage and angle is high voltage at light loads or $0 - 40\%$ and the magnitude of the voltage at high loads of 105% through

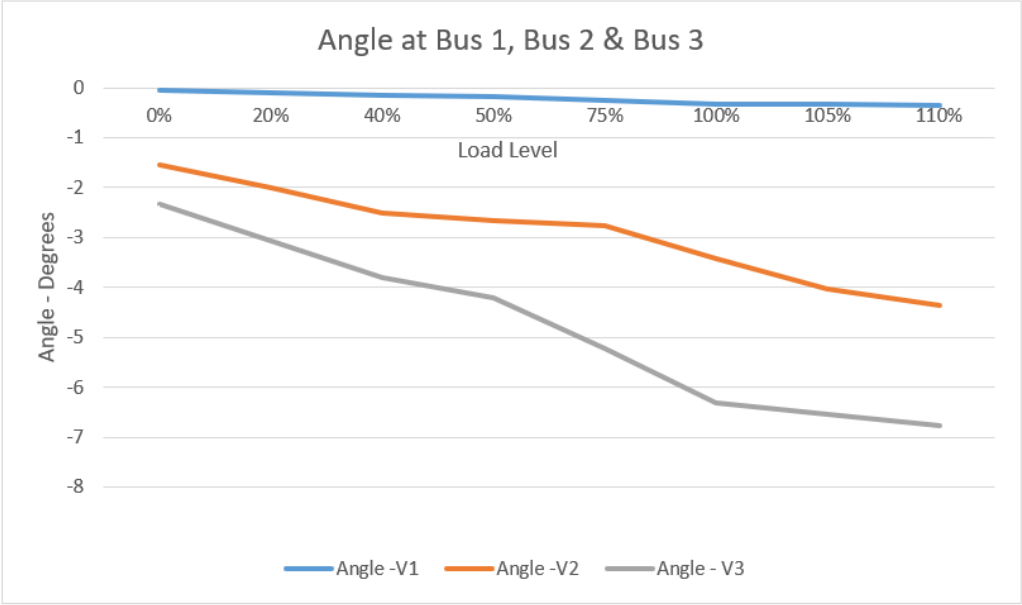

Figure 3.6: Voltage angle at each bus for varying load levels

110%.

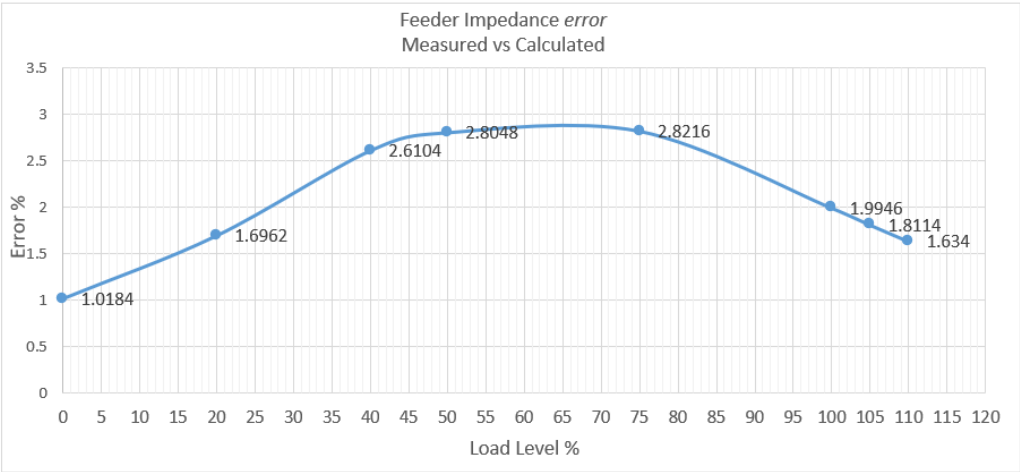

Figure 3.7: Graph of Feeder impedance % error at varying load levels of 0% through 110%

Lastly, Analyzing the impedance error at varying load levels gives an idea of the accuracy of the impedance validation technique used to derive an equivalent feeder circuit. At light load levels or no-load the error is determined to be 1.0184%, and rises steadily through 50% load. From 50% system load through 75%, the error marginally

Table 3.3: Single A-phase circuit for Figure 2

System Characteristic	Feeder Detail
System Voltage	2.4kV lint to neutral
Nodes	124
Line Sections	121
Shunt Capacitors	300 kVar (3 units at 100 kvar each)
Line Fuses	18
Line Switches	22
Spot Loads	62
Connected Load	298 KVA - A-phase
Demand at Peak Load	S = 283 - j64 kVA
DER Generation	0

ranges from 2.6104 to 2.8216%, at mid load. As the load levels increase to 100% and on to 110%, the error decreases from 2.8216% down to 1.634%. The fact that the impedance error rises and falls from no-load through 110% loading gives rise to further investigation of the methodology used to develop the equivalent feeder model.

3.3 Single Phase Analysis of Original Feeder

The previous analysis was conducted on a three phase circuit. However, now the same circuit will be evaluated similarly by strictly looking at the A phase complex power, at each of the three buses. By looking at the A-phase, the system voltage is 2.4kV line to neutral. Table 3.5 below provide characteristics of the single phase circuit now under study.

The single phase version of Figure 3.1, the original circuit offers great insight into how the original circuit operates. By comparison the original circuit had approximately one third of the power from the original circuit. However, as seen in Table 3.6, phase A, B and C are loaded at 291.4, 256.5 and 354.8 kVA respectively. Clearly C-phase is loaded more heavily than A and B-phase. Phase C is loaded at 40% while phase A and B are loaded at 32% and 28% respectively.

Table 3.4: Data for single A-phase circuit at 0-110% loading

Load Level	P_1	P_2	P_3	Q_1	Q_2	Q_3 w/o Cap	V_1	V_2	V_3	$\angle V_1$	$\angle V_2$	$\angle V_3$	ε %
0%	11.9	2.6	0.1	244	132	138	2500	2700	2800	0.12	2.23	3.33	1
20%	64	29.4	16.9	213	115.6	124	2400	2400	2400	0.15	2.82	4.23	2.8963
40%	117.9	56.4	33.8	180.6	97.8	111	2400	2400	2300	0.17	3.44	5.17	2.8947
50%	145	69.9	42.3	163	88.6	104	2400	2400	2300	0.19	3.83	5.74	2.8873
75%	214.5	104.2	63	116.4	64	87	2400	2300	2300	0.22	4.56	6.93	2.8997
100%	286.3	139	84.8	64.2	39.3	68.8	2400	2300	2300	0.27	5.58	8.5	2.9026
105%	300.7	146.1	89	53.7	34.1	64.9	2400	2300	2300	0.27	5.59	8.61	2.9074
110%	318	153	93.3	42.3	28.7	61	2400	2300	2300	0.27	5.77	8.9	2.9063

Table 3.5: Three phase loading of the original circuit

Phase	kVLL	kVLN	i (A)	kVA	kW	kVAR
A	4.4	2.5	115.5	291.4	281	-77.1
B	4.4	2.5	101.7	256.5	230.7	-112.2
C	4.4	2.5	140.7	354.8	354.1	-22.7
			Total:	891	866	-212

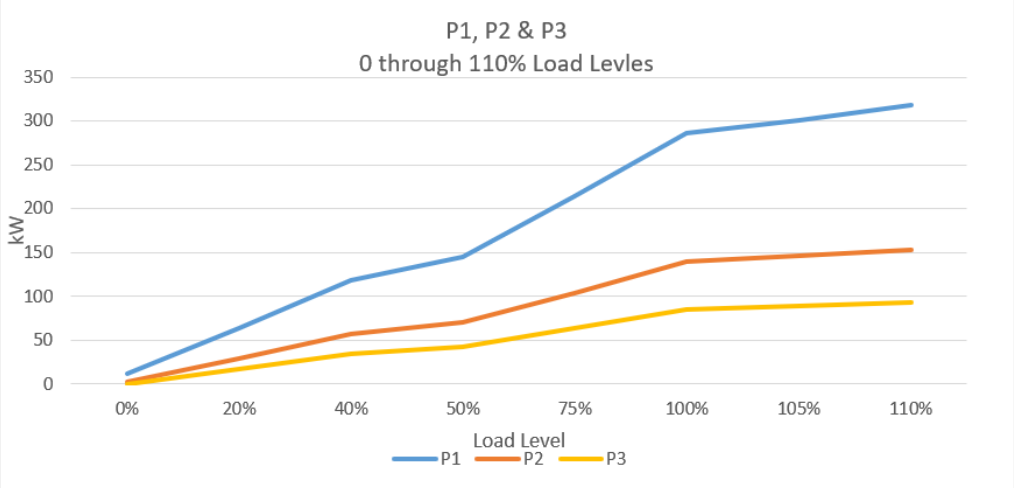

Figure 3.8: Graph of Feeder impedance % error at varying load levels of 0% through 110%

Second critical difference in the single phase circuit is the interaction of Q1 and Q3. At 100% loading, the effect of the capacitors at the end of the line ss clear. Between 100% and 110 % loading the capacitors at Bus 3 drive the reactive power above the

reactive power at Bus 1 or Q1. This interaction of Bus 1 and Bus 3 is evident in Figure 3.8 depicting the kVar at Bus 1, Bus 2 and Bus 3 form $0-110\%$ loading. The voltage at each of the buses is relatively flat from Figure 3.9. The voltage at Bus 1 ranges high at 2.5 to 2.8 kV under no-load conditions. However as load is added to the system, the voltage profile remains relatively flat. Similarly with the voltage angle in Figure 3.10.

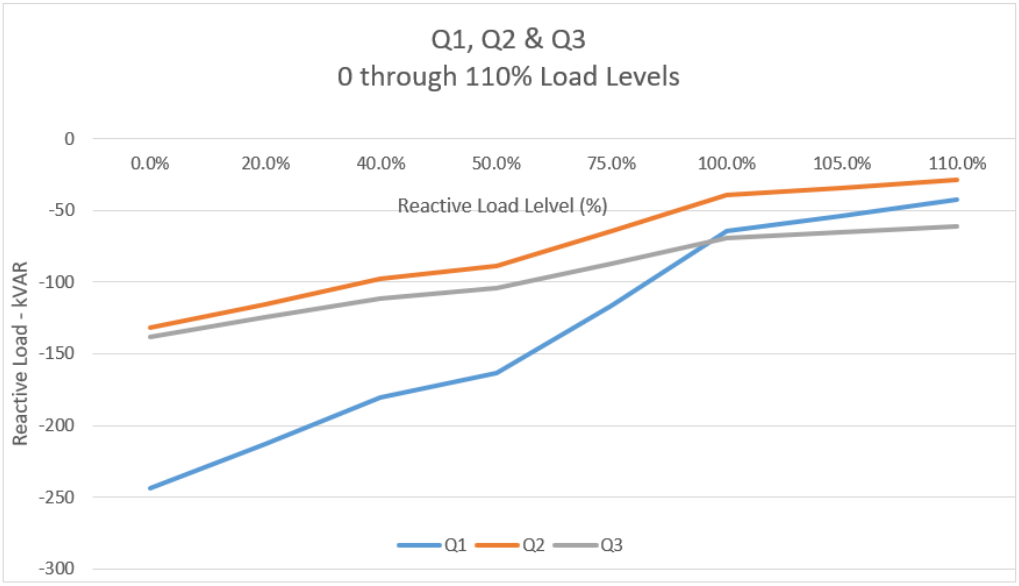

Figure 3.9: Graph of Feeder impedance % error at varying load levels of 0% through 110%

One of the more important observations from the A-phase circuit is the impedance error. Similar to the analysis of Q1, Q2 and Q3, the percent error shown in Figure 3.12 indicates that the losses increase as the circuit is loaded beyond 100% loading. The increase in the impedance error can be explained by the fact that the circuit was designed for unity power factor at 100% peak load. Hence the 100kVar capacitor banks at the end of the line are exhausted int their ability to maintain unity power factor as the sytem Q begins to exceed the kVar capability of the banks past 100% loading. The I^2R and the I^2X losses begin increase as the load increases, however, the I^2X losses have a greater effect on the system impedance error as there are not

enough reactive resources to counter the increased reactive requirements under over loading conditions of 105 and 110%.

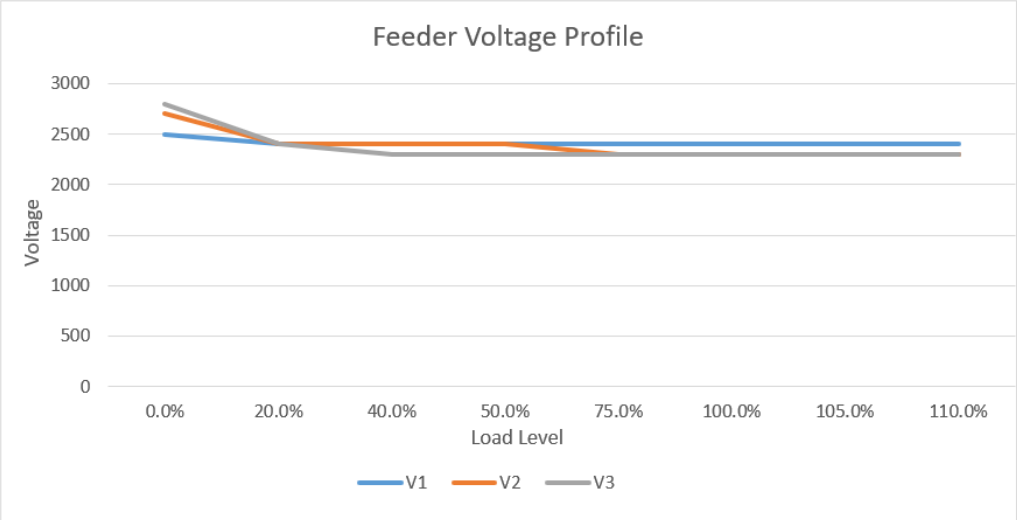

Figure 3.10: Graph of Feeder impedance % error at varying load levels of 0% through 110%

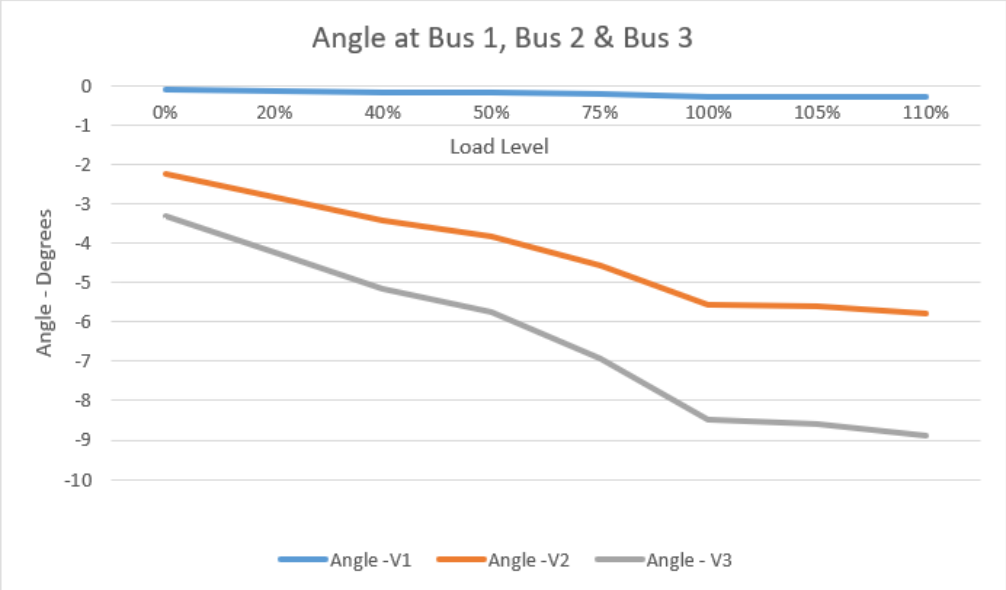

Figure 3.11: Graph of Feeder impedance % error at varying load levels of 0% through 110%

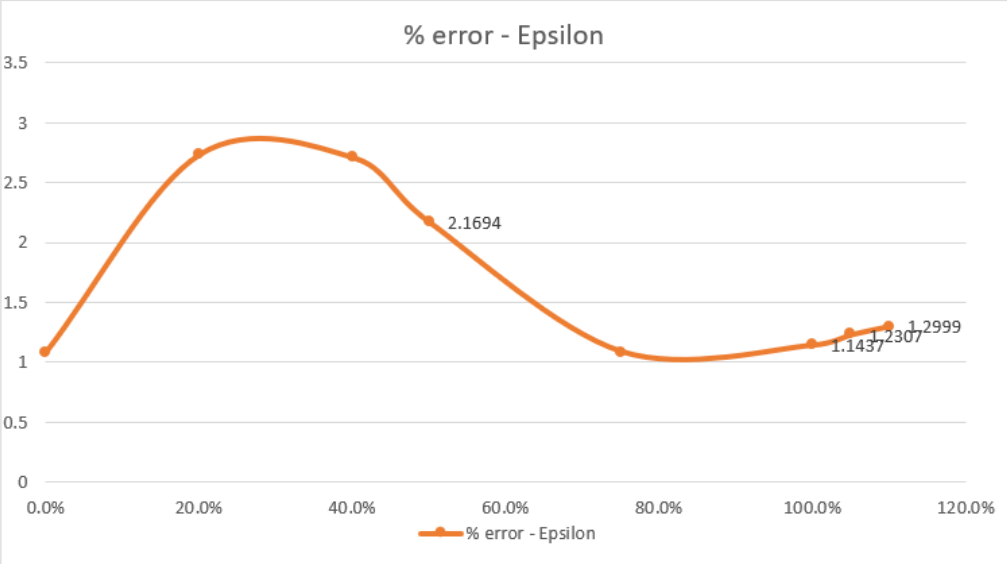

Figure 3.12: Graph of Feeder impedance % error at varying load levels of 0% through 110%

3.4 Impedance Analysis of Random Circuit

The next step in validating the impedance model procedure is to analyze a random circuit using the impedance methods outlined above on the test circuit. The test circuit employs both random line impudence's ZL1 and ZL2, loads and source voltages. The system can best be described as two loads, S1 and S2, connected by two single phase distribution lines served from a 2.4kV source. The random circuit can be seen in Figure 3.7. The exercise here is to analyze the circuit using classic nodal analysis and Kirchoff's Current and Voltage Laws. Initially the circuit will be analyzed using manual or hand calculations. Once these calculation are validated and deemed accurate and consistent Kirchoff's Laws, a power flow will be conducted on the circuit where voltage, angle, active and reactive powers will be analyzed. The last step will be to analyze the impedance error using the same procedure used to evaluate the original circuit. **Step 1:** Using Kirchoff's Voltage and Current Law's solve for I1, I2, Z1 and Z2 in Figure 3.7:

$$S1 = V1 \times I1^{*} \tag{3.18}$$

$$I1 = \frac{S1}{V1} = \frac{200 \times 10^{3} \angle 36.87^{\circ}\ \text{kVA}}{2300 \angle 0^{\circ}} (\text{conj}) = 86.96 \angle -36.84^{\circ}\ \text{A} \tag{3.19}$$

$$I1 = \frac{S1}{V1} = \frac{100 \times 10^{3} \angle 25.841^{\circ}\ \text{kVA}}{2300 \angle 0^{\circ}} (\text{conj}) = 43.47 \angle -25.87^{\circ}\ \text{A} \tag{3.20}$$

$$Z1 = \frac{V1}{I1} = \frac{2300 \angle 0^{\circ}\ \text{V}}{86.96 \angle -36.87^{\circ}\ \text{A}} = 26.45 \angle 36.87^{\circ}\ \Omega = 21.16 + j15.87 \tag{3.21}$$

$$Z2 = \frac{V2}{I1} = \frac{2300 \angle 0^{\circ}\ \text{V}}{43.47 \angle -25.87^{\circ}\ \text{A}} = 52.92 \angle 25.84^{\circ}\ \Omega = 47.63 + j23.07 \tag{3.22}$$

Combining the series combination of ZL2 and Z2:

$$\text{Z23} = \text{ZL2} + \text{Z2} \ = (0.442 + j.6919) + (47.63 + j23.07) \tag{3.23}$$

$$\text{Z23} = 53.601 \angle 26.3^{\circ} = 48.05 + j23.75 \tag{3.24}$$

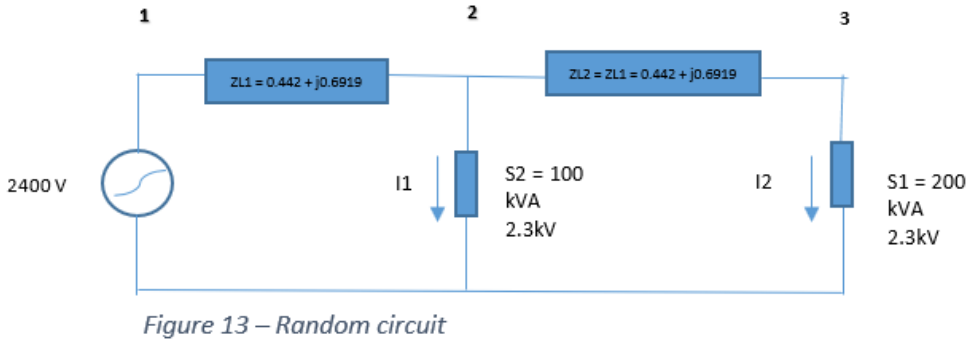

Figure 3.13: Random Circuit

Calculate the parallel combination of Z1 and Z23:

$$\text{Z1}||\text{Z23} = \frac{\text{Z1} \times \text{Z23}}{\text{Z1} + \text{Z23}} == \frac{(21.16 + j15.87) \times (48.05 + j23.75)}{21.16 + j15.87 + 48.05 + j23.75} \tag{3.25}$$

$$Z1||Z23 = 17.13\angle 3.51^\circ = 14.287 + j9.459 \tag{3.26}$$

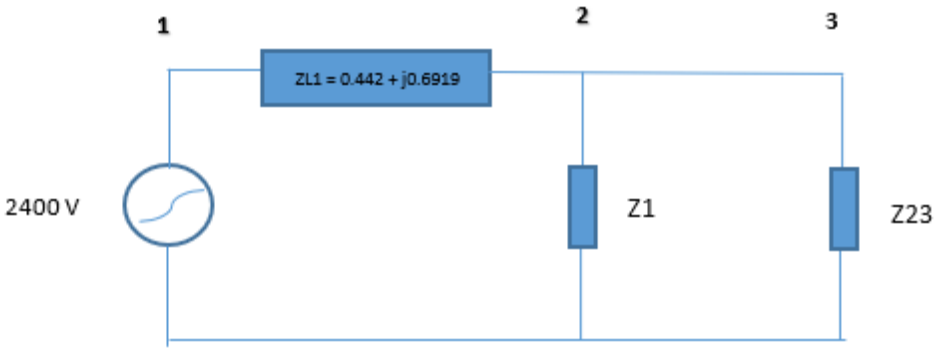

Figure 3.14: Further circuit reduction, combining parallel combination of Z23 and Z1

Determine the equivalent system impedance by adding the series combination of ZL1 and Z1 || Z23:

$$Z_{System} = ZL1 + Z1||Z23 = (0.442 + j.6919) + (14.287 + j9.459) \tag{3.27}$$

$$Z_{System} = 17.89\angle 34.58^\circ = 14.73 + j10.15 \tag{3.28}$$

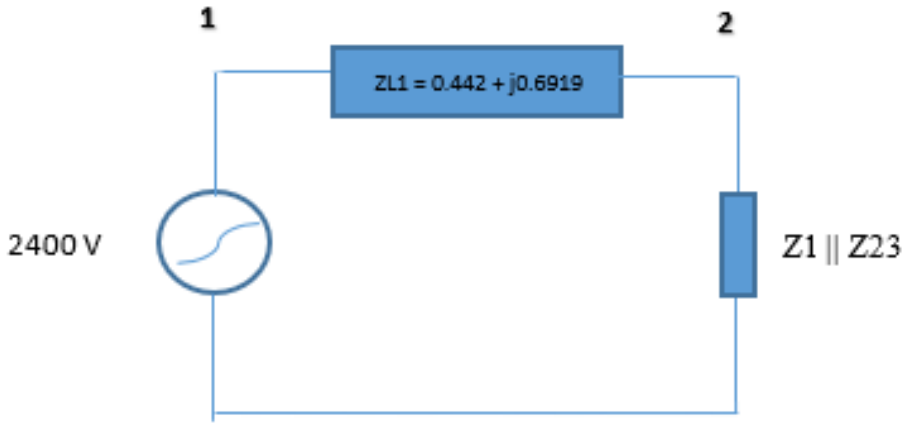

Figure 3.15: Equivalent system impedance

$$I_{Total} = \frac{V1}{Z_{System}} = \frac{2.4x10^3 \angle 0° \text{V}}{17.89 \angle 34.58°} = 134.17 \angle -34.58° \text{ A} \tag{3.29}$$

$$S_{Total} = V1 \times I^*_{Total} = 322.01 \angle 34.58° \text{ kVA} \tag{3.30}$$

$$= 265.12 + j182.76 \text{ kVA} \tag{3.31}$$

Re-calculate V2, I1, V3 and I2 and compare these values to the nameplate values of the two loads:

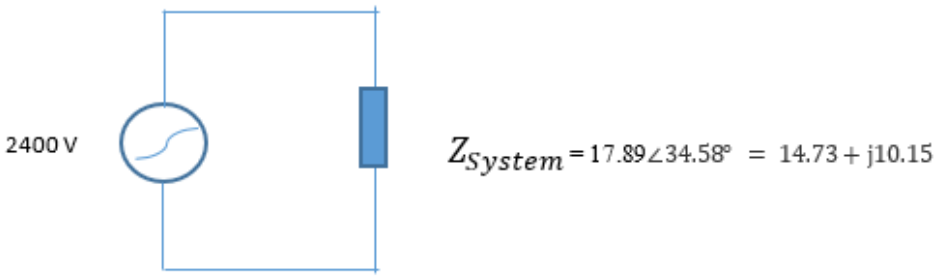

Figure 3.16: Original circuit now used to calculate operating values

$$V2 = 2400 \angle 0° - (134.17 \angle -34.58°) x (0.442 + j.6919) \tag{3.32}$$

$$V2 = 2298.88 \angle -1.07° \tag{3.33}$$

$$I1 = \frac{V2}{Z1} = \frac{2298.88 \angle -1.07° \text{ V}}{26.45 \angle 36.87^{\Omega}} (\text{conj}) = 86.96 \angle -36.84° \text{ A} = 86.916 \angle 37.94° \text{ A} \tag{3.34}$$

$$V3 = V2 - (I_{Total} - I1) \times ZL2 = 2298.88 \angle -1.07 \circ - (134.17 \angle 34.58° - 86.916 \angle 37.94°) \tag{3.35}$$

$$V3 = 2265.08 \angle -1.57 \circ \text{V} \tag{3.36}$$

$$I2 = \frac{V3}{Z2} = \frac{2265.08 \angle -1.57° \text{ V}}{52.92 \angle 25.84°} = 42.82 \angle -27.41° \text{ A} \tag{3.37}$$

Table 3.7: Sample circuit system characteristics

System Characteristic	Feeder Detail
System Voltage	2.4kV sinlge phase
Nodes	8
Line Sections	7
Shunt Capacitors	0
Line Fuses	0
Line Switches	0
Spot Loads	2
Connected Load	300 kVA
Demand at Peak Load	S = 265 + j 183 kVA
DER Generation	0

Table 3.6: Comparison of nameplate to operating values for sample circuit

Circuit Parameter	Nameplate Values	Operating Values
V1	2400	N/A
V2	2300	$2298.88\angle -1.07°$
V3	2300	$2265.08\angle -1.57°$ V
I1	$86.96\angle -36.84°$ A	$86.916\angle 37.94°$ A
I2	$43.47\angle -25.87°$ A	$42.82\angle -27.41°$ A
S1	200 kVA @0.8 pf lagging	199.73 kVA @0.8 pf lagging
S2	100 kVA @0.9 pf lagging	96.99 kVA @0.9 pf lagging

The next step confirming the impedance procedure is to build the random circuit in Power Flow, and load the circuit from 0 through 110% and compare the error of the measured impedance to the calculated impedance as was done in the original 4kV test circuit. The sample circuit is similar to the original circuit except that the sample circuit is a single phase 2.4 kV circuit with only eight nodes, seven sections and 300kVA of connected load consisting of two spot loads, 200kVA and 100 kVA respectively.

Table 3.8: 300 kVA sample Circuit Data

Load Level	P1	P2	P3	Q1	Q2	Q3 w/o Cap	V1	V2	V3	$\angle V_1$	$\angle V_2$	$\angle V_3$	ε %
0%	0	0	0	0.4	0.2	0.1	2400	2400	2400	0	0	0	1
20%	50	50	18	33	33	9	2400	2400	2400	0	0.06	0.11	2.8936
40%	100.4	100.3	36.1	65.8	65.9	17.5	2400	2400	2300	0	0.12	0.23	2.8947
50%	126.6	125.4	45.1	82.5	82.5	21.9	2400	2400	2300	0	0.16	0.28	2.8873
75%	188.9	188.4	67.7	124.7	124.4	33	2400	2300	2300	0	0.24	0.42	2.8997
100%	252.3	251.7	90.4	167	166.6	44	2400	2300	2300	0	0.31	0.56	2.9026
105%	265.1	264.4	95	176	175.1	46.3	2400	2300	2300	0	0.33	0.59	2.9074
110%	277.8	277.1	99.5	184.7	183.6	48.5	2400	2300	2300	0	0.35	0.62	2.9063

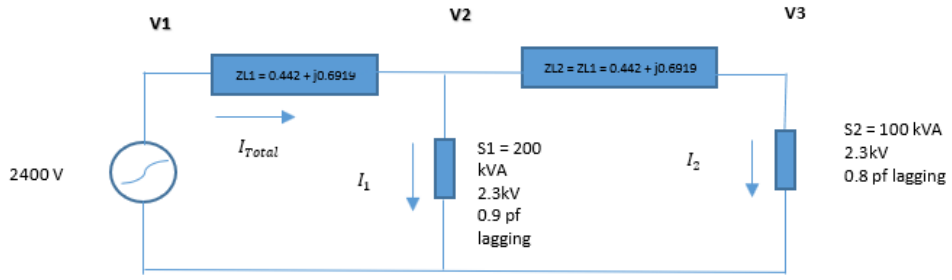

Figure 3.17: Sample circuit one-line diagram

Eight iterations of Power Flow were ran to gather the data in table 3.4 below. Again, Matlab code was developed to analyze the the impedance error. Data from table 3.4 was enetered into the Matlab code. However, before analyzing the impedance error data, a closer look at the performance of circuit parameters is necessary to understand simple and random circuit.

Figure 3.13 gives an overview of the active powers at Bus 1, Bus 2 and Bus 3. As can be seen in the graph, Bus 1 and Bus 2 have virtually the same active power wherein P1 equals P2 at every load level. This is quite differenet from the original circuit where there were several connected loads between Bus 1 and Bus 2. In the sample circuit, there are no loads between Bus 1 and Bus 2, only the impedance of the conductor. The active power ranges from 0 kW to 277.9 kW at 110% load.

Reactive power in the circuit behaves similarly to active power for Bus 1 and Bus 2. Q1 and Q2 are virtually equal. The reactive power for Bus 2 and Bus 3 are only

the reactive power seen in the two loads S1 and S1.

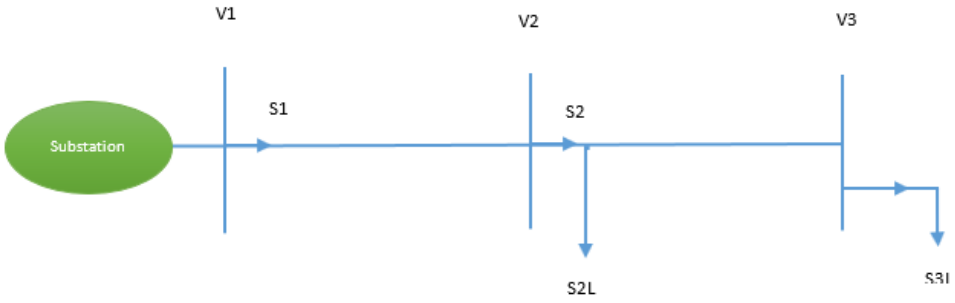

Figure 3.18: Active powers at varying load levels

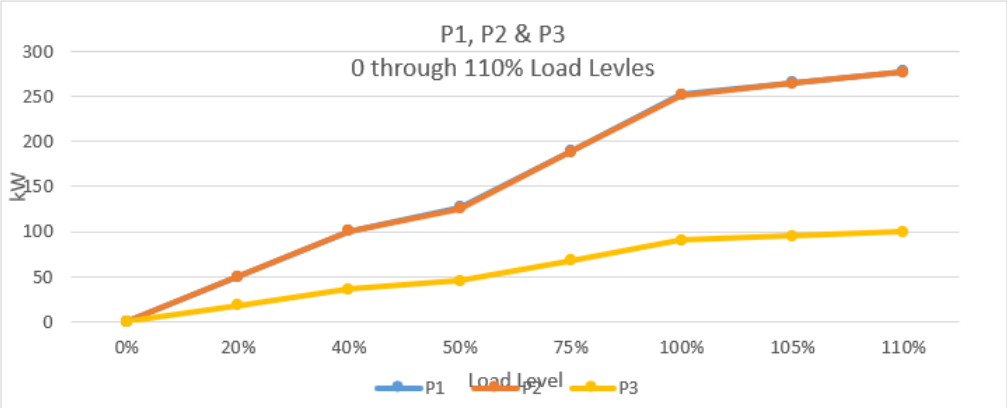

Figure 3.19: Reactive power

The voltage at Bus 1, the source bus is held strong at 2.4 kV through all load levels. V2 is similarly held strong at 2.4 kV up through the $50-75\%$ load level where V2 drops to 2.3kV. V3 begins to drop off at the 40% load levels and then still is flat through 110%. Unlike the original circuit, the load for the sample circuit is held between 2.3 and 2.4 kV, or less than 4% voltage drop and no high voltage issues under no-load conditions. Like the flat voltage profile for V1, V2 and V3 across all load levels, the angles for each of the busses is held steady. The angle of reference bus V1 is held at 0 for all load levels. As expected the angle for V2 and V3 gradually grow apart as load increases.

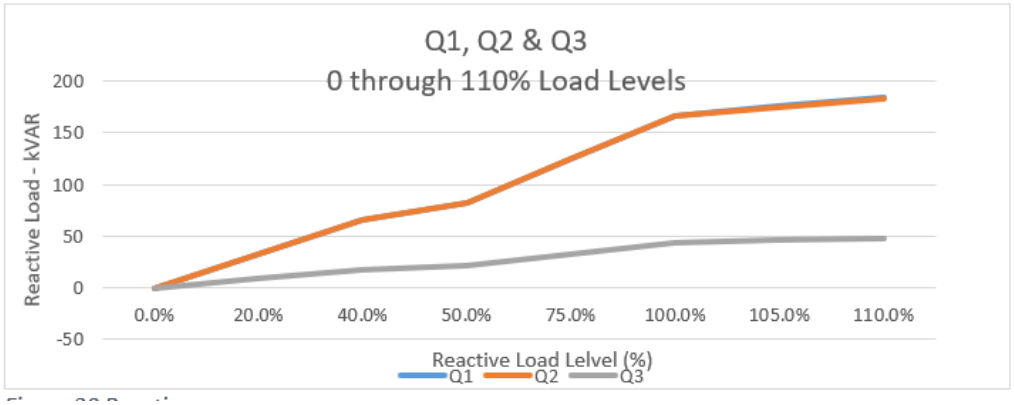

Figure 3.20: Random circuit feeder voltage profile

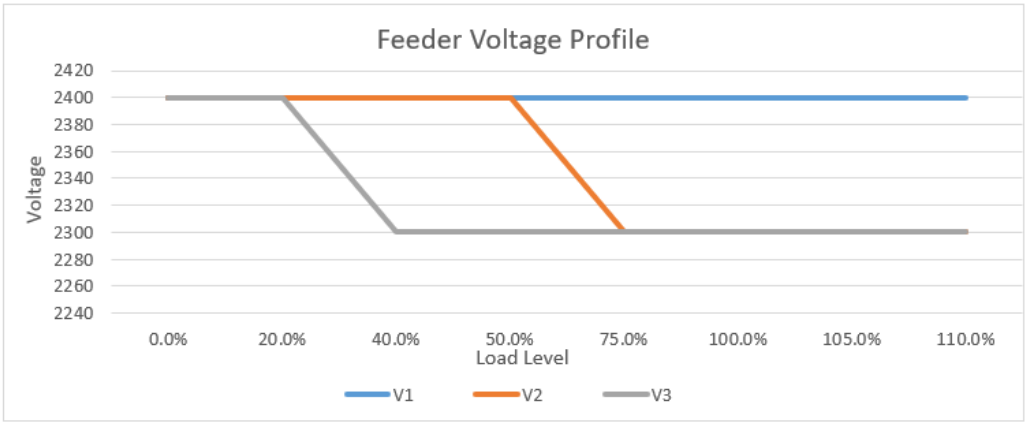

Figure 3.21: Voltage angle for V1, V2 and V3

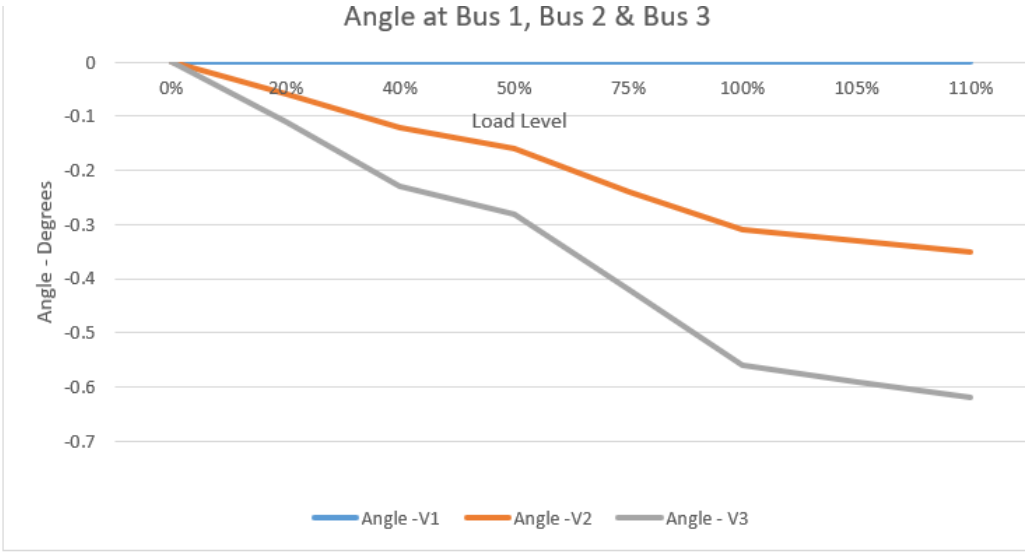

Figure 3.22: Reactive power Q1, Q2 and Q3

The impedance error for the sample circuit is 1.0% at no-load and then stays relatively flat at approximately 2.9% for all other load levels. The sample circuit appears to be much more predictable in its behavior across all load levels as the procedure used to confirm the impedance of the circuit returns approximately the same results across all load levels. There are several reasons as to why the original circuit responds differently at no load and overload conditions. One reason for the discrepancy is that the original circuit is a three phase balanced circuit. In reality the circuit is unbalanced. Some of the nodes between the busses are not balanced which causes the voltage, complex power and current to be different for each bus. Thus, for each Power Flow iteration a value for voltage and complex power had to be selected out of the three phases.

A second reason for the discrepancy in the error is that the sample feeder is only eight nodes and less than fifteen hundred feet in length. The original circuit is almost $42,000$ feet in length for a single phase and nearly $127,000$ feet when counting all three phases. The length of the feeder creates a significant difference in how the impedance of the circuit may react to the procedure being used here. At no load conditions, the original circuit still sees 24 kW of active load and 704 kVar of reactive load. The mostly inductive unloaded circuit acts are mostly capacitive and causes the voltage to rise to 4.7 kV at Bus 3.

A third reason for the discrepancy at no load and high load conditions is the number of loads, both spot loads and transformers that are connected between the busses. The sample circuit is a clean circuit with only two loads.

It appears that the impedance validation procedure returns slightly different results at $20-40\%$ load levels and at $105-110\%$ overload conditions. The results under low and medium or typical loading conditions of $40-100\%$ seem to show that the model is accurate. At 100% loading the procedure returns an equivalent system impedance within 1% of a scaled down sample circuit. The worst case for the model is at 110%

loading where the difference in the two circuits is approximately 1.3%. Given the difference in scale of the circuits in terms of complexity, number or nodes, and the sheer unbalanced nature of the circuit, the impedance validation procedure seems to be relatively accurate. A final test for the procedures may be to analyze a single phase of the original circuit comparing those results to the simple sample circuit.

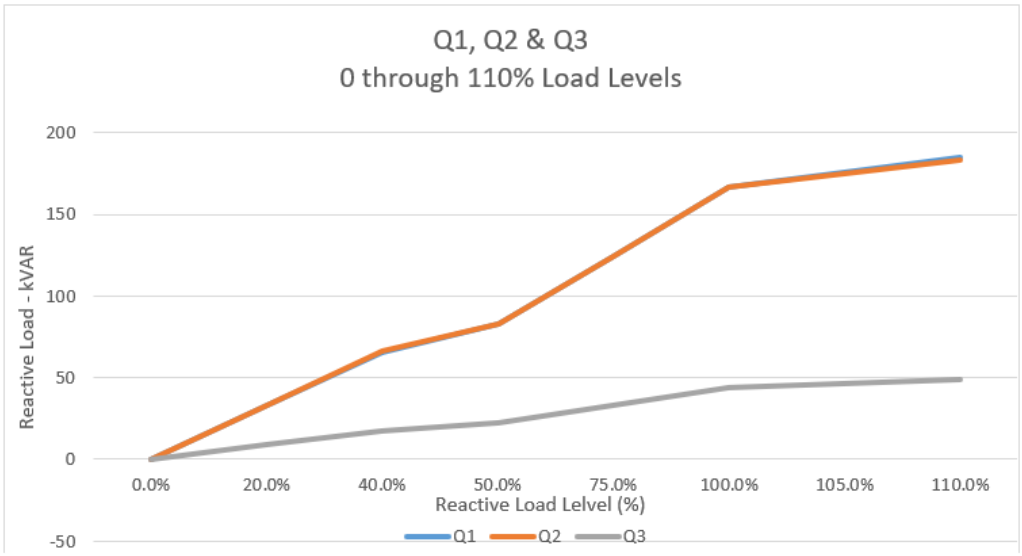

Figure 3.23: Error comparison for sample circuit and original circuit

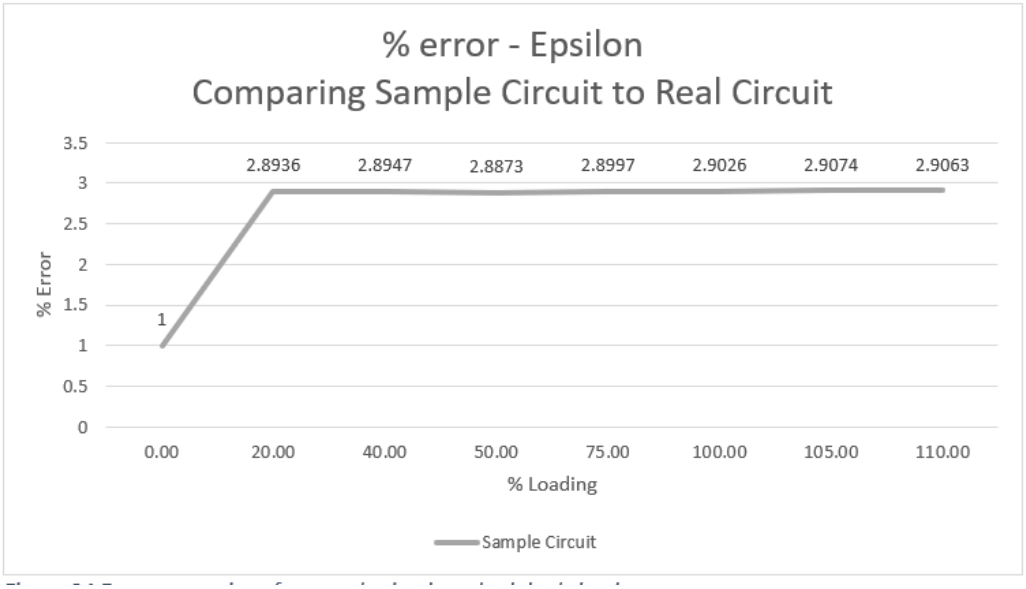

Figure 3.24: Randomly selected distribution feeder circuit

3.5 Manual Analysis of Random Feeder form $0 - 110\%$ Load Levels

To further evaluate the impedance of random circuit at various load levels, steps 1 through 5 below were performed to determine the percent error between Zystem and the parallel combination of the impedance of the loads.

Step 1: Using Kirchoff's Voltage & Current Law's solve for I1, I2, Z1 and Z2 in Figure 3.7:

$$S1 = V1 \times I1^* \tag{3.38}$$

$$\mathrm{I1} = \frac{S1}{V1} = \frac{200 \times 10^3 \angle 36.87^\circ \text{ kVA}}{2300 \angle 0^\circ \text{ V}} (\text{conj}) = 86.96 \angle -36.84^\circ \text{ A} \cdots\cdots @100 \text{ \% Load} \tag{3.39}$$

$$\mathrm{I2} = \frac{\mathrm{S1}}{V1} = \frac{100 \times 10^3 \angle 25.841^\circ \text{ kVA}}{2300 \angle 0^\circ \text{ V}} \text{ (conj)} = 43.47 \angle -25.87^\circ \text{ A} \tag{3.40}$$

$$\mathrm{Z1} = \frac{\mathrm{V1}}{\mathrm{I1}} = \frac{2300 \angle 0^\circ \text{ V}}{86.96 \angle -36.87^\circ \text{ A}} = 26.45 \angle 36.87^\circ \, \Omega = 21.16 + j15.87 \tag{3.41}$$

$$\mathrm{Z2} = \frac{\mathrm{V2}}{\mathrm{I2}} = \frac{2300 \angle 0^\circ \mathrm{V}}{43.47 \angle -25.87^\circ \text{ A}} = 52.92 \angle 25.84^\circ \, \Omega = 47.63 + j23.07 \tag{3.42}$$

Step 2: Combine the series combination of ZL2 and Z2:

$$\begin{aligned} \mathrm{Z23} &= \mathrm{ZL2} + \mathrm{Z2} \\ &= (0.442 + j.6919) + (47.63 + j23.07) \\ &= 53.601 \angle 26.3^\circ = 48.05 + j23.75 \end{aligned} \tag{3.43}$$

Step 3: Calculate the parallel combination of Z1 and Z23:

$$\begin{aligned} \mathrm{Z1||Z23} &= \frac{\mathrm{Z1} \times \mathrm{Z23}}{\mathrm{Z1} + \mathrm{Z23}} \\ &= \frac{(21.16 + j15.87) \times (48.05 + j23.75)}{21.16 + j15.87 + 48.05 + j23.75} \\ &= 17.13 \angle 33.51^\circ \\ &= 14.287 + j9.459 \end{aligned} \tag{3.44}$$

Determine the equivalent system impedance by adding the series combination of ZL1 and Z1 || Z23:

$$Z_{System} = ZL1 + Z1||Z23 = (0.442 + j0.6919) + (14.287 + j9.459) \tag{3.45}$$

$$Z_{System} = 17.89\angle 34.58^{\circ} = 14.73 + j10.15 \tag{3.46}$$

Step 5: Calculate the percent impedance error:

$$\%\text{error} = \frac{\text{Z}_{\text{system}}}{\text{Z1}||\text{Z2}} \cdots\cdots \text{Plot \% error at all load levels} 0 - 110\% \tag{3.47}$$

Table 3.9: Load levels for testing the random circuit and the percent error

Load Level	S1	S2
0%	0	0
10%	$20 \times 10^3\angle 36.87^{\circ}$	$10 \times 10^3\angle 25.84^{\circ}$
20%	$40 \times 10^3\angle 36.87^{\circ}$	$20 \times 10^3\angle 25.84^{\circ}$
30%	$60 \times 10^3\angle 36.87^{\circ}$	$30 \times 10^3\angle 25.84^{\circ}$
40%	$80 \times 10^3\angle 36.87^{\circ}$	$430 \times 10^3\angle 25.84^{\circ}$
50%	$100 \times 10^3\angle 36.87^{\circ}$	$530 \times 10^3\angle 25.84^{\circ}$
60%	$120 \times 10^3\angle 36.87^{\circ}$	$60 \times 10^3\angle 25.84^{\circ}$
75%	$150 \times 10^3\angle 36.87^{\circ}$	$75 \times 10^3\angle 25.84^{\circ}$
80%	$160 \times 10^3\angle 36.87^{\circ}$	$80 \times 10^3\angle 25.84^{\circ}$
90%	$180 \times 10^3\angle 36.87^{\circ}$	$90 \times 10^3\angle 25.84^{\circ}$
100%	$200 \times 10^3\angle 36.87^{\circ}$	$100 \times 10^3\angle 25.84^{\circ}$
105%	$210 \times 10^3\angle 36.87^{\circ}$	$105 \times 10^3\angle 25.84^{\circ}$
110%	$220 \times 10^3\angle 36.87^{\circ}$	$110 \times 10^3\angle 25.84^{\circ}$

The calculations for Z1, Z2 and Zsystem were performed in Matlab. The table 3.9

Table 3.10: Q added at each bus for each load level

Load Level	P1	P2	P3	Q1	Q2	Q3	Q1Add	Q2Add	Q3Add
0%	24	5	0	-704	-369	0	0	0	0
20%	186	73	24	-616	-329	11	88	40	11
40%	352	140	48	-522	-288	21	94	41	10
50%	435	174	90	-476	-268	41	46	20	20
75%	650	259	90	-343	-215	51	133	53	10
100%	869	345	120	-200	-160	55	143	55	4
105%	914	363	126	-171	-149	57	29	11	2
110%	959	380	132	-140	-138	60	31	11	3

shows the impedance error of the random circuit is approximately1% at all load levels. The system impedance that accounts for ZL1 and ZL2 as compared to the parallel combination of the impedance's of the loads S1 and S2 or Z1 and Z2, holds steady at all load levels. This is a critical finding as for any change in load and voltage, the impedance error does not change.

3.6 Analysis after Removal of Reactive Support at Each Load Level

Now we will test the the hypothesis that percent error is constant at various load levels. Testing this hypothesis will also test the hypothesis that losses are constant through all load levels. Figure **??** indicates that when the reactive support is removed, at the increments added at each load level, the %error does not change much based on load level.

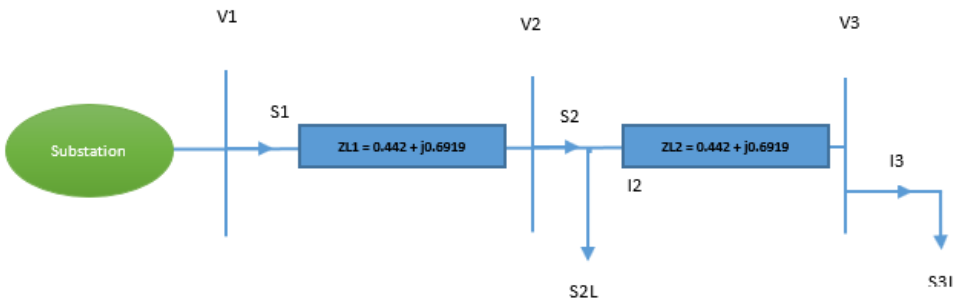

Figure 3.25: %error with reactive support and with the reactive support removed

3.7 Evaluation of Line Losses Between Bus 2 and Bus 3

Further examining impedance error at various load levels the next exercise is to focus on the line losses between Bus 2 and Bus 3. The hypothesis is that the line losses should increase as the load on the sample system increases from 0% through 110%. The percent error method used to determine the line and system impedance's can be further refined once more information is obtained about the line losses absorbed in ZL2. Ideally we would like to see an impedance that does not change for any increase or decrease in active and reactive power drawn by the circuit. To determine the line losses, I2 and V2 will be measured at Bus 2, and another voltage measurement for V3 will be taken at Bus 3. Sloss will be used to calculate ZL2 as we did with the original circuit in Figure 3.17.

$$\mathrm{S_{loss}} = I^{*}(\mathrm{V2} - \mathrm{V3})\ \mathrm{kVA} \tag{3.48}$$

$$\mathrm{ZL2_{calculated}} = \frac{\mathrm{S_{loss}}}{|\mathrm{V2} - \mathrm{V3}|^{2}}\ \mathrm{ohms} \tag{3.49}$$

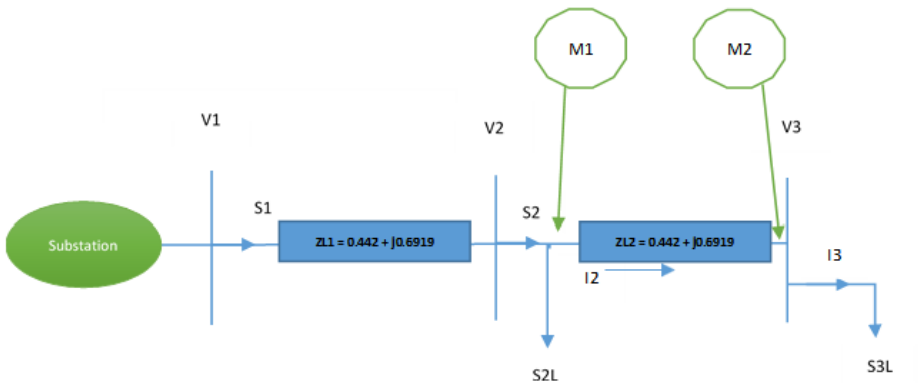

Figure 3.26: %error with reactive support and with the reactive support removed

Once $\mathrm{S_{loss}}$ and ZL2 are determined at each load level, $\mathrm{ZL2_{calcualted}}$ will be compared to $\mathrm{ZL2_{actual}}$ to evaluate both the error impedance error and losses. An accurate model must properly account for the circuit losses.

Table 3.11: 300 kVA Random System Data

Load Level	V2 (kV)	V3 (kV)	S23 (kVA)	P23 (KW)	Q23 (kVar)	PF at Node 2	I23 (A)	I23 (deg)	I23
0%	2.3672	2.3672	0.15	0	-0.15	0.00000	0.0634	90.0000	0.0634i
20%	2.3622	2.3576	19.95	16.03	11.88	0.80351	8.4452	36.5335	6.7858+ 5.0274i
40%	2.3572	2.348	40.0828	32.1162	23.9828	0.80125	16.9966	36.7507	13.6186+ 10.1693i
50%	2.3546	2.3432	50.1851	40.1862	30.0603	0.80076	21.3007	36.7973	17.0567+ 12.7588i
75%	2.3483	2.331	75.5347	60.4236	45.3264	0.79994	32.137	36.8752	25.7078+ 19.2846i
100%	2.3419	2.3187	101.0315	80.7611	60.7042	0.79937	43.0893	36.9304	34.4441+ 25.8900i
105%	2.3406	2.3163	106.1489	84.8409	63.7935	0.79926	45.294	36.9402	36.2018+ 27.2208i
110%	2.3393	2.3138	111.2725	88.9249	66.8874	0.79916	47.5035	36.9497	37.9631+ 28.5550i

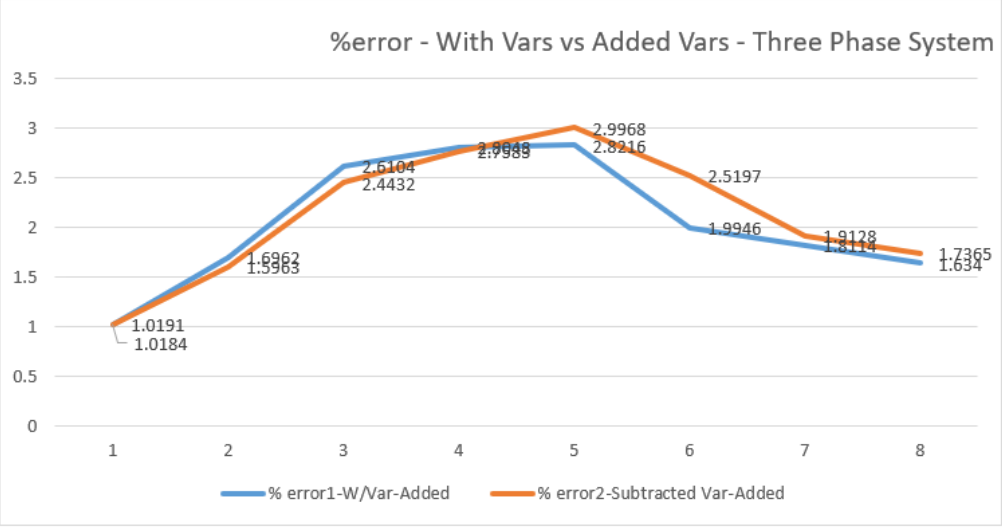

Figure 3.27: %error with reactive support and with the reactive support removed

3.8 Summary

In chapter 3 the impedance of an actual distribution feeder was determined using measured and calculated values. It was demonstrated taht the power network can be analyzed appropriately for for purposes of studying the impact of high penetration of DERs. A valid impedance model was developed and validated when comparing measured impedance to impedance calculated from network characteristics. We proved

that the equivalent circuit derived when using the six step procedure to be valid for all load levels using the iterative Newton Raphson iterative technique. In chapter 4 the implementation methodology is presented where the system response sensitivities is evaluated for a power network feeder to begin looking at how to optimize DER penetration levels. The chapter also presents the concept of modeling ans system identification. More importantly, the following chapter lays out the steps necessary for building transfer functions using system identification techniques and model order reduction. Chapter 3 is critical to formulating the basic principle for this work related to impedance modeling. System impedance does not change and is critical to building models for this work. As previously noted, the specific contributions of this work are the development of framework to develop and validate models from power networks for use in every day planning at the utility. Secondly, this work established a framework for developing aggregated transfer function parametric models based on System Identification. Last an thirdly this work create a framework to understand the effects of DERs on power system voltage at varied DER penetrations levels and under different system operating conditions.

CHAPTER 4: SENSITIVITY ANALYSIS of POWER GRID BASED ON POWER FLOW JACOBIAN

4.1 Introduction

In this chapter we develop the sensitivity analysis of the power grid based on the classic power flow Jacobian. We begin the development of sensitivity analysis by applying circuit analysis theory to a linear time-invariant RLC circuit. Our goal her is to prove that the complex physical structure of the power network can be reduced and analyzed like a basic circuit. Circuit analysis is coupled with the Newton Raphson power flow iterative technique to derive the Bus Admittance Matrix using the product of square matrices. In order to successfully analyze and dynamically model the radial distribution systems on a larger scale, deriving the bus admittance matrix and the Jacobian is critical to analyzing and developing dynamic models that can be used on a larger scale. The chapter also presents the challenge of voltage control on distribution feeders when confronted with high penetrations of DERs. The issue of high voltage is presented by manipulating the power flow equations along with demonstrating the importance of being able to validate the R/X ration a network. Mathematical derivations prove the need for DERs to begin to absorb reactive power art high penetrations levels and that the higher R/X ratios cause greater sensitivities when dealing with high voltage. Lastly, Chapter 3 present three voltage control strategies that can be used to manage network voltage.

4.2 Application of Circuit Analysis

Linear time-invariant RLC circuits having a sinusoidal voltage source, classic circuit theory using Ohm's Law and Kirchhoff's Voltage Law's for nodal and loop analysis

apply as follows:

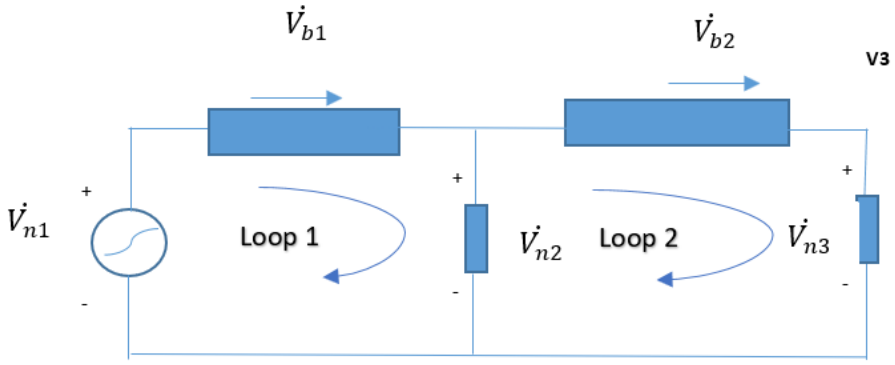

Figure 4.1: Circuit Analysis

Ohm's Law:

$$\dot{I}_b = Y_b \dot{V}_b \tag{4.1}$$

Kirchoff's Current Law:

$$Ax\dot{I}_b = \dot{I}_n \tag{4.2}$$

Kirchoff's Voltage Law:

$$Bx\dot{V}_b = 0 \tag{4.3}$$

Where $\dot{I}_b$ is complex branch current vector

Y_b is the diagonal matrix of system addmittances

$\dot{V}_b$ Is a complex branch voltage vector

The direction of vectors $\dot{I}_b$ and $\dot{V}_b$ shall be consistent. KCL requires that :

$$Ax\dot{I}_b = \dot{I}_n \tag{4.4}$$

Where $\dot{I}_n$ is a nodal current vector

A is the node to branch incidence matrix given that

$$A_{ij} = \begin{cases} 1, & \text{if branch } j \text{ is directed away from node } i \\ -1, & \text{if branch } j \text{ is directed towards from node } i \\ 0, & \text{if the branch } j \text{ is not incident to node } i \end{cases} \tag{4.5}$$

All rows if the injection current matrix $\dot{I}_n$ represents KCL for a node. Given that physically each branch current is directed from one node to the next node, the addition of all row currents eventually end in zero as defined by Kirchoff's Current Law. Thus for a system with n nodes, only n-1 row of the current vector $\dot{I}_n$ are considered independent. The reference node corresponds to the removed node.

In order to capture KVL in matrix from, a loop matrix B is then represented by:

$$B_{ij} = \begin{cases} 1, & \text{if branch } j \text{ is in loop } i \text{ and direction is the same} \\ -1, & \text{if branch } j \text{ is in loop } i \text{ and direction is opposite} \\ 0, & \text{if branch } j \text{ is not in loop } i \end{cases} \tag{4.6}$$

Thus, Kirchoff's Voltage Law can be written as

$$Bx\dot{V}_b = 0 \tag{4.7}$$

Each row of the voltage vector $\dot{V}_b$ represents Kirchoff's Voltage Law for a loop. Only independent loops are represented in vector $\dot{V}_b$. Thus, only independent loops are required to follow KVL where an independent loop is defined as a loop where not all the branches in the independent loop are found in other independent loops.

For a given radial distribution system independent loops can be derived by a branch with two shunt loads. For modeling purposes an assumed shunt branch can be placed with branch can be replaced with branch voltage to serve as the nodal voltage as shown in Figure 4.1. Thus from Figure 4.1 and KVL, we arrive at:

$$\dot{V}_b = A^T \dot{V}_n \tag{4.8}$$

$$\dot{V}_b = A^T \dot{V}_n \tag{4.9}$$

Rearranging and combining Ohm's Law (Equation 4.1), KCL (Equation 4.2) and Equation 4.9 from above derive Equation 4.10 as follows:

$$AY_b A^T \dot{V}_n = \dot{I}_n \tag{4.10}$$

Assuming that we know the nodal voltages at the first node or the source node, and the nodal current injections at the remaining $n-1$ nodes, the following Equation 4.11 can be derived from Equation 4.10 as follows:

$$A_{n-1} Y_b \begin{pmatrix} A_s^T & A_{n-1}^T \end{pmatrix} \begin{pmatrix} \dot{V}_s \\ V_{n-1} \end{pmatrix} = \dot{I}_{n-1} \tag{4.11}$$

Where,

$$A = \begin{bmatrix} \dot{A}_s \\ \dot{A}_{n-1} \end{bmatrix}, \tag{4.12}$$

$$\dot{V}_n = \begin{bmatrix} \dot{V}_s \\ \dot{V}_{n-1} \end{bmatrix}, \tag{4.13}$$

and

$$\dot{I}_n = \begin{bmatrix} \dot{I}_s \\ \dot{I}_{n-1} \end{bmatrix}. \tag{4.14}$$

4.3 Newton Raphson Power-flow

$A_{n-1}$is a square matrix. All branches in a radial distribution system are directed away from the source node, towards the successive nodes through to the end of the

feeder.

$$A^T e_n = 0 \tag{4.15}$$

Or alternatively

$$A_s^T + A_{n-1}^T e_{n-1} = 0 \tag{4.16}$$

e_n and e_{n-1} are unity column vectors with dimension n and $n-1$, respectively. It follows that Equation 4.11 is reduced to:

$$A_{n-1}^T Y_b A_{n-1}^T (V_{n-1} - V_s e_{n-1}) = \dot{I}_{n-1} \tag{4.17}$$

$A_{n-1}^T Y_b A_{n-1}^T$ is the classical Bus Admittance Matrix derived from each node. The Bus Admittance Matrix is symmetrical around the main diagonal. Thus the Bus Admittance Matrix if derived using the product of three square matrices.

On radial distribution systems, such is our interest, the voltage measured from one node to the next is relatively small. Using this assumption, the Jacobian matrix for HDH^T. H is an upper triangular matrix based on system topology and D is a block diagonal matrix. Shunt devices such as capacitor banks, constant impedance loads can be changed to node injections using initial and updated nodal voltages. Accepting the assumption that changes in nodal voltages are small, and that shunt branches can be converted to constant power injections, this sets us up nicely leverage the Newton Raphson method to solve the power flow and analyze radial distributions systems.

$$\begin{bmatrix} \Delta P \\ \Delta Q \end{bmatrix} = \begin{bmatrix} M & N \\ R & W \end{bmatrix} \times \begin{bmatrix} \Delta \delta \\ \Delta V \end{bmatrix} \tag{4.18}$$

$$M_{ij} = -V_i V_j (G_{ij} \sin \delta_{ij} - B_{ij} \cos \delta_{ij}),\ j \neq i \tag{4.19}$$

$$M_{ii} = V_i \sum_{j \in i, j \neq i}^{n} V_j (G_{ij} \sin \delta_{ij} - B_{ij} \cos \delta_{ij}) \tag{4.20}$$

$$N_{ij} = -V_i V_j (G_{ij} \cos \delta_{ij} - B_{ij} \sin \delta_{ij}),\ j \neq i \tag{4.21}$$

$$N_{ii} = -V_i \sum_{j \in i, j \neq i}^{n} V_j (G_{ij} \cos \delta_{ij} + B_{ij} \cos \delta_{ij}) - 2V_i^2 G_{ij} \tag{4.22}$$

$$R_{ij} = V_i V_j (G_{ij} \cos \delta_{ij} + B_{ij} \sin \delta_{ij}) \tag{4.23}$$

$$R_{ii} = -V_i \sum_{j \in i, j \neq i}^{n} V_j (G_{ij} \cos \delta_{ij} + B_{ij} \cos \delta_{ij}) \tag{4.24}$$

$$W_{ij} = -V_i V_j (G_{ij} \sin \delta_{ij} - B_{ij} \cos \delta_{ij}),\ j \neq i \tag{4.25}$$

$$W_{ii} = -V_i \sum_{j \in i, j \neq i}^{n} V_j (G_{ij} \sin \delta_{ij} - B_{ij} \cos \delta_{ij}) - 2V_i^2 B_{ii} \tag{4.26}$$

The Admittance Y_{ij} or $G_{ij} + jB_{ij}$ is the entry into the admittance matrix. Revisiting the fact that the difference in voltage between successive nodes is marginal, similarly the diagonal admittance is equal to the summation of the node admittance as given below:

$$G_{ii} += B_{ii} = \sum_{j \in i, j \neq i}^{n} (G_{ij} + jB_{ij}) \tag{4.27}$$

The Jacobin can be reduced to the below set of equations for systems without shunt branches:

$$M_{ij} = -V_i V_j B_{ij} \cos \delta_{ij}, j \neq i \tag{4.28}$$

$$M_{ii} \approx -V_i \sum_{j \in i, j \neq i}^{n} V_j B_{ij} \cos \delta_{ij} \tag{4.29}$$

$$N_{ij} \approx -V_i V_j G_{ij} \cos \delta_{ij}, j \neq i \tag{4.30}$$

$$N_{ii} \approx V_i \sum_{j \in i, j \neq i}^{n} V_j G_{ij} \cos \delta_{ij} \tag{4.31}$$

$$R_{ij} \approx V_i V_j G_{ij} \cos \delta_{ij} \tag{4.32}$$

$$R_{ii} \approx -V_i \sum_{j \in i, j \neq i}^{n} V_j G_{ij} \cos \delta_{ij} \tag{4.33}$$

$$W_{ij} \approx -V_i V_j G_{ij} \cos \delta_{ij}, j \neq i \tag{4.34}$$

$$W_{ii} \approx -V_i \sum_{j \in i, j \neq i}^{n} V_j B_{ij} \cos \delta_{ij} \tag{4.35}$$

4.4 Jacobian

Approximated power flow equations show that matrices M, N, R and$W$ have properties of symmetry and sparsity as the Nodal Admittance Matrix and can be formed as follows:

$$\begin{aligned} M =& W = A_{n-1} K_B A_{n-1}^T \\ R =& - N = A_{n-1} K_G A_{n-1}^T \end{aligned} \tag{4.36}$$

K_B and K_G are diagonal matrices with entries of:

$$V_i V_j B_{ij} \cos \delta_{ij} \tag{4.37}$$

and

$$V_i V_j G_{ij} \cos \delta_{ij} \tag{4.38}$$

Thus in solving for $\Delta\delta$ and $\Delta V/V$, we now have

$$\begin{bmatrix} \Delta P \\ \Delta Q \end{bmatrix} = \begin{bmatrix} A_{n-1} \\ A_{n-1} \end{bmatrix} \begin{bmatrix} K_B & K_G \\ -K_G & K_B \end{bmatrix} \begin{bmatrix} A_{n-1}^T \\ A_{n-1}^T \end{bmatrix} \begin{bmatrix} \Delta\delta \\ \Delta V/V \end{bmatrix} \tag{4.39}$$

A_{n-1} is the upper triangular matrix where all diagonal entries are equal to 1 and all non-zero off-diagonal entries are -1. We have proven that the Jacobian can be formed as a product of three square matrices like the Nodal Admittance Matrix and can be sued to solve for $\Delta\delta$ and $\Delta V/V$.

4.5 Voltage Control on High Penetration Feeders

DERs are generation resources that are typically placed near electrical loads such as residential loads on a feeder. DER generation supply household loads. Surplus

generation is exported back to the grid - this reverse power flow is the catalyst for voltage rise along the feeder. Voltage rise thus voltage control is a limiting factor to the amount of PV that can be injected into the feeder violating: ANSI C84.1 voltage limits, and utility distribution planning criteria for nominal voltage of 0.95 to 1.05 pu.

High voltage worsens in DERs supply peak production under light loads - not necessary a problem for feeders with mostly industrial and commercial loads. Peak PV production is coincident with peak load. Overvoltage is noticeable when: Over half of residential loads have PV or existing baseline voltage is high without or before DER addition.

High voltage issues are prevalent in long distribution feeders where long lines are designed with line voltage regulators set to maximum to boost line voltage as high as possible or where accommodating voltage drop further down the radial feeder. Electric utilities planning and operating radial distribution feeders need revised study procedures and solutions to accommodate maximum DERs while avoiding overvoltage.

4.5.1 Overvoltage in Radial Distribution Systems

Voltage drop across a distribution feeder (Figure 4.2) is given by the following equation:

$$\begin{aligned} \Delta V &= V_S - V_R \\ &\approx \frac{P \times R + Q \times X}{V_s} \\ &= \frac{(P_L - P_G)R + (Q_L - Q_G)X}{V_s} \end{aligned} \tag{4.40}$$

Similarly, the voltage rise phenomenon for high penetration feeders the term $(P_L - P_G)R$ turns negative at light load which results in an increase in ΔV in the negative direction.

Figure 4.2: Radial distribution system

Power system stability primarily falls into two categories, angle stability and voltage stability. On the distribution network, angle stability is not of primary concern since the difference in angle between buses is extremely small on the order of a tenth or a hundredth of a degree and thus is n0t necessary to analyze. On the other hand, voltage stability is broken down by large disturbance and small signal disturbances. On the distribution network, small signal voltage disturbance is of concern the nominal voltage must be maintained within a 5 percent tolerance. Absorbing Q_G can mitigate high voltage at the expense of reduced . For this purpose, KVA name plate ratings is used to determine the maximum power. In order to hold DER terminal voltage constant, $\Delta V = 0$ and $\Delta Q \approx (R/X)\Delta P$. For common feeder conductor such as 1/0 ACSR, $R/X \approx 1$, thus KW-rise is directly proportional to VARs required to be absorbed. Furthermore, the under excited DER system is not feasible for IBRs.The higher the R gives greater sensitivity to over voltage. It means long feeders with high R/X ratios is strong indicator of the need for VAR absorption or hightened voltage control. Overvoltage is more prominent at light load conditions. Q_G exports exacerbate over voltage. There are several ways that the voltage can be controlled that comply with Kirchoff's Voltage and Current Law's. Perhaps the easiest control strategy is power factor control. Today most utilities require DER sites to operate at unity power factor where reactive power absorption is held to zero. A second option when using power factor to control the voltage is to underexcite the DER creating an off unity and leading power factor wherein the DER is absorbing reactive power from the network to maintain voltage stability. Alternatively, voltage can be controlled us-

ing Voltage-Reactive Control or Volt-Var Control. Under Volt-Var control the DER dynamically controls it reactive output depending on system conditions wherein reactive power is either absorbed or injected into the network. The last option for voltage control is Voltage-Active Power Control or Volt-Watt. Under Volt-Watt control the DER site is required to dynamically lower or raise active power output for what is commonly referred to as curtailment.

4.6 Summary

In conclusion, this chapter presents a sensitivity analysis of the power grid based on the classic power flow Jacobian. We begin the development of sensitivity analysis by applying circuit analysis theory to a linear time-invariant RLC circuit. Our goal her is to prove that the complex physical structure of the power network can be reduced and analyzed like a basic circuit. Circuit analysis is coupled with the Newton Raphson power flow iterative technique to derive the Bus Admittance Matrix using the product of square matrices. In order to successfully analyze and dynamically model the radial distribution systems on a larger scale, deriving the bus admittance matrix and the Jacobian is critical to analyzing and developing dynamic models that can be used on a larger scale. The chapter also presents the challenge of voltage control on distribution feeders when confronted with high penetrations of DERs. The issue of high voltage is presented by manipulating the power flow equations along with demonstrating the importance of being able to validate the R/X ratio of a network. Mathematical derivations prove the need for DERs to begin to absorb reactive power art high penetrations levels and that the higher R/X ratios cause greater sensitivities when dealing with high voltage. This Chapter is pivotal to the analytical Law's of Physics and the flow and analysis of electric circuits and thus is paramount to formulating the basic principle for this work. The powerflow equations and the iterative methods employed to solve power networks must be validated and used to collect system data used for model development. As previously noted, the specific contributions of this

work are the development of framework to develop and validate models from power networks for use in every day planning at the utility. Secondly, this work established a framework for developing aggregated transfer function parametric models based on System Identification. Last and thirdly this work creates a framework to understand the effects of DERs on power system voltage at varied DER penetrations levels and under different system operating conditions. The next chapter analyzes the system response sensitivities of a radial distribution network. A more in depth look at voltage response along the feeder is undertaken looking closely at the sensitivities around voltage active and reactive power allocations. The next chapter is the initial step to proving that parametric models of the power system can be used to predict system voltage for given DERs penetration levels.

CHAPTER 5: IMPLEMENTATION METHODOLOGY

5.1 Introduction

In this chapter the system response sensitivities of a radial power network are investigated. A detailed analysis of voltage response at the head, middle and end of the feeder is evaluated for purposes of further analyzing voltage response. Analysis and performance of sensitivities for voltage, active and reactive power are developed. Models are constructed form observed data wherein voltage response sensitivities are assessed at critical points in the feeder. Pivotal to the overall contribution is the use of control system theory and more specifically, system identification are use to extract key information about the relationship between input and output data.Input output relationships are used to identify power network models for the dynamical system. A System Identification Methodology and framework is presented. Techniques for model order reduction and presented to derive optimal system models that capture system dynamics. A methodology is also presented that allows the system identification and model order reduction framework to be scaled to a larger and more complex networks. Chapter 5 is the first step to proving that parametric models of power networks can be developed and used to predict the effects of DERs on voltage. The specific contributions of this work are the development of framework to develop and validate models from power networks for use in every day planning at the utility. Secondly, this work established a framework for developing aggregated transfer function parametric models based on System Identification. Last an thirdly this work create a framework to understand the effects of DERs on power system voltage at varied DER penetrations levels and under different system operating conditions.

5.2 System Response

5.2.1 System Response Sensitivities - Head, Middle and End

Voltage control is critical to maintaining reliability on a radial feeder. Particularly, voltage response at head, middle and end of the feeder are critical measurements of the ability to increase DER penetration levels. Optimizing DER penetration levels and Distribution Planning Methods is to analyze voltage response and changes in voltage along feeders may inform useful voltage control strategies.

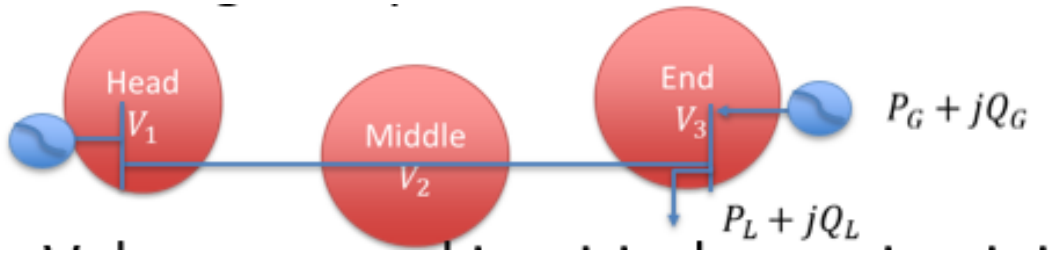

Figure 5.1: System Response Sensitivities

If $V_{baseline}$ = Steady state voltage prior to DER addition, V_{new} = Steady state voltage after DER addition, then System stability criteria is given by:

$$V_{new} - V_{Baseline} = \Delta(i.e. \Delta V_1, \Delta V_2, \Delta V_3) \tag{5.1}$$

where

$$\Delta V = \begin{cases} 0.1 \text{ pu} \\ \text{positive} \end{cases} \tag{5.2}$$

The above must be true for all load levels at each bus and for all DER penetration levels at each bus.

System response sensitivities can be characterized as follows:

$$V_{\text{senstivities}} = \begin{cases} V_1 \longrightarrow \Delta V_1 \\ V_1 \longrightarrow \Delta V_2 \\ V_1 \longrightarrow \Delta V_3 \\ V_2 \longrightarrow \Delta V_2 \\ V_2 \longrightarrow \Delta V_3 \\ V_3 \longrightarrow \Delta V_3 \end{cases} \tag{5.3}$$

Similarly, system response sensitivities $V,\ P, :\ Q$ at each bus can be calculated by the following:

$$\begin{vmatrix} \frac{\delta v_1}{\delta p_1} & \frac{\delta v_2}{\delta p_1} & \frac{\delta v_3}{\delta p_1} \\ \frac{\delta v_1}{\delta Q_1} & \frac{\delta v_2}{\delta Q_1} & \frac{\delta v_3}{\delta Q_1} \end{vmatrix} \begin{vmatrix} \frac{\delta v_1}{\delta p_2} & \frac{\delta v_2}{\delta p_2} & \frac{\delta v_3}{\delta p_3} \\ \frac{\delta v_1}{\delta Q_2} & \frac{\delta v_2}{\delta Q_2} & \frac{\delta v_3}{\delta Q_2} \end{vmatrix} \begin{vmatrix} \frac{\delta v_1}{\delta p_3} & \frac{\delta v_2}{\delta p_3} & \frac{\delta v_3}{\delta p_3} \\ \frac{\delta v_1}{\delta Q_3} & \frac{\delta v_2}{\delta Q_3} & \frac{\delta v_3}{\delta Q_3} \end{vmatrix} \tag{5.4}$$

5.3 Analysis and Performance Metrics

Analyze autonomous voltage-reactive power control strategies at multiple DERs connected to the same feeder. Understand whether and how these controls cooperate with existing voltage and VAR control systems. Assess the performance of distributed voltage-reactive power controls at the distribution feeder level. Evaluate mitigation options required at the distribution feeder level to enable more aggressive reactive power based voltage control.

5.4 Modeling and Identification

Constructing models from observed data is a fundamental element in science. Several methodologies and nomenclatures have been developed in different application areas. In the control area, the techniques are known under the term System Identification. Generally there are two kinds of modeling approaches being either developing a model from basic theoretical principles and physical laws or assuming a general

model class which envelops the system under investigation and estimating a representative of that class based on the experimental data. The theoretical models are good for understanding the physical phenomena which drive the observed system behavior. However the many physical parameters which appear in these models are difficult to measure or estimate in practice especially for large scale or complex systems. On the other hand the system identification models can be easily fitted to experimental data and unknown parameters estimated directly. However with these models the underlying physical phenomena become implicit in the model. For control and system optimization purposes it is more important to have a good model of input output behavior than the exact physical interpretation of the model parameters so the system identification models are preferred in the dissertation.

Control system analysis techniques can be used to critically analyze the sensitives and stability around DER penetration levels. Voltage response sensitivities across the feeder provide enough information to analyze the system at varying DER penetration levels. Optimal voltage control strategies and penetration levels can be identified for unique feeder types (voltage, substation rating, load characteristics, etc..)

5.5 System Identification

System Identification (SI) is the process of extracting information about a dynamic system from measured input-output data. The expected outcome is the identification of a model which may be static or dynamic, deterministic or stochastic, linear or nonlinear. And resulting model is used for simulation, controller design, or further analysis. System Identification can also be used to identify controllability matrix, observability matrix, an observer or Kalman filter gain.

System Identification is the term that has been coined by Zadeh (1956) for the model estimation problem for dynamic systems in the control community. Two main avenues can be seen for the development of the theory and methodology (Gevers, 2006): One is the realization avenue, that starts from the theory how to realize

linear state space models from impulse responses, Ho and Kalman (1966), followed by Akaike (1976), leading to so-called subspace methods, e.g. Larimore (1983) and Van Overschee and DeMoor (1996). The other avenue is the prediction-error approach, more in line with statistical time-series analysis and econometrics. This approach and all its basic themes were outlined in the pioneering paper Astrom and Bohlin (1965). It is also the main perspective in Ljung (1999). Identify the System or construct a model from measured data to:

- Estimate approximate models of dynamic systems
- Dynamic systems - key is the next state depends on the previous state.
- Predicting output y(t) at time t depends on all or some previous measured inputs and outputs
- Purpose of the model is to accurately achieve prediction or control of the system

A main feature of dynamical systems is that the future depends on the past. Thus a prediction of the output $y(t)$ at time t, either being constructed by ad hoc reasoning or carefully calculated in a stochastic framework, depends on all or some previous measured inputs and outputs,

$$Z_{t-1} = y(t-1), u(t-1), y(t-2), u(t-3), \cdots . \tag{5.5}$$

Let us denote the prediction by $y(t|t-1) = g(Z_{t-1})$. In case the system is not fully known, this prediction will be parameterized by a parameter θ (which typically is finite-dimensional, but could also conceptually capture nonparametric structures) so the prediction is

$$\hat{y}(t|\theta) = g(Z_{t-1}, \theta) \tag{5.6}$$

The distinguishing features as well as the bulk of efforts in System Identification can, somewhat simplistically, be described as:

1. Invent parameterizations $\hat{y}(t|\theta)$, suitable to describe linear and nonlinear dynamic systems. For underlying state-space realizations, realization theory has been an important source of inspiration. Questions of how prior physical knowledge can best be incorporated form another central issue.

2. Translate the core material of Section 2 to properties of estimated systems, as well as estimation procedures.

3. Find effective ways to estimate θ numerically for the chosen parameterizations. The curve-fitting criterion (5) forms a beacon for these efforts in the prediction error approach, typically leading to nonlinear opti- mization by iterative search. The realization avenue has developed techniques based on SVD and QR factorizations.

4. The typical intended use of the model in this context is for prediction or control. This means that models of the noise affecting the system often are essential.

5. Experiment design now becomes the selection of input signal. The effects of the experiment design can be evaluated from the core material, but can be given concrete interpretations in terms of model quality for control design, e.g. Gevers (1993). Specific features for control applications are the problems and opportunities of using inputs, partly formed from output feedback, e.g. Hjalmarsson (2005). An important problem is to quantify the model error, and its contribution from the variance error and the bias error, cf. (11), "model error models", e.g. Goodwin et al. (1992).

The complete workflow chart of System Identification Methodology is presented in the 5.2.

5.5.1 Steps for System Identification

1. Design and build a random 2.4kV feeder in Power Flow

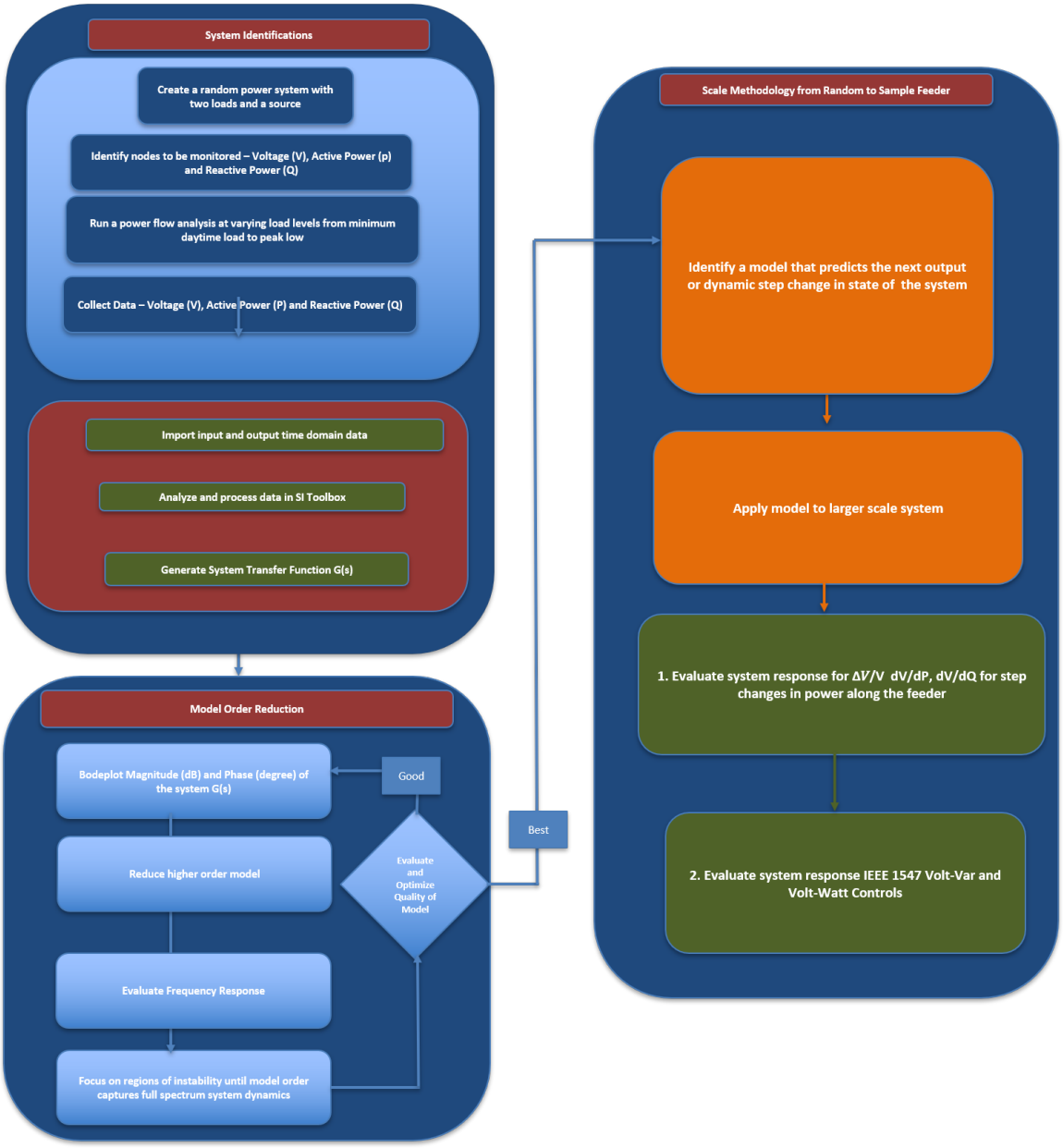

Figure 5.2: Flowchart of System Identification Methodology

- 300kVA peak load consisting of two spot loads
- Two loads - 100kVA and 200kVA distribution

2. Initialize the Power Flow case with flat start load allocation at 40-110
3. Batch run Powerflow at varying load levels
4. Identify nodes to be monitored
5. Collect measured system data from feeder at selected monitored nodes
    - Inputs - Active power (P) and Reactive power (Q) at each node
    - Outputs - Voltage (V) at each node
6. Import input and output time-domain data in toolbox
7. Analyze and process input and output data
    - piecewise constant - zero-order hold
8. Generate Transfer Function G(s)
    - @ nodes 1, 2 and 3
    - Mathematical relationship between inputs and outputs
    - Linear Time Invariant System
9. Model Quality - Validate the accuracy of the models in the frequency domain with a step response - Assess %fit
10. Reduce System Order
    - Analyze the magnitude and frequency of the Bodeplot
    - Focus on regions of instability and low energy
11. Repeat step 6 through 8 until an acceptable approximation of the system is derived

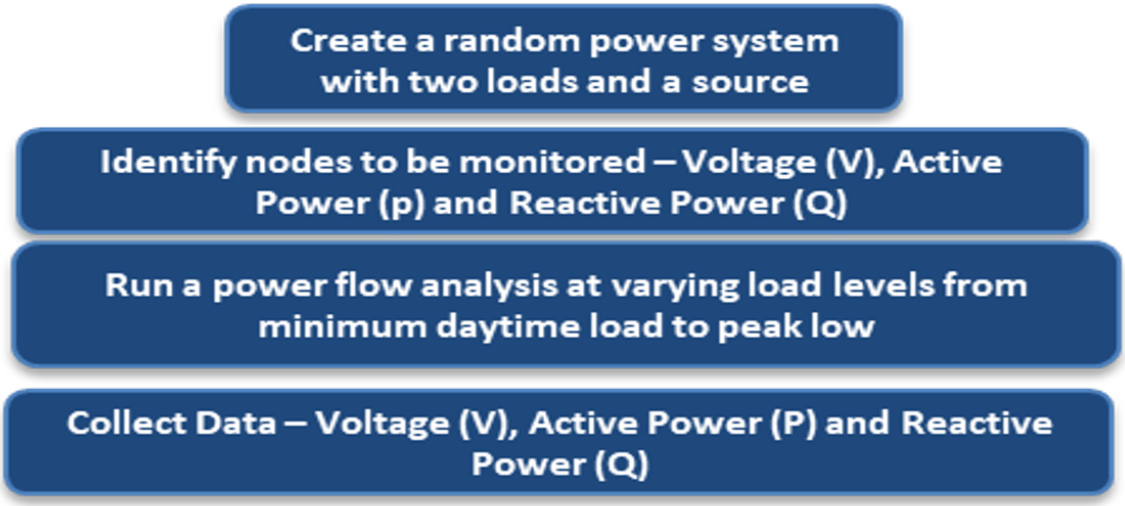

Figure 5.3: Flowchart of System Identification Methodology

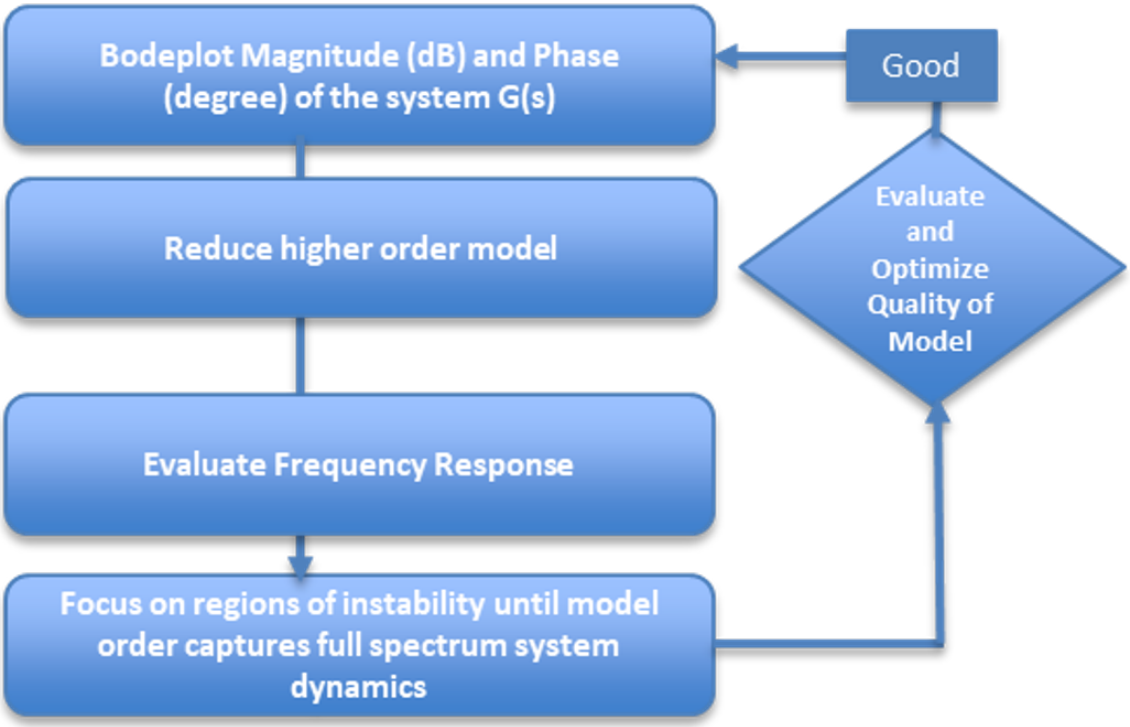

Figure 5.4: Flowchart of System Identification Methodology

5.6 Typical model structures

As was noted above the basic assumption in system identification is that the real system behavior falls into certain *model class*. The model class is a bounded parametric or non-parametric set of model formulas which describe how to calculate the output system signal based on the input system signal. So if we denote the model class as $\mathcal{M}(\theta) = \{y = F(u)\}$ where $\theta \in R^n$ is particular parametrization of the model class with n dimensional Euclidean vector, the system identification assumption is that $F_{real} \in \mathcal{M}(\theta)$. If the real system doesn't belong to the model class then the estimated model will be biased and giving an approximation to one or another degree. From this it follows that it is critical how we choose the model structure (or model class). The model structure should be rich enough to capture the real system but also should be efficient to not evade overestimation. The problem with overestimation or overfitting is that by extending the model class we always can fit the experimental data, i.e. minimizing model error $y(t) - y_m(t)$, but at the cost of model generalization properties. So if we give different (unknown) input to the model the chance we miss the real system response is larger whit overfitted model. Lets review most common model structures.

Linear time-invariant state-space model of the form

$$\begin{cases} \dot{x}(t) = Ax(t) + Bu(t) \\ y(t) = Cx(t) + Du(t) \end{cases} \tag{5.7}$$

where $x(t) = (x_1, x_2, \ldots, x_n)^T \in R^n$ is hidden state vector, $u(t) = (u_1, u_2, \ldots, u_m)^T \in R^m$ is the input signals vector and $y(t) = (y_1, y_2, \ldots, y_l)^T \in R^l$ is a vector of output signals. Here n, m and l are the dimensions of the state, input and output vector spaces. Matrices $A \in R^{n \times n}$, $B \in R^{n \times m}$, $C \in R^{l \times n}$ and $D \in R^{l \times m}$ are matrices with appropriate dimensions which gives the correlation between spaces. In more

general form we can have time varying structure where A, B, C and D are time or parameter dependent. And in its most general setting we can have nonlinear state-space structure with $\dot{x}(t) = f(x,u)$ and $y(t) = g(x,u)$. The state space structure is universal in sense that every real system of ordinary differential equations can be represented in such a form. When trying to estimate the model parameters from experimental data it is more appropriate to use the discrete time equivalent of the model where instead of time derivative $\dot{x}(t)$ we have $x(k+1)$ with $k \in Z$. The drawback of estimating parameters of state space model is that number of free parameters is $n \times n + n \times m + l \times n + l \times m$, or the more inputs, outputs or hidden states the more parameters to estimate. One solution is to apply canonical state-space descriptions.

Another equivalent class of models is the transfer matrix set of models which can be given with

$$\begin{pmatrix} y_1(s) \\ y_2(s) \\ \dots \\ y_l(s) \end{pmatrix} = \begin{pmatrix} W_{11}(s) & W_{12}(s) & \dots & W_{1m} \\ W_{21}(s) & W_{22}(s) & \dots & W_{2m} \\ . & . & \dots & . \\ W_{l1}(s) & W_{l2}(s) & \dots & W_{lm} \end{pmatrix} \begin{pmatrix} u_1(s) \\ u_2(s) \\ \dots \\ u_m(s) \end{pmatrix} \tag{5.8}$$

where $y_i(s) = \mathcal{L}[y_i(t)]$ and $u_i(s) = \mathcal{L}[u_i(t)]$ are Laplace transforms of the output and input signals with $s = \sigma + j\omega \in C$ being a complex variable. Elements of the transfer matrix

$$W_{ij}(s) = \frac{y_i(s)}{u_j(s)} = \frac{s^m + b_{i,j,1}s^{m-1} + b_{i,j,2}s^{m-2} + \ldots + a_{i,j,m}}{s^n + a_1 s^{n-1} + a_2 s^{n-2} + \ldots + a_n} \tag{5.9}$$

are linear fractional transfer functions which represent a particular correlation between the i-th output with the j-th input. The parameters $b_{i,j,k}$ and a_k have to be estimated from the experimental data. There are various canonical forms that can minimize the number of parameters. In a simplest case we can assume that the matrix is diagonal meaning that $W_{ij} = 0$ when $i \neq j$ and $W_{ii} \neq 0$.

In discrete time models the data are fed to the model with the fixed sample rate T_S which should be properly selected depending on the frequency range of the system we want to focus on. In continuous time models one the frequency range of the system is infinite because any interval of real number is uncountable set and hence represents infinite information. However in practice we always measure data with certain frequency so the frequency range and information content are always limited. From discrete time models the most common linear structures are autoregressive model with exogenous input (ARX), autoregressive moving average model with exogenous input (ARMAX), Box-Jenkins (BJ) model and output error (OE) model. Also there are nonlinear analogs to these structures like nonlinear ARX model (NARX). In system identification ususally the procedure starts with estimation of ARX model of the form

$$A(q^{-1})y(k) = B(q^{-1})u(k) + e(k), \tag{5.10}$$

where

$$A(q^{-1]}) = 1 + a_1 q^{-1} + a_2 a^{-2} + \dots a_{na} q^{-na} \tag{5.11}$$

$$B(q^{-1]}) = 1 + b_1 q^{-1} + b_2 a^{-2} + \dots b_{nb} q^{-nb} \tag{5.12}$$

The q^{-k} is time-delay operator with $q^{-k}y(t) = y(t-k)$ with $k \in Z^+$ being the discrete time. From discrete time we can reconstruct $t = kT_S$, when we know the sample time. The $e(k)$ is so called residual or latent term which represent model error. The goal of parameter estimation is to minimize the magnitude of the $e(k)$ and in this way to capture most of the experimental information into model parameters a_i and b_i. This ARX model is single input single output (SISO). However in our case we focus on MIMO models - multiple input multiple output. In this case we have

$$A_i(q^{-1})y_i(k) = \sum_{j=1}^{m} A_{ij}y_j(k) + B_{ij}u_j(k) \tag{5.13}$$

with $i = 1 \ldots n$ is the index of the output signal and $j = 1 \ldots m$ is the index of the input signal. A_{ij} and B_{ij} represent the correlation between channels when $i \neq j$.

5.7 Model parameter estimation

The central problem in identification after selecting the appropriate model structure $\mathcal{M}(\theta)$ how to estimate the actual value of θ. So in order to do this we define a cost function as

$$J(\theta) = \sum_{k=1}^{N} (y(k) - y_m(k))^2 = \sum_{k=1}^{N} e^2(k) \tag{5.14}$$

Here the signal $y_m(k)$ is either the simulated model output or predicted model output. Which one will be used depend on the intended purpose of the model - for simulation or prediction.

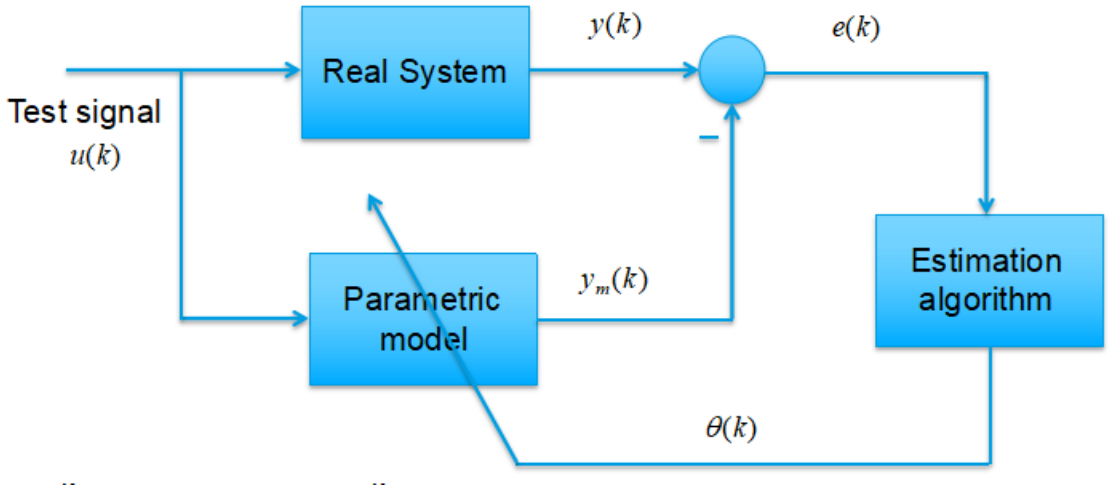

Figure 5.5: General identification approach

The purpose of system identification is to calculate an optimal values of the parameters to minimize the value of $J(\theta)$ such that

$$\hat{\theta} = Argmin_{\theta} \left(J(\theta) \right). \tag{5.15}$$

Values of the parameters $\hat{theta}$ which minimize the functional $J(\theta)$ are obtained with numerical optimization method. Some of the structures like ARX are linear with

respect to parameters so there can be found a unique minimizer. In other model types like ARMAX or BJ which are nonlinear with respect to parameters there is not guarantee that we can find an unique extremal value and the result depends on the initial model paramters. In general $\hat{theta}$ will depend on the actual data which are measured and on the length of the dataset which are more or less uncertain. Hence parameter estimates $\hat{theta}$ are random variables with certain mean and variance. A central topic in theory of system identification is to determine the conditions for unbiased estimates such that

$$lim_{N\to\infty}\hat{\theta}(N) = \theta_0 \tag{5.16}$$

where θ_0 are the parameters of the true system which we want to estimate with the optimization method.

5.8 Information content in the identified models

As we discussed above there are two kinds of model structures - continuous time and discrete time. In continuous time model all signals $x(t)$ are functions $x : T \to \mathbf{R}$ where $T = [0, \infty)$ is the set of time instants, identical with positive reals R^+. In discrete time models the time is discretized with sample rate $F_S = 1/T_S$, with $T_S > 0$ being the sample time representing the fixed interval used to collect the data in the data-set. Obviously the smaller the sample time more information is collected from the environment and hence the resolution of signals will be better. In discrete time the signals are represented as ordered set of values like $x_d(k)$ where $x_d : Z^+ \to \mathbf{R}$. Connection between continous time and discrete time models is $t = kT_S$.

For system analysis and design it is convenient to represent information about signals in frequency domain with the help of Fourier transform

$$X(j\omega) = \mathcal{F}(x(t)) = \int_{-\infty}^{\infty} x(t)e^{-j\omega t}dt \tag{5.17}$$

which represent the signals as linear combination of periodic signals $e^{-j\omega t}$. We can use equivalently Laplace transform $X(s)$ where $s = \sigma + j\omega$ and basis signals are e^{-st} with σ being a damping. So each signal can be represented either in temporal or frequency domain. The information content in a particular signal depend on the sampling frequency F_S. The higher the sampling rate the higher the information content.

5.9 Apply Methodology to Random Feeder

Figure 5.6 shows a layout of simple power system with three test nodes V_1, V_2 and V_3. At V_1 we have the power generator which is modeled as an ideal sinusoidal source. Voltages V_2 and V_3 are applied at two lagging loads are simulated rated at 2.3 kV, respectively consuming 200 kVA and 100 kVA with lagging power factors of 0.9 and 0.8. In the example network we have modeled the impedance of the power lines denoted as $Z_{L,1} = Z_{L,2} = 0.44 + j0.69$. Also in Figure 5.6 you can see a power flow diagram where we have substitution node, and the branching nodes V_2 and V_3. With S_1 and S_2 we have denoted the active power transmitted over the transmission lines and with $S_{2,L}$ and $S_{3,L}$ we have denoted the the power flow through both loads.

Table 5.1: System parameters

Circuit Parameter	Nameplate Values	Operating Values
V1	2400	N/A
V2	2300	$2298.88\angle -1.07°$
V3	2300	$2265.08\angle -1.57°$ V
I1	$86.96 \angle -6.84°$ A	$86.916\angle -37.94°$ A
I2	$43.47\angle -25.87°$ A	$42.82\angle -7.41°$ A
S1	200 kVA	199.73 kVA
	@0.8 pf lagging	@0.8 pf lagging
S2	100 kVA	96.99 kVA
	@0.9 pf lagging	@0.9 pf lagging

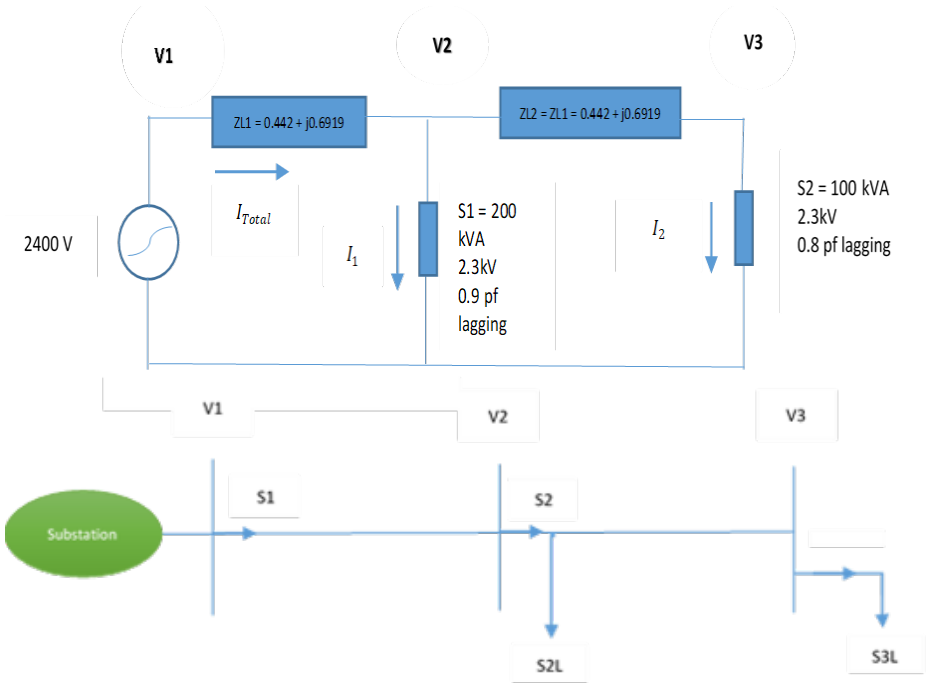

Figure 5.6: Apply Methodology to Random Feeder

In the table 5.1 we have summarized the numerical parameters of the power system for the examined electrical steady state. Due to reactive loads in nodes 2 and 3, the voltages V_2 and V_3 are with phase delay with respect to voltage at V_1. The table also compares the nominal load values and operating steady state values calculated during simulation.

In a real situation the loads of the system at nodes 2 and 3 will not be fixed and will vary depending on seasonal or daily basis. The actual nature of the load profile is predictable and this can be foretasted to a certain degree. Thus we cannot say exactly what will be values as inevitably there exist some uncertainty. Table 5.2 presents simulation results for varying loading in nodes 2 and 3 from 0 to 110%.

5.9.1 Model Order Reduction

In the above example we have examined a simple system model which can be analysed with various methods - analytic, numerical simulation, vector diagrams and others. However for large scale systems which contains thousands of nodes solution

Table 5.2: Power profile variation

% Load	V1 (kV)	V2 (kV)	V3 (kV)	P1	P2	P3	Q1	Q2	Q3
0	2.4	2.3672	2.3672	0	0	0	-0.4	-0.2	-0.1
20	2.4	2.3621	2.3578	50	50	18	33	33	9
40	2.4	2.3569	2.3483	100.4	100.3	36.1	65.8	65.9	17.5
50	2.4	2.3544	2.3435	126.6	125.4	45.1	82.5	82.5	21.9
75	2.4	2.3479	2.3315	188.9	188.4	67.7	124.7	124.4	33
100	2.4	2.3413	2.3193	252.3	251.7	90.4	167	166.6	44
105	2.4	2.34	2.3169	265.1	264.4	95	176	175.1	46.3
110	2.4	2.3387	2.3144	277.8	277.1	99.5	184.7	183.6	48.5

of the respective system of equations is still possible but due to the large number of variables it might be difficult for the designer to grasp the general properties of the investigated system - like stability, resonances, settling time and others. In order to obtain such economical as mathematical formula description we have to inevitable apply some approximation technique, also known as model reduction. The model reduction and approximation theory is very large and highly developed field. Generally there are two approaches for order reduction - theoretical and experimental. The theoretical approach relies on first obtaining the full analytical model of the large scale system and then using various methods like balanced state space realization to exclude the low energy states. Another approach is to apply test signals to the system and describe its input-output behavior with a approximate model.

Such model reduction is closely related to System Identification, cf. Section 4.3. It is therefore interesting to follow convexification attempts for model order reduction problems, see Souet al. (2008), and see if they have implications on system identification loss function formulations.

System identification is really system approximation. We attempt to find a model of acceptable accuracy from data, and the resulting model is by necessity an approximation of the true description. This means that the topics of model reduction and model approximation are closely related to identification. Now, model reduction is in itself a huge research area with a wide scope of application areas (e.g.

www.modelreduction.com). It could rightly have been listed as one of the communities around the core, Section 3, but it lacks the data-estimation component. It is true that a model reduction perspective has been in focus for some work in system identification, but I am convinced that the identification community could learn a lot more by studying the model reduction research - especially for nonlinear systems.

5.9.2 Linear Systems - Linear Models

Model reduction for linear models is quite well understood. Balanced realizations, Moore (1981), show how the different states contribute to the input-output map and are a rational ground for reducing the state dimension by projecting the state-space to certain subspaces. As noted in the original contribution this is pretty much like Principal Component Analysis (PCA) in linear regression (and related to how the state space is selected in subspace methods, cf. Section 4.2). Linear model reduction can be a very useful tool in system identification (cf. the command balred in the System Identification Toolbox, Ljung (2007)), for example when concatenating single-output models to a bigger model. My impression is, though, that this possibility is much underutilized.

5.9.3 Nonlinear Systems - Linear Models

The situation becomes much more difficult and interesting when we want to approximate a nonlinear system with a linear model, (which is typically what happens in practice when you build linear models.) Certain issues are well understood, like what is the linear second-order equivalent to a nonlinear system, Ljung (2001), but the results can be surprising as seen from the following example (Enqvist, 2005):

Example Consider the static and (slightly) nonlinear system

$$y(t) = u(t) + 0.01u_3(t) \tag{5.18}$$

For a certain (non-Gaussian and bounded) input, its linear second order equivalent

is dynamic with a Bode plot as shown in Figure 5.8. It has a very high gain for low frequencies, and is very different from the Bode plot obtained by just ignoring the small nonlinear term. It is this linear model with the strange low frequency gain that an output error identification method will produce for data from (19). Such investigations of nonlinear systems that are "perturbations" of linear ones are also carried out by Schoukens, Pintelon and coworkers, e.g. Schoukens et al. (2003)

5.9.4 Nonlinear Systems - Nonlinear Models

The most challenging problem is when we would like to approximate a nonlinear system with a simpler nonlinear model. For effective identification of nonlinear models, this is a topic which must be understood. There is a quite extensive literature on this problem, but this is not the place to provide a survey of that. Let it suffice to note that among the approaches we see (1) linearization followed by reduction of the linear model, with its states fed back into the nonlinear model, (2) mimicking the balanced realization thinking in terms of contributions to observability and controllability, Scherpen and Gray (2002), and (3) various nonlinear Galerkin methods (truncations of function expansions). There also exist some Matlab packages for nonlinear model reduction, e.g. Sun and Hahn (2006).

BodePlot - Magnitude and Phase of Bus 1

Figure 5.7 shows the frequency responses of the bus 1 voltage with respect to input power. The important frequency range for system dynamics is from 0.3 to 2.5 rad/sec which indicates potential instability and large peaks. Another observation is that the 30th order transfer function can be reduced to more manageable 10th order system with less than 1dB absolute error.

Table 5.3: Estimated transfer functions from experimental data P_1,P_2,P_3 - active power inputs, Q_1,Q_2,Q_3 - reactive power inputs, V_1 - output signal

Input, Output Data	5 Poles and 4 Zeros, Transfer Function	Model Validation Fit, 5 Pole & 4 Zeros (%)
V1, P1	$\text{TF1} = \frac{2.486 * s^4 + 50.13 * s^3 + 10.37 * s^2 + 72.64 * s - 6.446}{s^5 + 0.9038 * s^4 + 3.466 * s^3 + 2.675 * s^2 + 0.2819 * s + 0.01427}$	100%
V1, P2	$\text{TF2} = \frac{15.11 * s^4 - 11.73 * s^3 + 91.69 * s^2 - 66.71 * s + 19.05}{s^5 + 2.371 * s^4 + 5.839 * s^3 + 6.709 * s^2 + 3.698 * s + 4.977e^{-09}}$	87.86%
V1, P3	$\text{TF3} = \frac{0.5678 * s^4 + 15.7 * s^3 + 16.14 * s^2 + 24.73 * s + 7.281}{s^5 + 1.424 * s^4 + 3.758 * s^3 + 4.468 * s^2 + 0.723 * s + 0.324}$	89.98%
V1, Q1	$\text{TF4} = \frac{4.88 * s^4 + 14.07 * s^3 + 28.87 * s^2 - 1.072 * s + 4.842}{s^5 + 0.7093 * s^4 + 3.752 * s^3 + 1.947 * s^2 + 0.7355 * s + 0.08243}$	97.63%
V1, Q2	$\text{TF5} = \frac{1.02 * s^4 + 32.85 * s^3 + 3.536 * s^2 + 46.74 * s - 22.52}{s^5 + 1.321 * s^4 + 3.825 * s^3 + 4.476 * s^2 + 1.236 * s + 2.528e^{-09}}$	76.55%
V1, Q3	$\text{TF6} = \frac{5.626 * s^4 + 1.934 * s^3 + 16.77 * s^2 + 1.149 * s + 2.077}{s^5 + 2.366 * s^4 + 3.642 * s^3 + 6.488 * s^2 + 1.642 * s + 0.0003083}$	94.52%

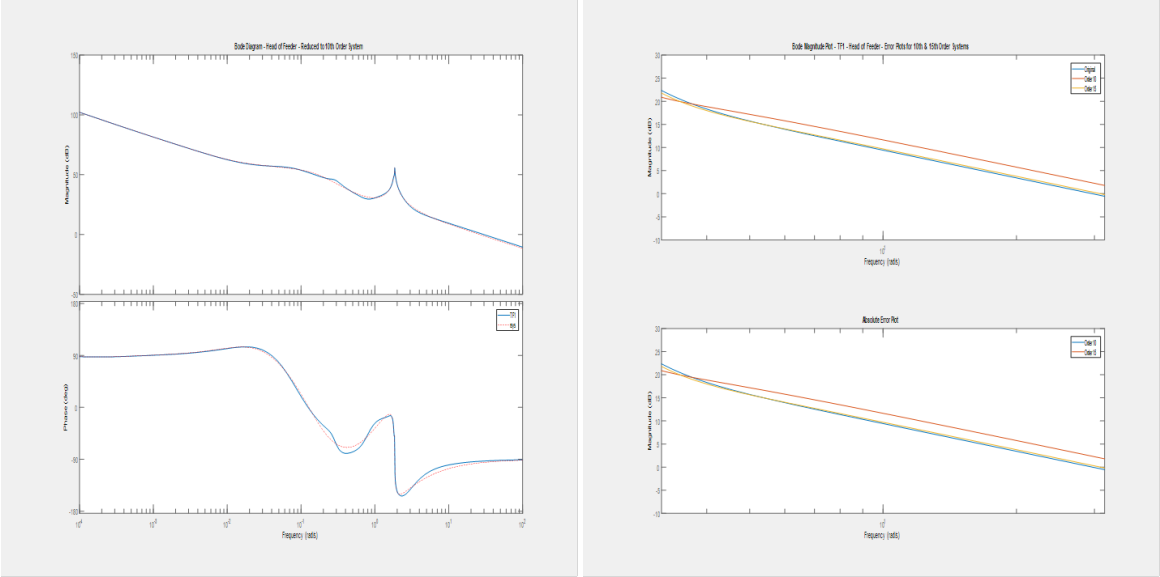

Figure 5.7: BodePlot - Magnitude and Phase of Bus 1

BodePlot - Magnitude and Phase of Bus 2

Figure 5.8 show the frequency response of the bus 2 voltage with respect to the input power. There the focus region is between 0.3 to 2.5 rad/sec where can be observed oscillatory behaviors and large peaks. Again the 30th order transfer function is reduced to more manageable 10th order system with less than 1dB absolute error.

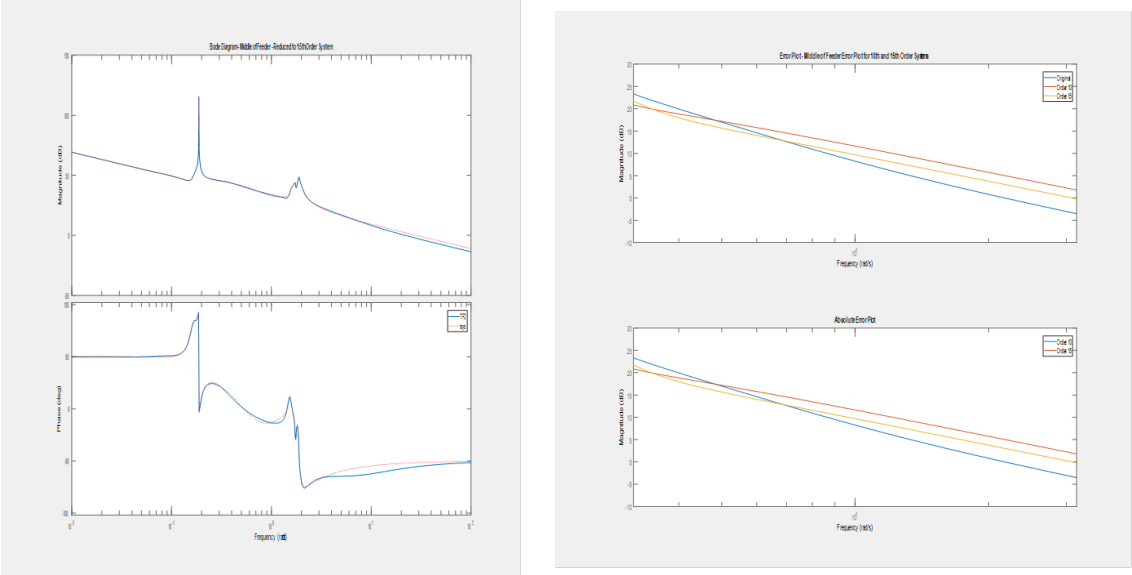

Figure 5.8: BodePlot - Magnitude and Phase of Bus 2

BodePlot - Magnitude and Phase of Bus 3 Again from the Bode plot of frequency response in bus 3 voltage in Figure 5.9 focus region is 0.3 to 2.5 rad/sec where oscillatory behavior and large peaks are demonstrated and 30th order transfer function can be reduce to more manageable 10th order system with less than 1dB absolute error

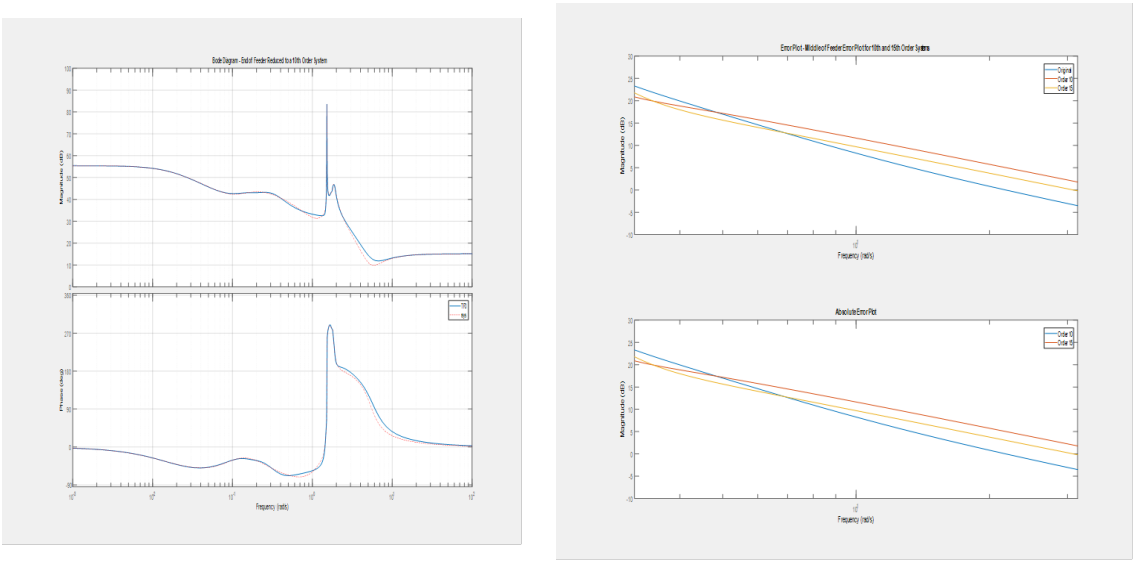

Figure 5.9: BodePlot - Magnitude and Phase of Bus 3

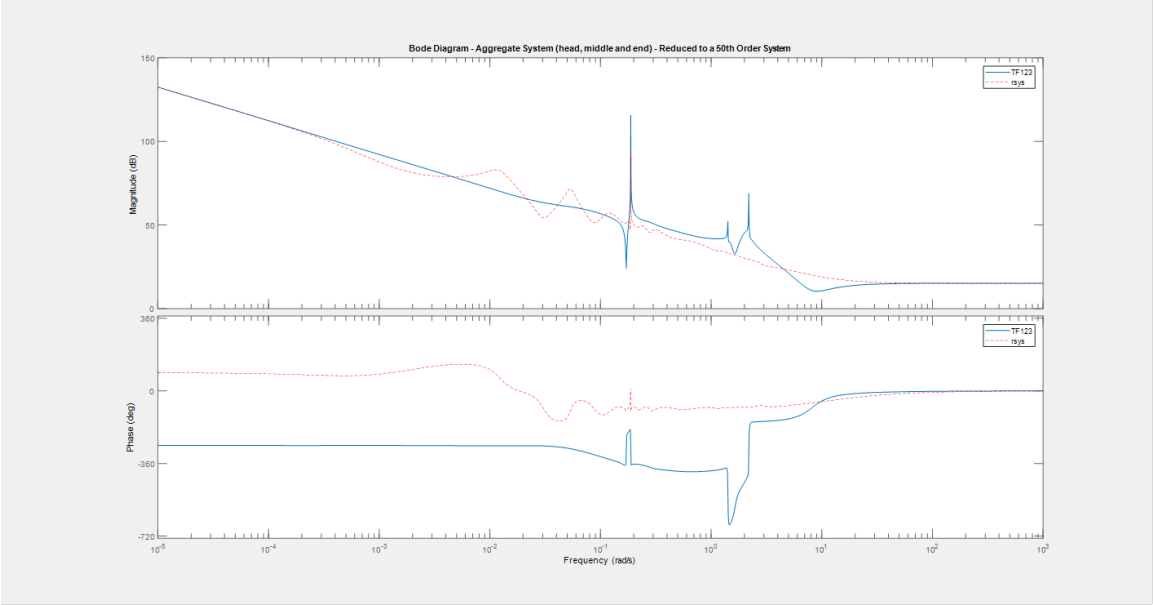

Figure 5.10: Bode Plot - Magnitude and Phase of Composite System

Frequency response diagrams for an example 90th order system are presented in Figure 5.10. There you can see several larger magnitude peaks over an extended range of frequencies. The focus region is similar to system response in other systems at lower frequencies. This 90th order system can be reduced to more manageable 50th order system without considerable loss of accuracy.

5.10 Summary

In this chapter sensitivities were performed around system response to perturbations for a radial power network are investigated. Voltage response was evaluated at the critical head, middle and end nodes of the feeder. A step by step methodology for system identification was presented where dynamical models can be constructed from observed input and output data. An important feature of dynamical systems is that past data can be predictive of future system response. The resulting approximate models from the system identification process is shown to be valuable in simulations, and controller design. System Identification can also be used to identify controllability and observability matrices. In the next chapter 6, we leverage the design methodology and system identification to test a novel framework to understand the effects of DERs on power system voltage at various penetration levels and under both normal and extreme system conditions. A search for simple numerical representations via system identification theory will be undertaken. The system identification methodology is applied to a random power network. The process of model order reduction is undertaken to optimize first pass developmental models. Briefly we revisit linear and nonlinear principles before developing our transfer function models. We use Bodeplot, magnitude and phase data to critically analyze and validate our models. Lastly in section 6.3 we apply the framework to understand the effects of DER on power system voltage to a much larger systems. The steps to derive the models used on the test systems are then repeated to to validate the propose framework on a larger scale. Chapter 5 proves that parametric models of power networks can be developed

and used to predict the effects of DERs on voltage. Critical to the specific contributions of this work are the development of framework to develop and validate models from power networks for use in every day planning at the utility. Secondly, this work established a framework for developing aggregated transfer function parametric models based on System Identification. Last an thirdly this work create a framework to understand the effects of DERs on power system voltage at varied DER penetrations levels and under different system operating conditions.

CHAPTER 6: APPLICABILITY OF THE PROPOSED APPROACH ON A LARGE SCALE REAL-LIFE FEEDER

The purpose of this chapter is to apply a methodology for investigation of a complex power grid system with DERs and dynamic loading profiles [20]. The problem with real-world power grids is their large dynamic order and uncertain load variations. Hence this chapter aims to approach this by searching for simple numerical representations by applying techniques from system identification theory[21]. The benefit of obtaining a simple or reduced order model of the power system is the insight for long term systematic properties - like steady state gain, dominating dynamical modes, resonance frequencies, phase delays, etc. Various model structures can be applied to this problem which generally fall into two large categories described as linear and nonlinear models [22]. The linear models have well recognized properties by larger scientific community and allows easier generalization and analysis. However these are only local approximations of the system which are valid only for a particular operating region. When the deviations from the operating point are larger then approximation accuracy degrades. The nonlinear models are better approximation of the real system, but they require individual mathematical treatment which is only effective if the nonlinear model is correctly estimated [23]. The estimation of the linear models on the other hand is faster and easier to verify and better fit for a practical applications. Chapter 6 endeavors to demonstrate that parametric models of power networks can be developed and used to predict the effects of DERs on voltage on large scale power systems. Chapter 6 is critical to the specific contributions of this work in the development of a framework to identify and validate models from power networks for use in every day planning at the utility. Secondly, this work establishes

a framework for developing aggregated transfer function parametric models based on System Identification [24, 25]. Last and thirdly this work creates a framework to understand the effects of DERs on power system voltage at varied DER penetrations levels and under different system operating conditions.

6.1 Introduction

One critical consideration when analyzing a three phase electric power delivery system is the issue of phase balance. Changes in single phase loading can cause load currents in phase conductors to be mismatched causing the phase voltages to become unbalanced [18]. In most cases the maximum voltage unbalance occurs at or near the end of the feeder. The actual amount of unbalance is a function of how well the single phase loads are balanced across the system on single-phase and double phase take-offs. The effects of an unbalanced system are many. For example, when three-phase motors receive an unbalanced voltage source, the imbalance causes negative sequence currents to circulate in the motor creating heat losses in the rotor. More severe effects occur when one phase is opened and the motor operates on single-phase power creates a temperature rise causing overheating and loss of life. The American National Standards for Electric Power Systems and Equipment, ANSI C84.1, recommends that "electric supply systems should be designed and operated to limit maximum voltage unbalance to 3 percent ..." According to the IEEE Red Book, IEEE Std 141-1993, Recommended Practice for Electric Power Distribution, the severity of voltage unbalance is determined as follows:

$$PercentVoltageUnbalance = 100 \times \frac{MaximumVoltageDeviation}{AverageVoltage} \tag{6.1}$$

Example:

Assume the following phase-phase voltages are measured on a feeder at any given

point: $A = 125\text{V}$, $B = 118\text{V}$ and $C = 114\text{V}$

$$AverageVoltage = \frac{125V + 118V + 114V}{3} = 119V \tag{6.2}$$

$$MaximumVoltageDeviation = 125V - 114V = 11V \tag{6.3}$$

$$VoltageUnbalance = 100 \times \frac{11V}{119V} = 9.24\% \tag{6.4}$$

In the example above, the phase voltage unbalance is 9.24% exceeding ANSI C84.1. Even with the known effects of an unbalanced systems, it is unrealistic to expect perfect balance and in reality perfect balance can never be achieved [17]. Typically, most utilities perform annual or seasonal balancing where single-phase taps are moved between phases to better balance the system. In the example above, the planning engineer would take the necessary steps to have load moved from the heavy loaded phase-C at 114 Vto the lightly loaded phase A.

Thus in this research it is assumed that the system is balanced in the steady-state. Additionally, utility scale DER plants added to the system are assumed to be added as a three-phase balanced supply in concert with the assumption of a three phase balanced system. While not a perfect assumption, the assumption is consistent with how electric distribution systems operate in practice by continuously balancing and re-balancing the system, and more realistic like actual field conditions.

In addition, another critical point to mention in this research is the area of stability for which we are performing the current research. The parametric models that will be developed with a focus on voltage stability of the power system as shown in the figures presented in subsequent sections. More specifically, small signal voltage stability similar to the voltage effects that a PV injections could have on the power system. Furthermore, the stability of the parametric models is not synonymous with the stability of the power system. When analyzing the parameters of the transfer function or parametric model, what we see in the phase and gain margin of the Bode

diagram is necessary to showcase the stability and validity of the derived model. To drive home the point, in a 60 HZ system one would expect to see around 380 rad/sec and in order to capture such frequency in a model the sampling frequency would need to be at least 1000 rad/sec which means a sample time of 0.001s or 1 millisecond. The data used in this research is typical 15-minute power system load, voltage and current data, and thus the instant research is squarely concerned with model accuracy and not power system frequency.

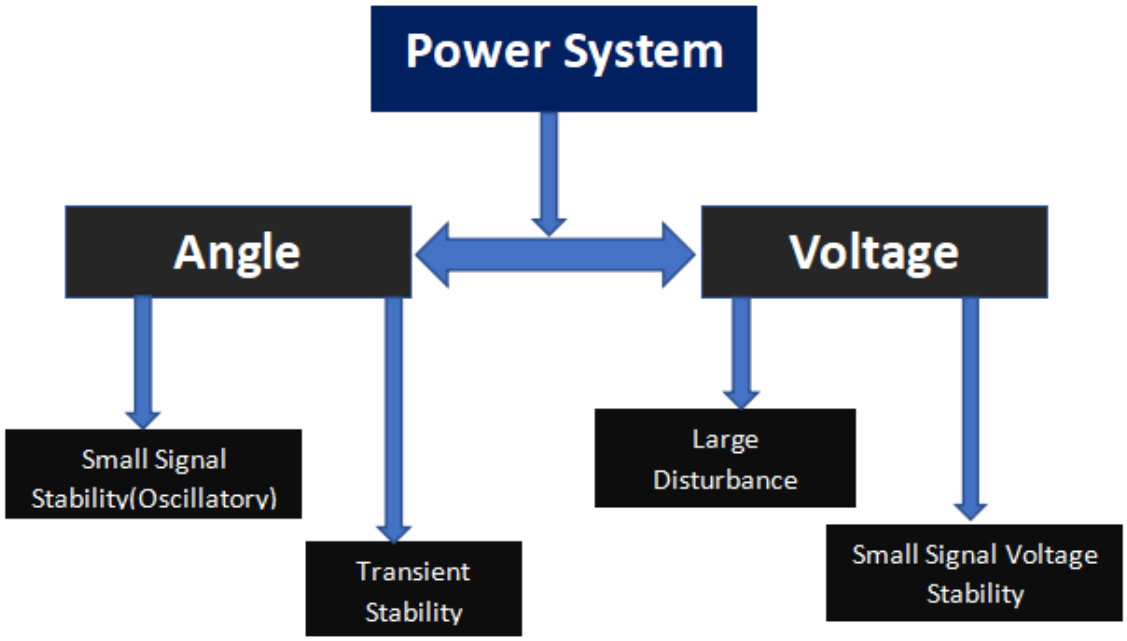

Figure 6.1: Fundamental power system parameters

6.2 Larger System - Applying Design and Implementation Methodology

The 11 step System Identification methodology developed in the previous chapter is useful in extracting information about a dynamic distribution system from measured input-output data [21]. Resulting models developed were used to understand the behavior of a small 300kVA power system modeled in Power Flow consisting of 8 nodes and 3 buses. The methodology could be further tested and thus applied to an 3000 node system:

- to analyze how a real distribution system will respond to step changes in power simulated by PV generation being added to the system
- further test system response to sensitiviteis in changes in active and reactive powers
- evaluate global dV/dP, dV/dQ across a feeder to understand system response as active and reactive power changes

Table 6.1 summarizes the parameters of the investigated example system to be investigated. Total load in the system is 10.17 GW, with power factor of 0.967, the total connected load is 13.7MVA, number of nodes is 3109 and number of residential loads is 4653. A 10kW PV plant is currently connected to the system [17]. The architecture of the system under investigation is illustrated at Figure 6.2 where the geographical extent of the system is evident. As widely known the main challenge with photo voltaic supported system is increased uncertainty due to cloud and weather dependence. This uncertainty can lead to oscillations of the node voltages and hence lead to power grid instability in an extreme case which is highly undesirable. Hence PV dependent system have to be extensively investigated with respect to their dynamic properties.

Table 6.1: System Data- Larger System Applying Design and Implementation Methodology

Total load kW	10,169	Total load kVAR	425.6
load PF %	96.70	Total KVA	13735.6
Feeder Load Factor %	41.00	Total load as a % of peak load	12.10
Number of Nodes	3109	Soruce Voltage	24kV
Spot Loads (C&I) %	875.00	Residential Loads	4653
PV Systems (1)	10kW		

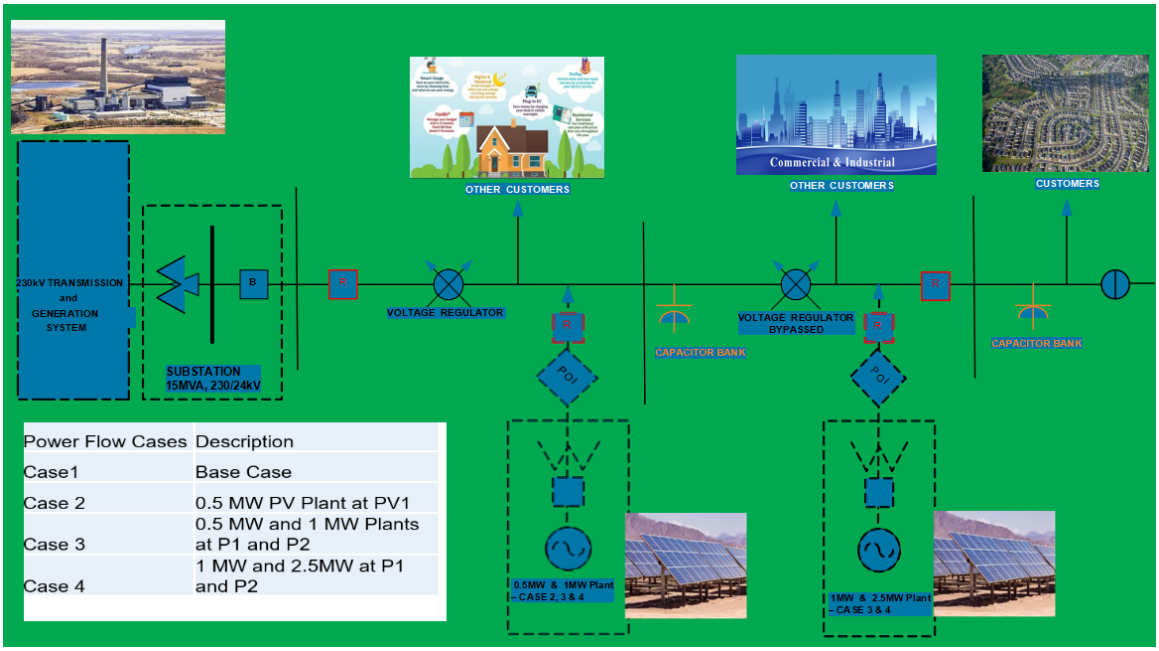

Figure 6.2: 24kV Feeder System Under Study

Static Gain Model

The static gain model for the system corresponds to the steady state of the system when $t \to \infty$. Usually system investigation from behavior point of view begins with identification of a static gain model which gives a general practical view of the plant under investigation [26]. The static gain is defined as a system gain after the transients settle. The resultant input-output characteristic of the plant is the first tool to judge the linearity of the system. If the static characteristic is nonlinear (curved, non one-to-one, discontinuous, saturated, etc.) then the dynamic plant would be nonlinear too. Generally each plant has partly linear and partly nonlinear behavior. Hence the black-box identification approach logically begins with determination of the best linear estimator (BLE) for the plant. After that the remaining nonlinear effect can be accounted for either as uncertainty in the linear model characteristics (confidence bounds, probability distributions, range of validity) or by incorporation of nonlinear blocks into system structure. In this regard the first effort is to try to introduce only static nonlinear block into system making it Hammerstein-Wiener kind or if that is

Table 6.2: Real Values - Larger System Applying Design and Implementation Methodology

Monitored nodes (head, middle and end)	Distance from source	V1-Low Side Trans-former	V1-High Side Trans-former	V2-middle	V3-end	P1-head	Q1-head	P2-middle	Q2-middle	P3-end	Q3-end
SOURCE_03552401, 33197005, 33206894, 33213672)	0	126.7	126.7	121.9	121.8	1648	-1175	714	87	61	10
SOURCE_03552401, 33197005, 33206894, 33213672)	7882.5	126.7	126.7	121.9	121.7	1813	-1129	785	106	67	12
SOURCE_03552401, 33197005, 33206894, 33213672)	16371.5	126.7	126.7	121.8	121.7	1977	-1084	856	125	73	13
SOURCE_03552401, 33197005, 33206894, 33213672)	25913	126.7	126.7	121.8	121.6	2141	-1039	927	144	78	15
SOURCE_03552401, 33197005, 33206894, 33213672)	27352.9	126.7	126.7	121.7	121.6	2310	-998	1000	164	85	17
SOURCE_03552401, 33197005, 33206894, 33213672)	39449.8	126.7	126.7	122.3	121.6	2480	-957	1073	183	91	18
SOURCE_03552401, 33197005, 33206894, 33213672)	43988.3	126.7	126.7	122	122.5	1149	-1174	217	92	-438	16
SOURCE_03552401, 33197005, 33206894, 33213672)	44911.8	126.7	126.7	122.1	122.6	650	-1171	-282	97	-438	16
SOURCE_03552401, 33197005, 33206894, 33213672)	44911.9	126.7	126.7	123.3	128.7	-3995	-1276	-4473	-72	-5362	601

Table 6.3: Per Unit Values - Larger System Applying Design and Implementation Methodology

monitored nodes (head, middle and end)	Distance from source	V1-Low Side Trans-former	V1-High Side Trans-former	V2-middle	V3-end	P1-head	Q1-head	P2-middle	Q2-middle	P3-end	Q3-end
SOURCE_03552401, 33197005, 33206894, 33213672)	0	1.0558	1.0558	1.0158	1.015	16.48	-11.75	7.14	0.87	0.61	0.1
SOURCE_03552401, 33197005, 33206894, 33213672)	7882.5	1.0558	1.0558	1.0158	1.01417	18.13	-11.29	7.85	1.06	0.67	0.12
SOURCE_03552401, 33197005, 33206894, 33213672)	16371.5	1.0558	1.0558	1.015	1.01417	19.77	-10.84	8.56	1.25	0.73	0.13
SOURCE_03552401, 33197005, 33206894, 33213672)	25913	1.0558	1.0558	1.015	1.013	21.41	-10.39	9.27	1.44	0.78	0.15
SOURCE_03552401, 33197005, 33206894, 33213672)	27352.9	1.0558	1.0558	1.01417	1.013	23.1	-9.98	10	1.64	0.85	0.17
SOURCE_03552401, 33197005, 33206894, 33213672)	39449.8	1.0558	1.0558	1.01917	1.013	24.8	-9.57	10.73	1.83	0.91	0.18
SOURCE_03552401, 33197005, 33206894, 33213672)	43988.3	1.0558	1.0558	1.017	1.0208	11.49	-11.74	2.17	0.92	-4.38	0.16
SOURCE_03552401, 33197005, 33206894, 33213672)	44911.8	1.0558	1.0558	1.0175	1.0217	6.5	-11.71	-2.82	0.97	-4.38	0.16
SOURCE_03552401, 33197005, 33206894, 33213672)	44911.9	1.0558	1.0558	1.0275	1.0725	-39.95	-12.76	-44.73	-0.72	-53.62	6.01

not enough then apply nonlinear dynamic model such as Volterra series or nonlinear networks [23]. The advantage of the Volterra series is that non-linear output depends on temporal inputs, retaining attributes of the system dynamics. However, obtaining these elevated as complexity nonlinear models is bound to collecting a richer and more complex data from the plant under investigation which practically is not always feasible or economically justified. Moreover many of the plants and systems in the power industry are engineered to primarily demonstrate linear (or in simple words intuitively anticipated) behavior in their function so the approach with linear models in their identification is well motivated. The problem with practical systems is their high number of system elements hence it is difficult to grasp the complete mathematical model by just writing the individual equations for the elements. Therefore system identification models offer simplified relationships which are justified from statistical point of view where the static characteristics give the information about correlation dependence between the selected input and outputs [27]. For the case of the power system the static gain model will show the correlation between input power terms and output voltages.

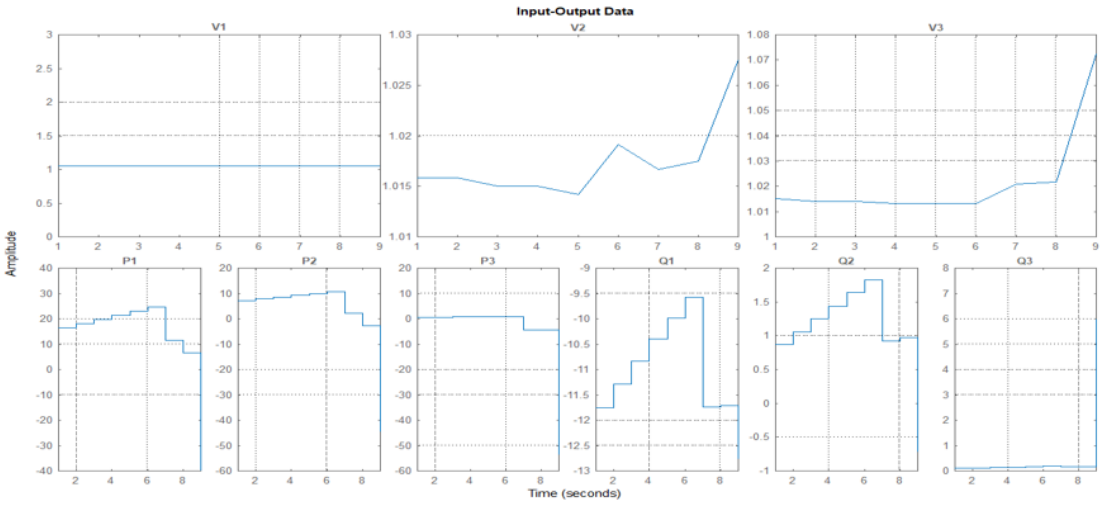

Figure 6.3: Identification data-set (Normalized quantities)

Figure 6.3 shows the identification data-set which is obtained by experiment with

the full power grid system. There are selected active power terms P_i and reactive power terms Q_i as inputs where $i = 1..3$ is the node index. And V_i represent respective node voltages. The static gain model is obtained with estimation of a linear model from the collected experimental data in normalized units. In this model the voltage V_1 depends on P_m and Q_n as below. Q_n and P_m are the active and reactive powers at each bus.

$$V_1 = 0.0358P_1 - 0.0365P_2 + 0.00093P_3 - 0.0642Q_1 - 0.0313Q_2 + 0.0101Q_3. \quad (6.5)$$

From equation 6.5 one can see the highest correlation is with P_1, P_2, Q_1 and Q_2 terms. Hence a long term increase in P_1, such as the addition of a solar plant, will lead to around 3.5 % increase in V_1. Also there is a negative correlation between V_1 and P_2, or when P_2 average value increases then V_1 will drop about 3.7 %. Similarly we have equations for voltage across the entire system such as:

$$V_2 = 0.0975P_1 - 0.1016P_2 - 0.00106P_3 - 0.03924Q_1 - 0.3666Q_2 - 0.0737Q_3 \quad (6.6)$$

and

$$V_3 = 0.0367P_1 - 0.0376P_2 + 0.000303P_3 - 0.0611Q_1 - 0.04202Q_2 + 0.00468Q_3. \quad (6.7)$$

6.2.1 ARX Model

After estimation of the model static characteristics we can proceed with obtaining a dynamical model to fit the temporal dynamics of the data-set [24, 25, 27]. There are many possible ways to estimate such a dynamic model. As noted in the introduction about system identification the models are either continuous or discrete time representations. This section presents the estimated ARX model from data-set in figure 6.3. The resulting model is given by following vector-matrix equation.

$$\begin{pmatrix} V_1(t) \\ V_2(t) \\ V_3(t) \end{pmatrix} = \begin{pmatrix} 1 & 0 & 0 \\ 0 & 0.082 & 0 \\ 0 & 0 & 0.903 \end{pmatrix} \begin{pmatrix} V_1(t-T_S) \\ V_2(t-T_S) \\ V_3(t-T_S) \end{pmatrix} + \begin{pmatrix} \xi_1(t) \\ \xi_2(t) \\ \xi_3(t) \end{pmatrix} \tag{6.8}$$

where $\xi_1(t) = 0$ due to fixed voltage at node 1 during the numerical Power Flow simulation,

$$\xi_2(t) = 0.095P_1 - 0.1P_2 - 0.001P_3 - 0.034Q_1 - 0.368Q_2 - 0.075Q_3, \tag{6.9}$$

and

$$\xi_3(t) = -0.002P_1 + 0.003P_2 - 0.003P_3 - 0.008Q_1 + 0.023Q_2 - 0.001Q_3. \tag{6.10}$$

6.2.2 State-space Model

Alternative model to ARX estimation is as was presented above the state-space representation [28]. Discrete-time linear grey-box model in matrix vector representation is

$$\begin{cases} x(t+T_S) = Ax(t) + Bu(t) \\ y(t) = Cx(t) + Du(t) + e(t) \end{cases}, \tag{6.11}$$

where $x(t)$ is hidden system state, $u(t) = (P_1, P_2, P_3, Q_1, Q_2, Q_3)^T$ is vector of input signals, $y(t) = (V_1, V_2, V_3)^T$ is vector of output signals. The input and output vector might be different as variables depending on the goals of the analysis we want to convey. The $A \in \mathbf{N} \times \mathbf{N}$, $B \in \mathbf{N} \times \mathbf{N_u}$, $C \in \mathbf{N_y} \times \mathbf{N}$ and $D \in \mathbf{N_y} \times \mathbf{N_u}$ are matrices of appropriate dimensions where N is the state space dimension, N_y is output space dimension and N_u is input space dimension. In the concrete example $A = 0.3988$,

$$B = (4.35, 4.35, 4.35, 4.35, 4.35, 4.35) \times 10^{-4}, \tag{6.12}$$

the output matrix C is

$$C = (1.239, 0.09823, 1.015)^T, \tag{6.13}$$

and input-output correlation matrix

$$D = \begin{pmatrix} 2.9 & -3.3 & 0.9 & -6.8 & -0.5 & 6.8 \\ 9.8 & -10.1 & 0 & -3.9 & -36.7 & -7.1 \\ 3 & -3.4 & 0.6 & -6.5 & -1.6 & 4.6 \end{pmatrix} \times 10^{-2} \tag{6.14}$$

Static Gain for ΔP_2 and ΔP_3

State space model as is like the all the dynamic model they contain information about the static gain of the system [28]. For the discrete state space model the static gain matrix is calculated with mapping the state space equation (6.11) in discrete Z-domain where $\mathcal{Z}\left(x(t+T_S)\right) = zx(z)$, with $z = e^{j\omega t}$. Hence after applying this transformation we get

$$y(z) = \left(C(zI - A)^{-1}B + D\right) \tag{6.15}$$

The steady state behavior of the system is obtained for $\omega = 0$ which makes $z = e^{j0t} = 1$ and the steady state matrix K_x becomes

$$K_x = C(I - A)^{-1}B + D = \begin{pmatrix} 0.03 & -0.03 & 0.01 & -0.07 & -0.01 & 0.07 \\ 0.1 & -0.1 & 0 & -0.04 & -0.37 & -0.07 \\ 0.03 & -0.03 & 0.01 & -0.06 & -0.02 & 0.05 \end{pmatrix} \tag{6.16}$$

To calculate static Gain of V_2 using Transfer Function for $\Delta P_2 = 10$ we have $\Delta V_2 = -0.1 \times 10 = -1$ and $\Delta V_3 = -0.03 \times 10 = -0.3$ or $\Delta V_2/\Delta V_3 = 3.33$ and $\Delta P_2/\Delta V_3 = -33$. For $\Delta P_3 = 10$ we have $\Delta V_2 = 0.0001 \times 10 = 0.001$ and $\Delta V_3 = 0.01 \times 10 = 0.1$ or $\Delta V_2/\Delta V_3 = 0.1$ and $\Delta P_3/\Delta V_3 = 100$.

V1, V2 and V3 Response from Active Power Inputs P1, P2 and P3

State space models are temporal models giving expressions for the hidden state

derivative in continuous time or for discrete difference in discrete time. However these models can be converted to frequency domain by taking respective representations of the derivative or discrete difference [22]. The model works like

$$V_3(t) = \mathcal{L}^{-1}\left(G\left(\mathcal{L}(P_1(t)), \mathcal{L}(P_2(t)), \mathcal{L}(P_3(t)), \mathcal{L}(V_2(t))\right)\right) \tag{6.17}$$

The transfer function is identified from experimental data sampled at 15 min intervals or 0.25 hours. The time domain for the whole model and figures are in hours. As a result from conversion from state space to frequency domain we get the following expressions for the V_1, V_2 and V_3

$$V_1(s) = \sum_{j=1}^{3}\sum_{i=0}^{4} \frac{b_{i,1,j}s^i P_j(s) + c_{i,1,j}s^i Q_j(s)}{s^5 + \sum_{i=0}^{4} a_i s^i}, \tag{6.18}$$

$$V_2(s) = \sum_{j=1}^{3}\sum_{i=0}^{4} \frac{b_{i,2,j}s^i P_j(s) + c_{i,2,j}s^i Q_j(s)}{s^5 + \sum_{i=0}^{4} a_i s^i}, \tag{6.19}$$

$$V_3(s) = \sum_{j=1}^{3}\sum_{i=0}^{4} \frac{b_{i,3,j}s^i P_j(s) + c_{i,3,j}s^i Q_j(s)}{s^5 + \sum_{i=0}^{4} a_i s^i}, \tag{6.20}$$

where polynomial in the denominator is the same for all the components and determine the stability and transient components driving the system behavior. Converted model parameters are presented in table 6.4. The parameters in the numerator of transfer functions are different for input signals P_i and Q_i and represent how these signals and their derivatives influence the respective voltages. Since the static gain for the system is obtain for $s \to 0$ it can be calculated from last column of the table.

Magnitude and phase frequency response of the system is plotted on Figure 6.4 for V_1 and also on Figures B.11 and B.12 for V_2, V_3. All bode plots share similar characteristics which are above zero for lower frequencies reaching 100dB and below zero dB for the higher frequencies. This behavior is typical for large scale systems. Also can be observed that the magnitude responses are very close for the separate

channels but the differences between them are into phase responses. From Figure 6.4 we see that responses for P_2 and Q_3 are negatively correlated to V_1.

Table 6.4: Transfer function model parameters obtained from state-space model

	s^4	s^3	s^2	s	1
a_i	2.668	2.307	0.8103	0.09961	-2.969×10^{-7}
V_1					
For P_1, $b_{1,1}$	0.1999	0.5613	0.3261	-0.002654	-0.02126
For P_2, $b_{1,2}$	-0.1617	-0.3064	0.3235	0.3821	0.07768
For P_3, $b_{1,3}$	0.4972	0.7735	-0.1959	-0.3275	-0.05224
For Q_1, $c_{1,2}$	-0.07876	-0.321	-0.385	-0.1371	-0.008561
For Q_2, $c_{1,3}$	-3.699	-8.428	-5.612	-1.328	-0.085
For Q_3, $c_{1,4}$	3.424	7.405	4.227	0.7783	0.0321
V_2					
For P_1, $b_{2,1}$	-0.4723	-0.9312	-0.2544	0.1132	0.03391
For P_2, $b_{2,2}$	0.4938	0.7556	-0.4304	-0.5915	-0.1239
For P_3, $b_{2,3}$	-0.03639	0.07859	0.5066	0.4018	0.08331
For Q_1, $c_{2,2}$	-0.1846	-0.3881	-0.1845	0.01065	0.01365
For Q_2, $c_{2,3}$	2.898	6.835	4.939	1.39	0.1356
For Q_3, $c_{2,4}$	0.2868	0.2821	-0.3725	-0.3106	-0.0512
V_3					
For P_1, $b_{3,1}$	-0.2158	0.6302	1.114	0.5015	0.06547
For P_2, $b_{3,2}$	0.3279	-2.31	-3.578	-1.647	-0.2392
For P_3, $b_{3,3}$	-0.1379	1.232	1.933	0.9666	0.1609
For Q_1, $c_{3,2}$	-0.09106	-0.1903	-0.02261	0.07873	0.02637
For Q_2, $c_{3,3}$	1.046	4.815	5.012	1.955	0.2618
For Q_3, $c_{3,4}$	-0.3036	-1.424	-1.798	-0.7688	-0.09886

Above are parameters of the transfer function numerator and denominator polynomials obtained from the state-space model to the frequency domain. It should be noted that as long as a single systems can be described with multiple state-space realizations, equivalent in their respective input and output behavior, there are different hidden states or linear combinations wherein the transfer function model is unique for the input-output behavioral pairs.

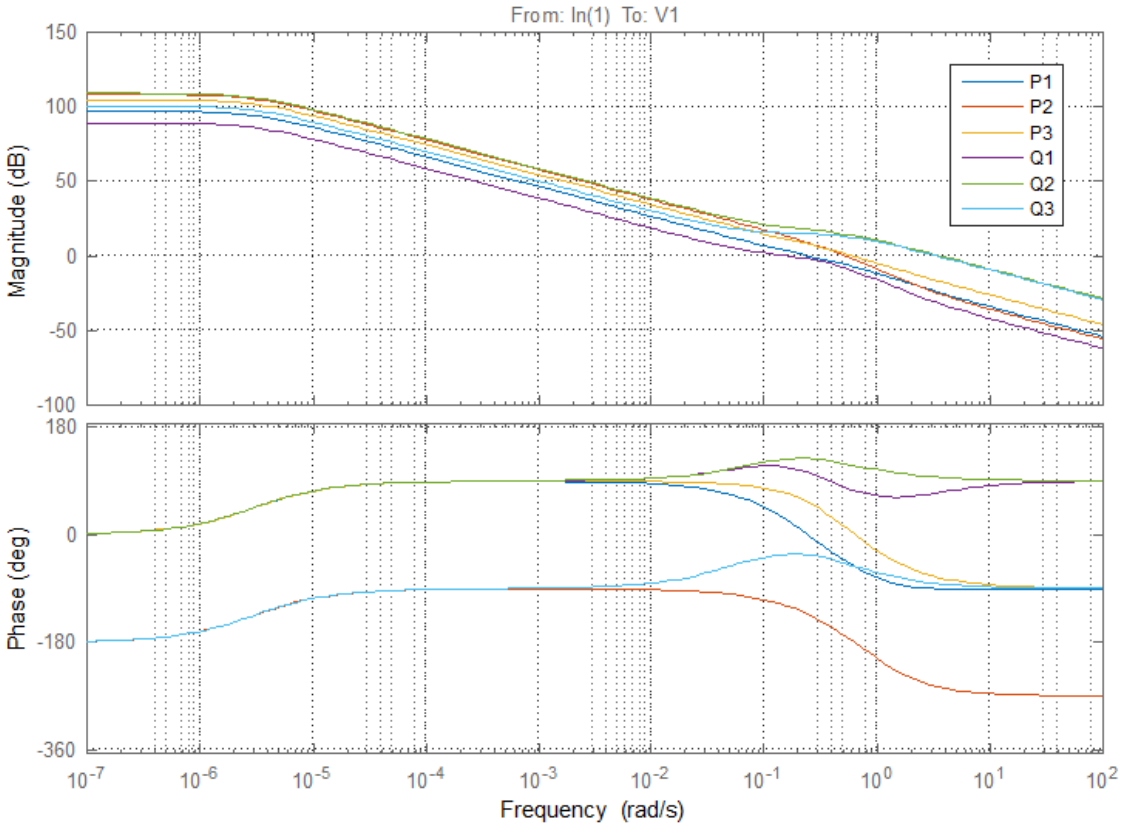

Figure 6.4: Magnitude and Phase Plot for V_1

However the selected inputs and outputs of the model are not necessary as we have them above - P_i and Q_i are inputs, V_i are the outputs. But for example we can estimate also transfer functions from V_2 to V_3

$$V_{32} = \frac{0.02322s^3 - 0.0156s^2 + 3.506s + 7.928}{s^5 + 0.1325s^3 + 0.06657s^2 + 21.52s + 7.847} \tag{6.21}$$

and from V_3 to V_2

$$V_{23} = \frac{0.08399 + 0.3508s^2 + 14.09s + 1.818}{s^5 + 0.01911s^3 + 0.1677s^2 + 0.9379s + 1.856} \tag{6.22}$$

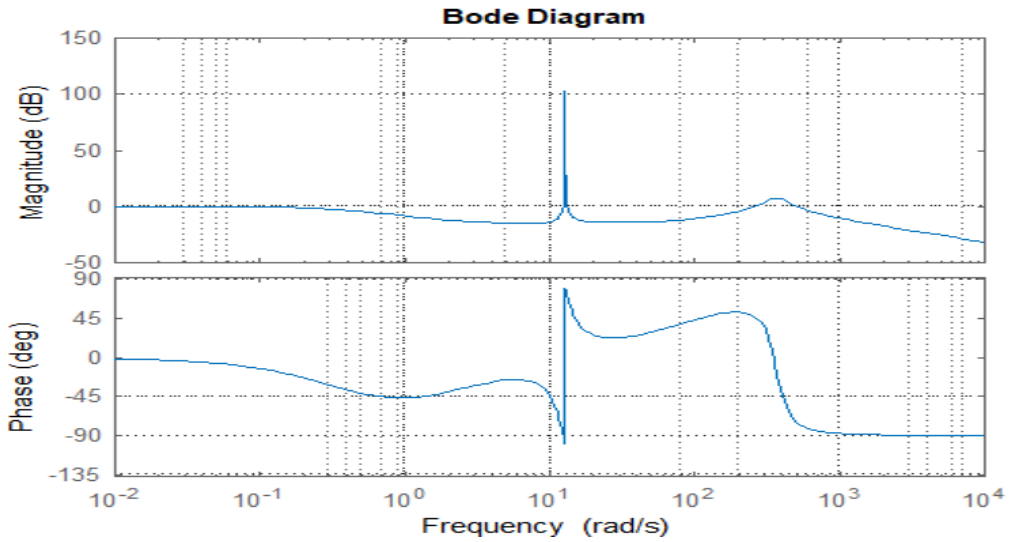

Figure 6.5: Transfer Function from input V_2 to V_3

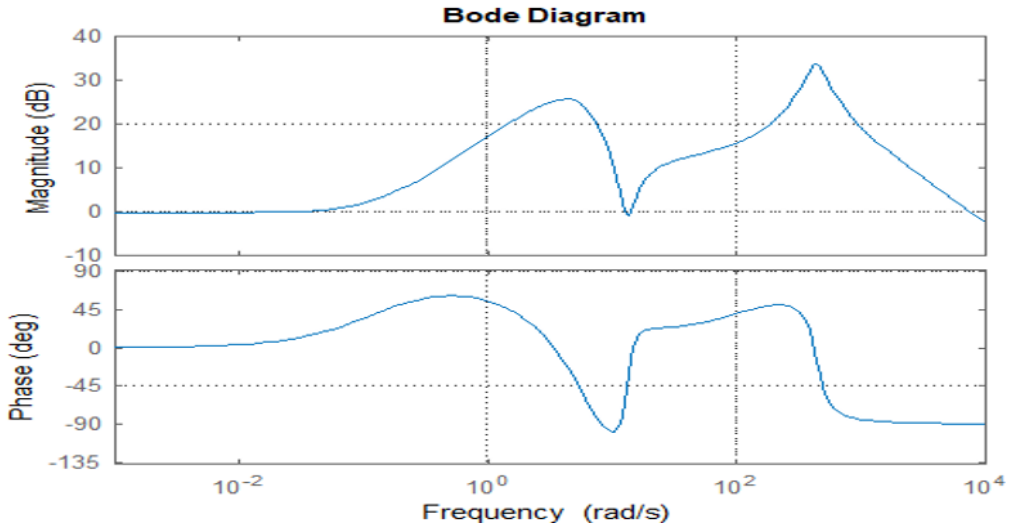

Figure 6.6: Transfer Function - V2 with V3 Input

The frequency domain responses of these transfer functions are presented on Figure

6.5 and 6.6. As can be seen the nature of these characteristics is more complicated due to strong resonance behavior.

From magnitude response for the transfer function V_{32} on figure 6.5 present narrow band resonance at 10 rad/sec which with height of about 100dB meaning amplification of 10000 times at that frequency. Considering the sharp increase in the phase response at that frequency we can conclude that this resonance is due to presence of complex zero pair in the transfer function numerator with large imaginary component. Another resonance appear at around 400 rad/sec, which due to decreasing phase is related to complex pole pair in the transfer function denominator.

In Figure 6.6 one can see that response for V_{23} transfer function is less aggressive compared to its inverse V_{32}. Again there are two resonances at 10 rad/sec and 400 rad/sec but they are highly damped.

Another model which can be estimated from data is for example a multiple input single output (MISO) model which represents the relation between the output voltage V3 and inputs P1,P2,P3 and V2. The advantage of this model is that we can obtain static gain correlation coefficient between V_3 and V_2.

$$
\begin{aligned}
V_3(s) = \frac{1}{s^5 + 0.28s^4 + 0.0227s^3}[& \\
& 0.0019s^4 P_1(s) + (0.00465s^4 + 0.001s^3)P_2(s) \\
& - (0.0021s^4 + 0.0012s^3)P_3(s) \\
& + (0.1128s^4 + 0.02494s^3 + 0.0015s^2)V_2(s)] \quad (6.23)
\end{aligned}
$$

Figure 6.7 presents the frequency response of the estimated model from P_1, P_2, P_3 and V_2 to V_3. On x-axis we have input harmonics frequency from 10^{-5} to 10 rad/s in logarithmic scale. On the top sub-figure we can see the magnitude frequency response which give the amplitude gain of the output sinusoidal signal. For linear models when

the input is sinusoidal at fixed frequency then the output is also sinusoidal at the same frequency. On the bottom sub-figure we present the phase delay between the input and output harmonics in degrees. The magnitude response $|P_1(j\omega)|$ is different as a structure compared to other inputs P_1, P_2 and V_2. There is a damping resonance at 0.3 rad/sec. Initially the characteristic for P_1 is above the P_2 and P_3 ones due to both differentiator block in this channel transfer function. However after 0.03rad/sec $|P_1(j\omega)|$ drops below the magnitude gains for P_2 and P_3 channels. The conclusion is that V_3 will be more sensitive to low frequency variation in P_1 than such variation in P_2 or P_3 but after certain frequency the sensitivity to P_1 variation is replaced with elevated sensitivity to 2nd and 3rd active power channels.

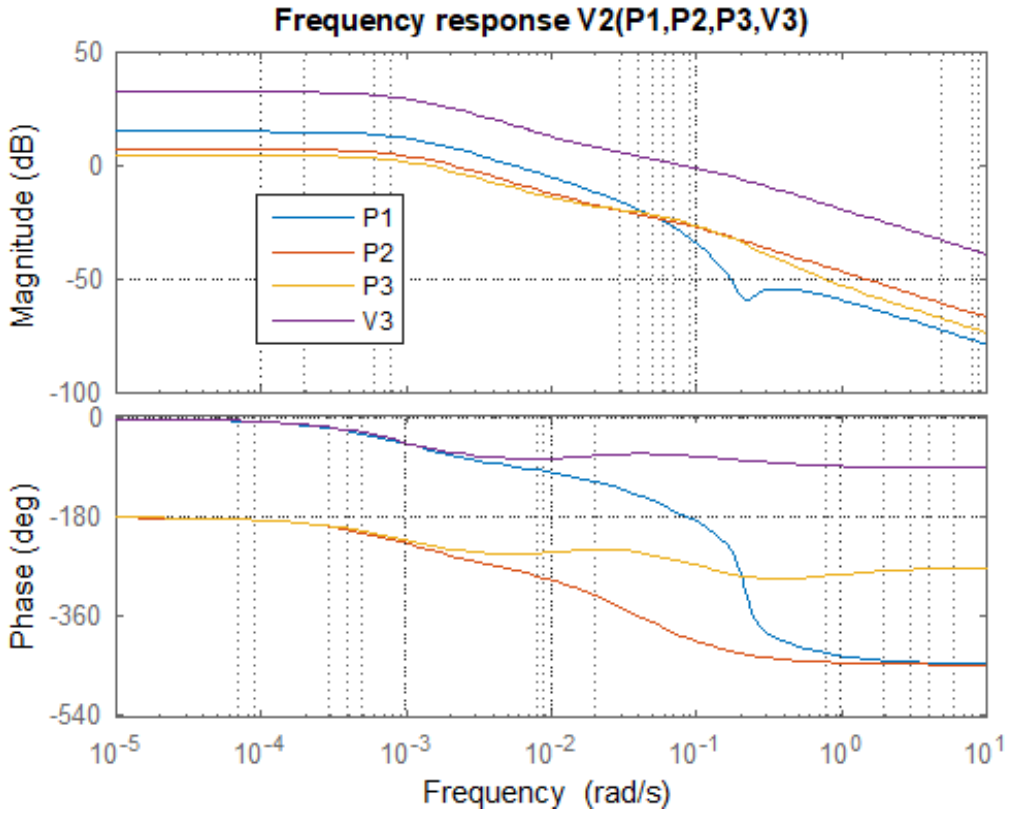

Figure 6.7: Frequency Response - V3

6.3 Time Domain or Temporal Analysis for Changes in Load

Step response $h(t)$ and impulse response $w(t)$ uniquely characterized the model, i.e. if you know the step/impulse response you can predict what will be the model output for a whatever input signals using Duhamel's integral formula [26]. The step signal is a reaction of the system to a constant unit signal $u(t) = 1(t)$. When the system has multiple input and multiple output as in the present analysis, the step response is a matrix $H(t)$ where each element $h_{ij}(t)$ represent the response of the output i when the unit signal $1(t)$ is applied at input j when all other inputs $k \neq j$ are equal to zero [29, 30].

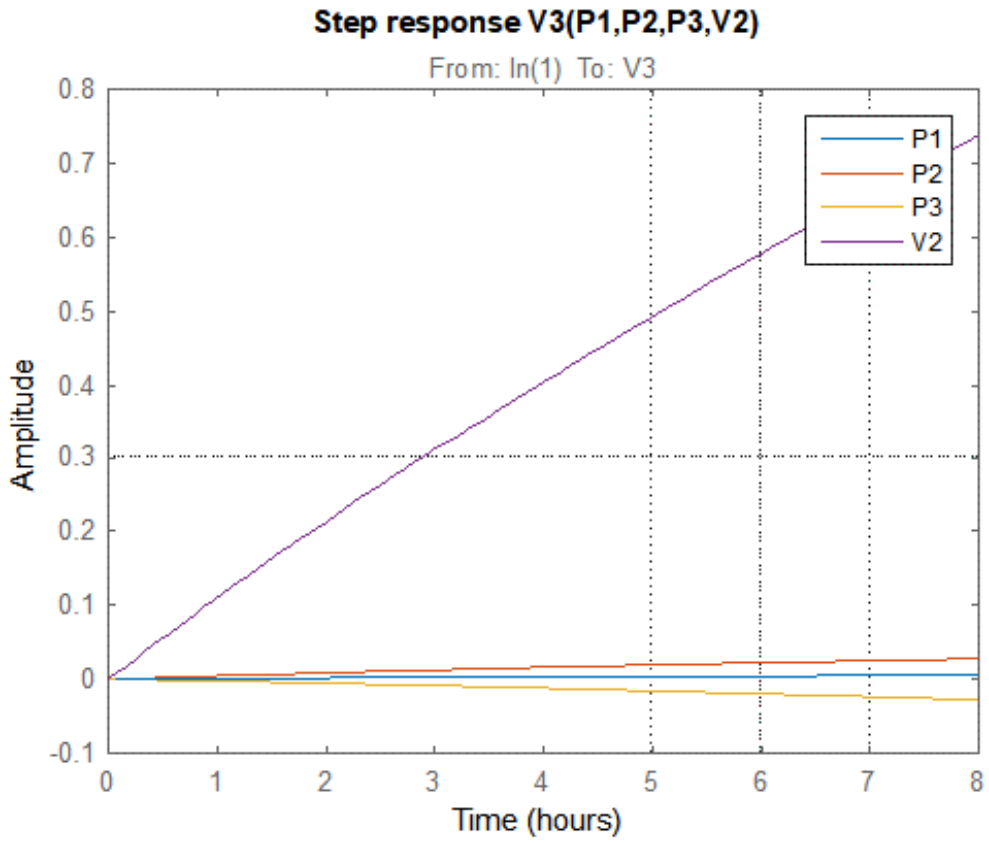

Figure 6.8: V_3 Temporal Analysis for Changes in Load (step)

Figure 6.8 shows the step response of V_3 for the model represented with equation (6.23). From this figure can be seen that the sensitivity of the voltage V_3 to V_2 is

higher than the sensitivity of the V_3 to power loads P_1,P_2 and P_3. Also we see that increase in power P_3 leads to decrease of V_3 however the increase of P_1,P_2 or V_2 leads to increase in V_3. The sensitivity of V_3 to the P_1 is too low and can be neglected. As can be seen a unit change in P_1 leads to very small change in V_3 compared to the other inputs

A similar statement can be made when observing the impulse response (figure 6.9) as was made for the step response. The highest sensitivity is to V_2 compared to P_1, P_2 and P_3. There is an obvious negative correlation between P_3 and V_3, no correlation with P_1 and positive correlation with P_2 and V_2. Here the impulse response represent the reaction of the system to a short impulse with unit energy at time 0.

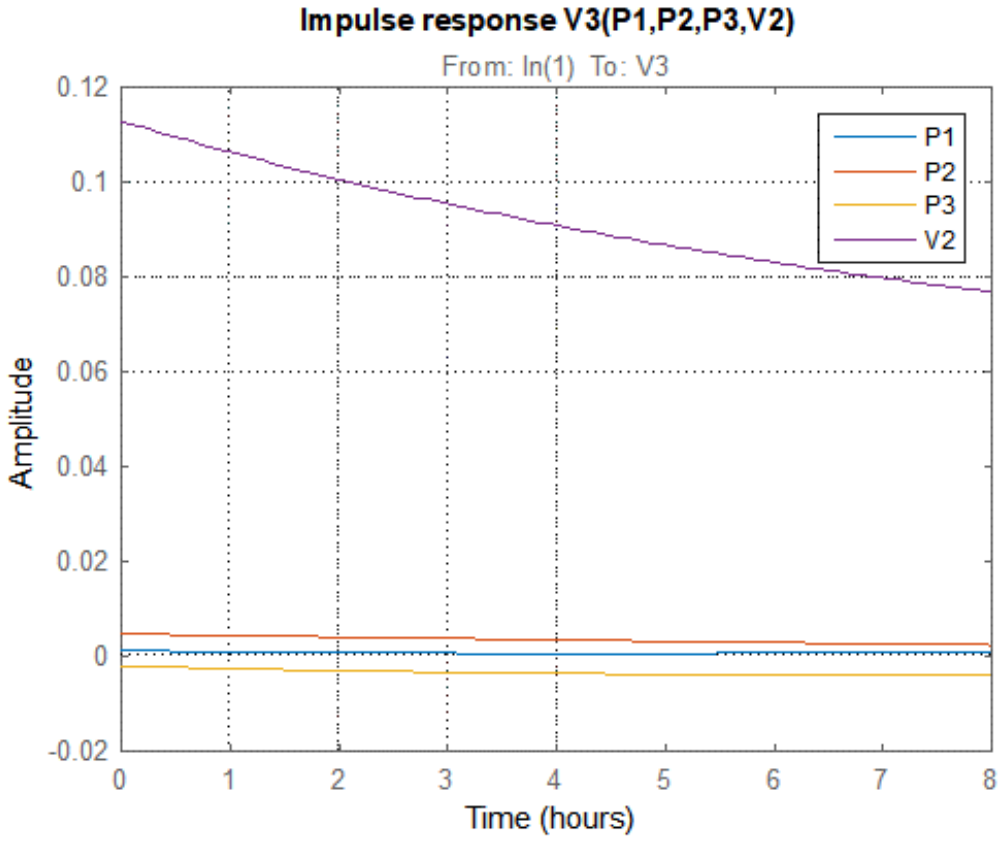

Figure 6.9: V_3 Temporal Analysis for Changes in Load (impulse)

As we can see in Figure 6.10 which present the comparison between fifth order model and experimental data the achieved level of fit is above 88%. The voltage is

increasing with time in dependence on P_1, P_2, P_3 and V_2. The differences between the model and experimental data is when the tangent angle is increased. The voltage on y-axis is in relative units, i.e. divided by 120V. The error can be further reduced by increase of the model order above five. However if we continue to increase the model order, and hence expand the dimensions of the model set, then we risk to make the model over-fitted to data[31]. In this case we have very large level of fit like above 98%, but unfortunately such fit can be achieved with large subset of model instances from the model set, each with their specific features. Therefore in case of over-fitting the generalization properties of the model are compromised and its high level of validity is only for the particular experimental data.

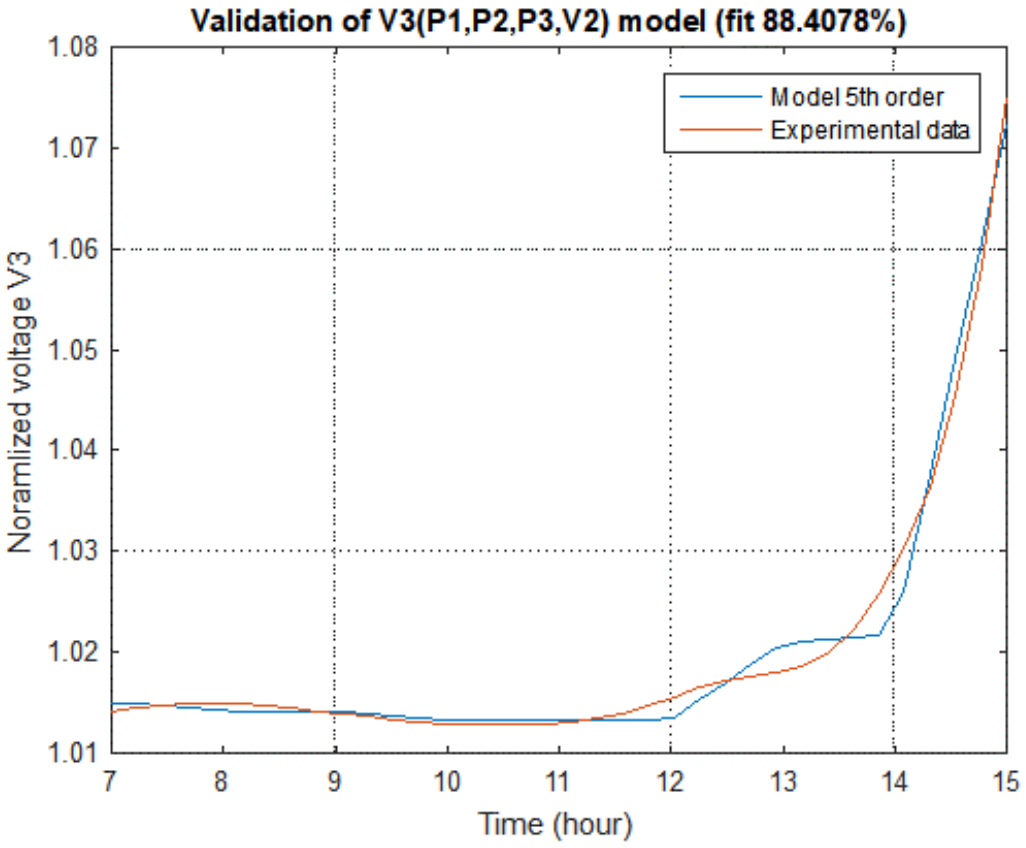

Figure 6.10: Model Validation for V3 - 5th Order Transfer Function

6.4 MIMO Transfer Function Model from Power Flow Simulation (sunny day)

The goal of this section is to estimate the transfer matrix model of the form $\vec{V} = W(s)\vec{P}$, where vector $\vec{V} = (V_1, V_2, V_3)^T$ contains the three node voltages and power vector $\vec{P} = (P_1, P_2, P_3, P_{pv})^T$ contains the active power consumed by the three nodes and also as a last component the generated active power P_{pv} from the photovoltaic power plant. The identification data set is created by collecting real-time data from power flow simulation software accounting for daylight changes and power consumption. Here $W(s)$ is a matrix of transfer functions relating i-th input to j-th output. In Figure 6.11 are summarized the input signals and the measured output signals from the real power system simulation. The goal of system identification is to estimate the components of the transfer matrix $W(s)$ such that to minimize the error between the output of the model and the output of the real system.

Figure 6.11: MIMO Model Comparison - Power Flow Simulation vs. Transfer Function Model

Figure 6.12 shows the comparison between the generated output from the estimation and output from the power flow simulation. Inputs are P_1, P_2, P_3 and P_{pv}. Outputs that have to be matched are V_1, V_2 and V_3. First the estimated model is of 5-th order. The time-base is in hours spanning from 0 to 24. As can be seen from the figures the fit is best at V_1 and V_3 signals which can be explained with their low-frequency variation. Usually the models fit better in lower frequencies because in the higher frequencies the nonlinear and sensor noise effects begin to develop and shadow the useful signal. For the voltage V_2 the fit is a little smaller around the places where the signal level changes fast from one direction to another. Such effects can be modelled with increasing model order so a 7-th order model is estimated to demonstrate this.

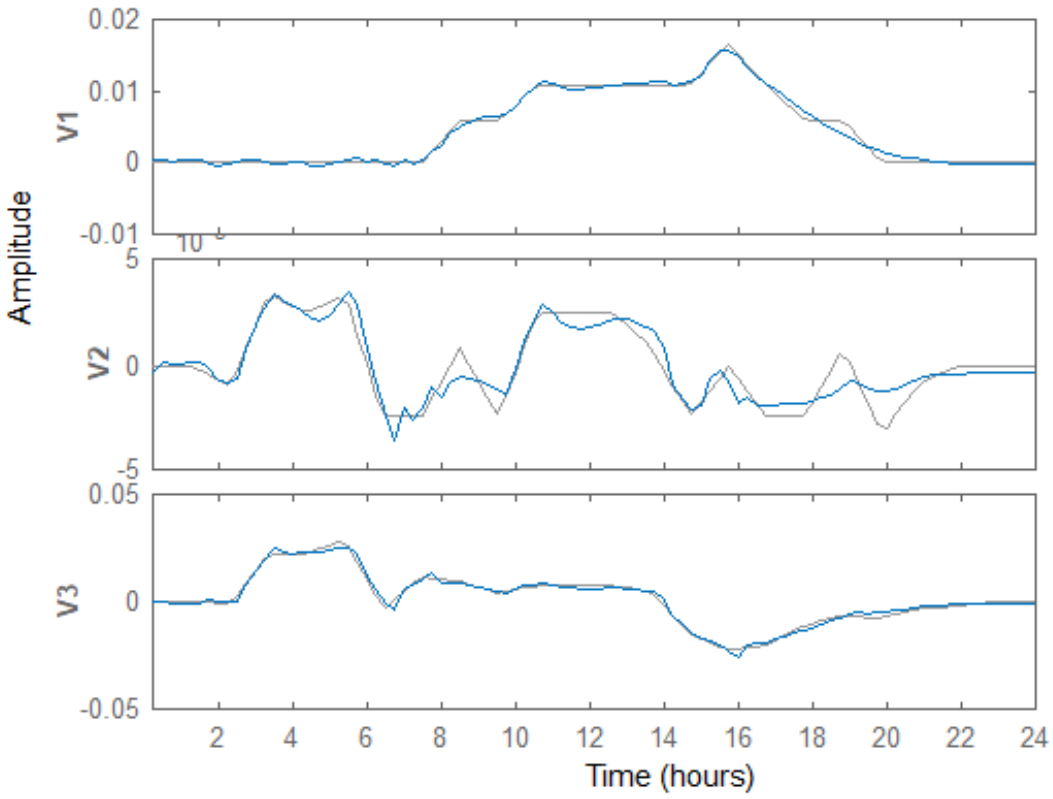

Figure 6.12: Validation with experimental data

The step and impulse responses uniquely characterized the model. That is to say

that if we know the step or impulse response we can definitively predict what will be the model output for a any given input signals. The step signal is the reaction of the system to a constant unit signal.

For the voltage transfer function of the first node V_1 we get the following result from identification

$$\begin{aligned} V_1 = \frac{1}{(s+0.3)(s+0.2)(s+0.1)^2}[&(-8\times10^{-4}(s+0.1)(s^2+0.5s+0.08)P_1 \\ &- 4.7\times10^{-5}(s+0.7)(s^2+0.3s+0.03)P_2 \\ &+ 0.002(s+0.09)(s^2+0.5s+0.07)P_3 \\ &+ 0.001(s+0.1)(s^2+0.5s+0.08)P_{pv}] \end{aligned} \quad (6.24)$$

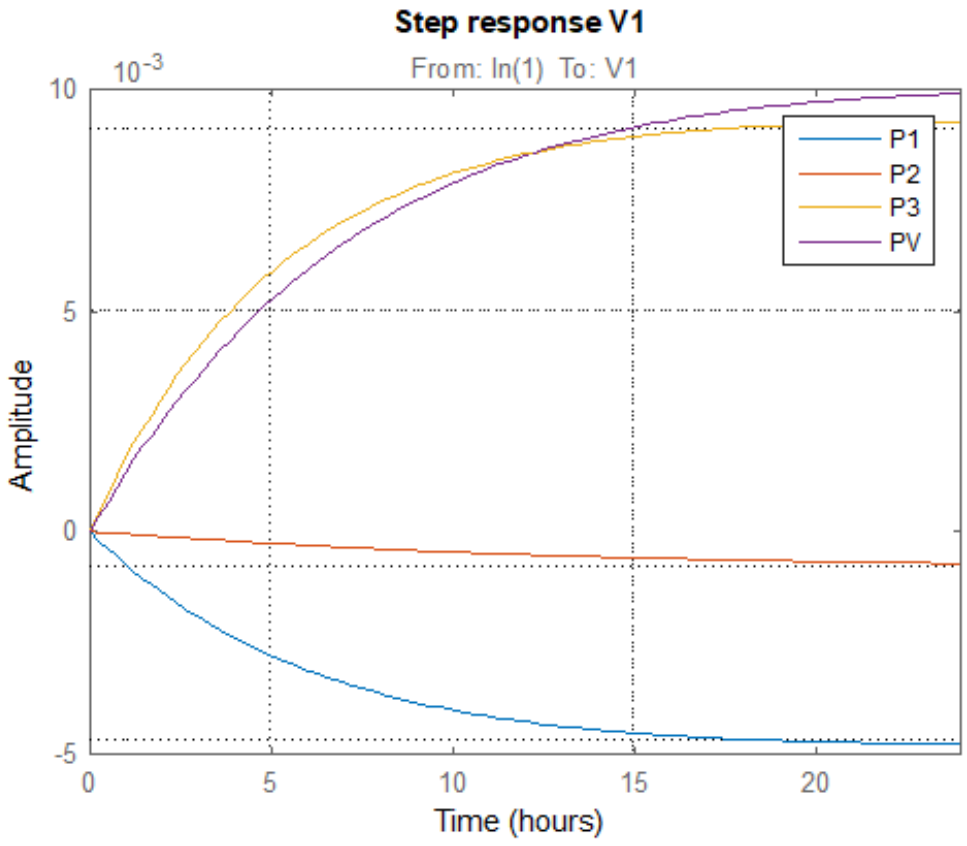

Figure 6.13: A time domain analysis for changes in load (step)

From the Figure 6.13 below we see that the sensitivity of the voltage V_1 to P_1,P_{pv},P_3 is higher than the sensitivity of the V_1 to P_2. Also we see that increases in power at P1 leads to decrease of V_1, however the increase of P_{pv} or P_3 leads to increase in V_1. The sensitivity of V_1 to P_2 is too marginal at best and can be neglected. As can u see a unit change in P_2 leads to very small change in V_1 compared to the other inputs.

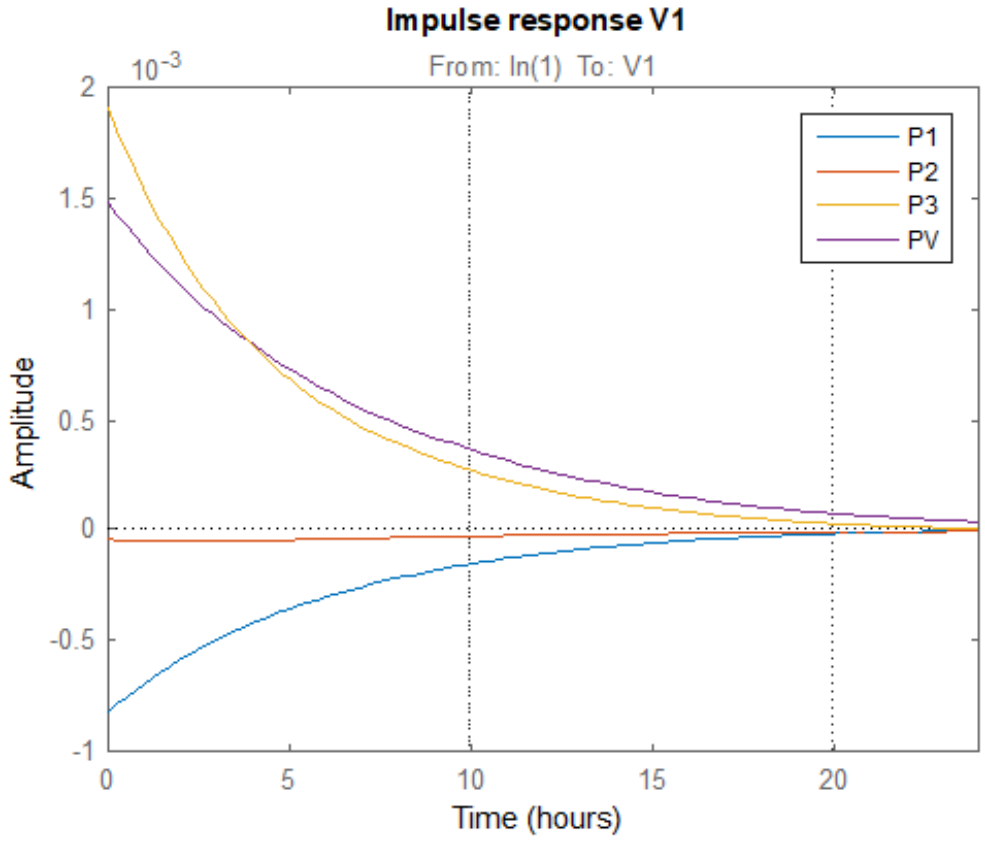

Figure 6.14: A time domain analysis for changes in load (impulse)

A similar statement can be made from the impulse response at Figure 6.14 as we did for the step response. Highest sensitivity to V_1 compared to P_1, P_3 and P_{pv}. A negative correlation between V_1 and P_1. There is no correlation with P_2, and positive correlation with P_3 and P_1. Further, the impulse response represents the reaction of the system to a short impulse with unit energy at time 0. All processes are aperiodic or sporadic without oscillation and ultimately converge to steady state value for around hour 20 hr. Thus, the sensitivity or effects on V_1 due to change in P_1,P_2 or P_{pv} are

long term.

Figure 6.15 compares the measured data about V_1 with the simulated output from the model given the input data for P_1, P_2, P_3 and P_{pv}. The value of fit 83% is acceptable, as we can see the model captures well enough the data variation. The difference between experimental data and the model is due to unobservable signals which are not included in this particular model like Q_1, Q_2 and Q_3. The other reason is reduced model order which I investigated is not big contribution on that difference and the third factor is possibly presence of some nonlinear effects acting on the data from the physical nature of the components in the system. We can see that the approximation is better when the V_1 changes and the error is bigger when V_1 is at steady state.

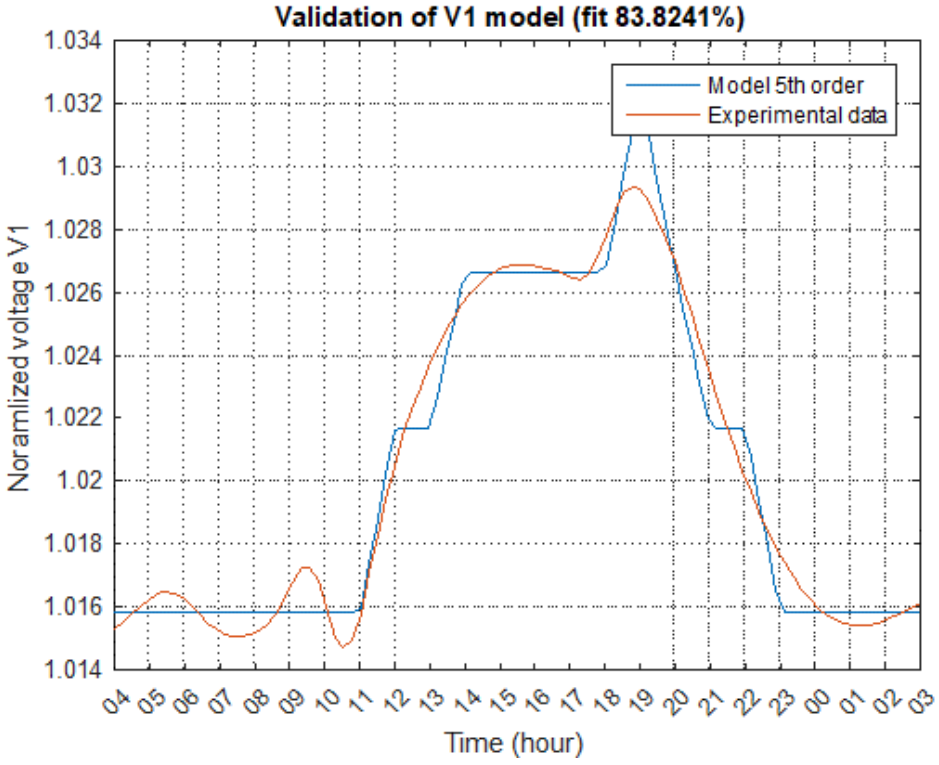

Figure 6.15: Validation of V_1 model

This transfer function model allow us to simulate whatever load profile we like. For example we have selected some 24hr load profile for P_1, P_2, P_3 and P_{pv}, as can be

seen from the bottom part of the Figure B.14.The upper part of the figure contains the temporal model response with respect to that load variation. The load profile might be selected from real data points or constructed from simulated data points to predict what would be the system behavior. From the magnitude response presented in the Figure 6.16 we see that the voltage V_1 is 100 times more sensitive to change in P_3 and P_{pv} than to change in P_2. The pass-band of the systems is around 0.1 rad/hr. The magnitude response means that we should expect aperiodic behavior of the system without overshoot or oscillation. The voltage V_1 is most sensitive to P_1, P_3 and P_{pv}. From the phase response we see that V_1 is synchronized with P_{pv} and P_3 and negatively correlated to P_1 and P_2 The delay of the response of V_1 to P_2 contains low frequency range than the response of V_1 to P_1. Hence the response of V_1 to P_1 is more delayed and slower.

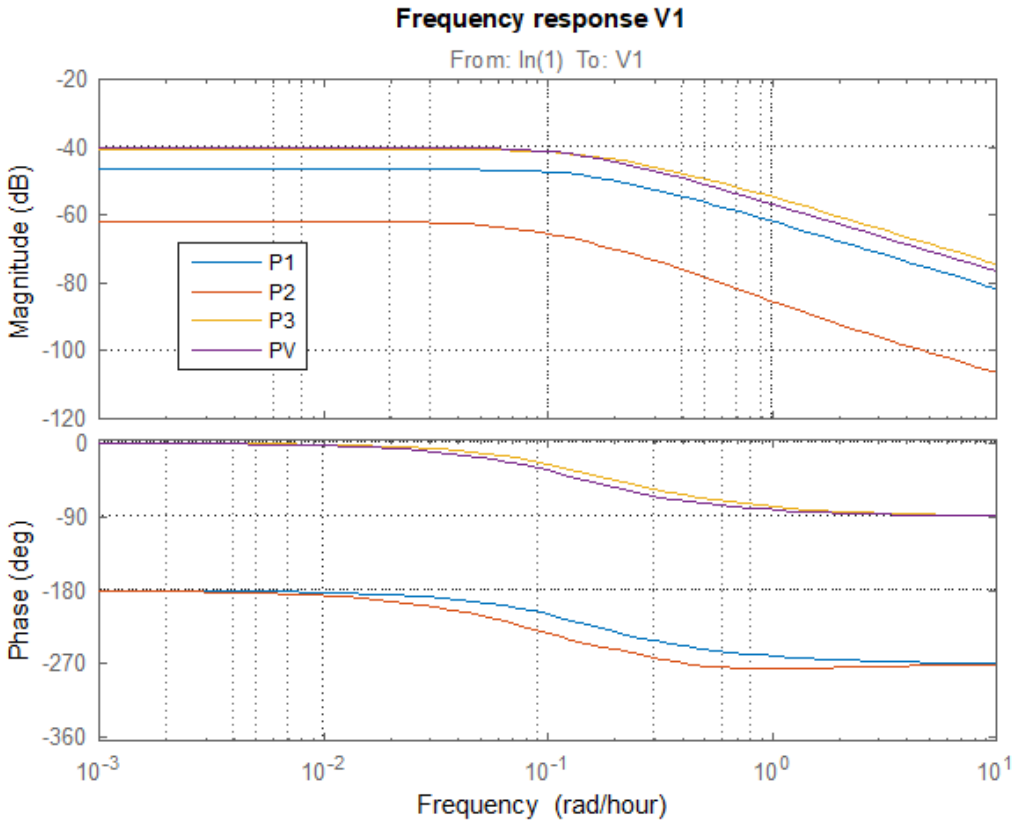

Figure 6.16: Frequency response of V_1

$$V_2 = \frac{10^{-4}}{(s+0.9)(s^2+0.6s+0.8)(s^2+0.3+3)(s^2+0.4s+7)}[$$
$$9.7(s^2+0.7s+0.9)(s^2-0.4s+2.6)(s^2+0.3s+8)P_1$$
$$-2(s-1)(s-0.7)(s^2+1.2s+0.7)(s^2-0.1s+7.5)P_2$$
$$-29(s^2+0.4s+0.9)(s^2-0.2+2.5)(s^2+0.3s+6.7)P_3$$
$$-20(s^2+0.3s+0.8)(s^2-0.2s+2.5)(s^2+0.4s+9)P_{pv}] \quad (6.25)$$

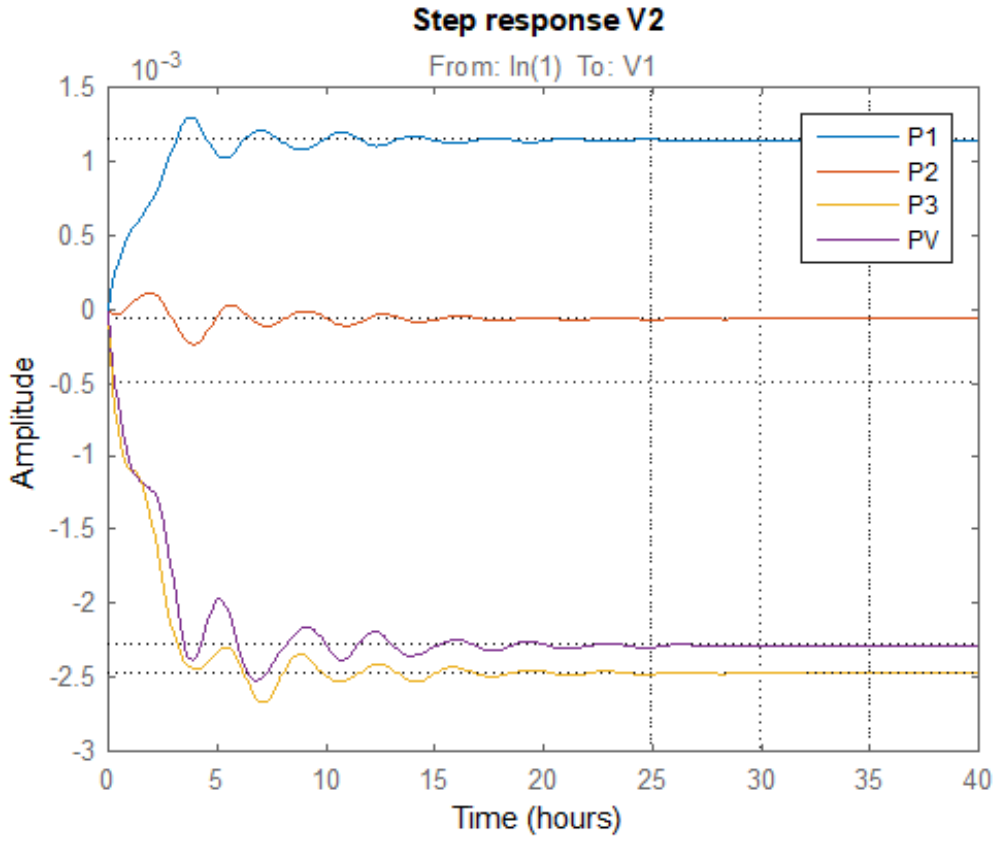

Figure 6.17: Temporal analysis for V2 - 7th order

Figure 6.17 presents the respective step response for the transfer function of $V_2(s)$ where is evident the oscillatory behavior during the transient. This oscillation extends the settling time of the process with several hours. From the figure it is interesting

to note the low sensitivity to P_2. Also it is evident a strong positive correlation between V_2 and P_1 as well as a strong negative correlation between V_2 and P_{pv} or P_3. The structure of the transient is preserved over the different input channels which is due to the common denominator. This is typical for the systems with linear fractional transfer functions because even if the denominators are different there can be calculated a common denominator. The reaction of V_2 with respect to P_3 and P_{pv} are very close meaning that adding power source at node 1 is functionally equivalent to increasing the load at node 3. Intuitively being a node in the middle node 2 is impacted by power consumption in the adjacent nodes.

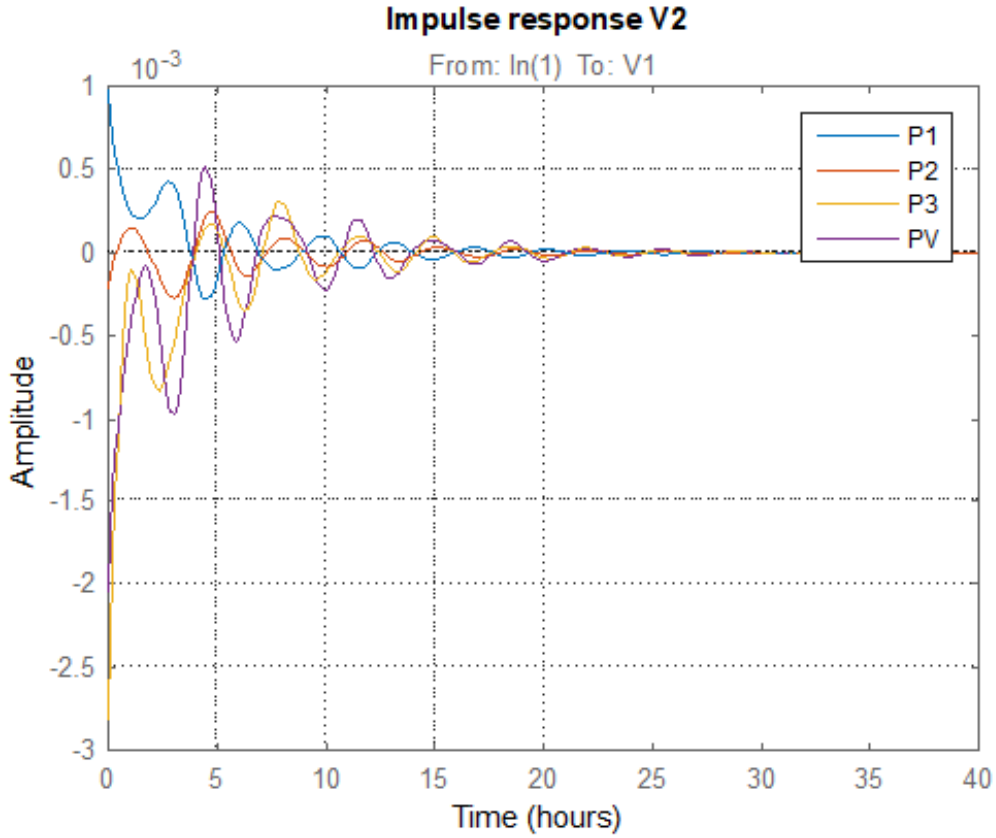

Figure 6.18: Temporal analysis for V2 - 7th order

More detailed look at the oscillatory behavior is presented at Figure 6.18 with the impulse response of the V_2 transfer function. There can be observed long term oscillations in V_2 signal for about 20 hours after the initial impulse deviation. The

impulse response is the reaction of the system to a short time impulse wave at time zero. The synchronized oscillations between P_3 and P_{pv} are also observed. The period of oscillation is around 1 hour. The settling time is around 15 hr which is calculating by noting the 5% range for the zero level. The initial values for different processes depend on their static gain and corresponds to the information from the step response characteristic. In control theory as we know the step and impulse response equivalently define the system behavior because $dh(t)/dt = w(t)$ (h being step response and w being the impulse response).

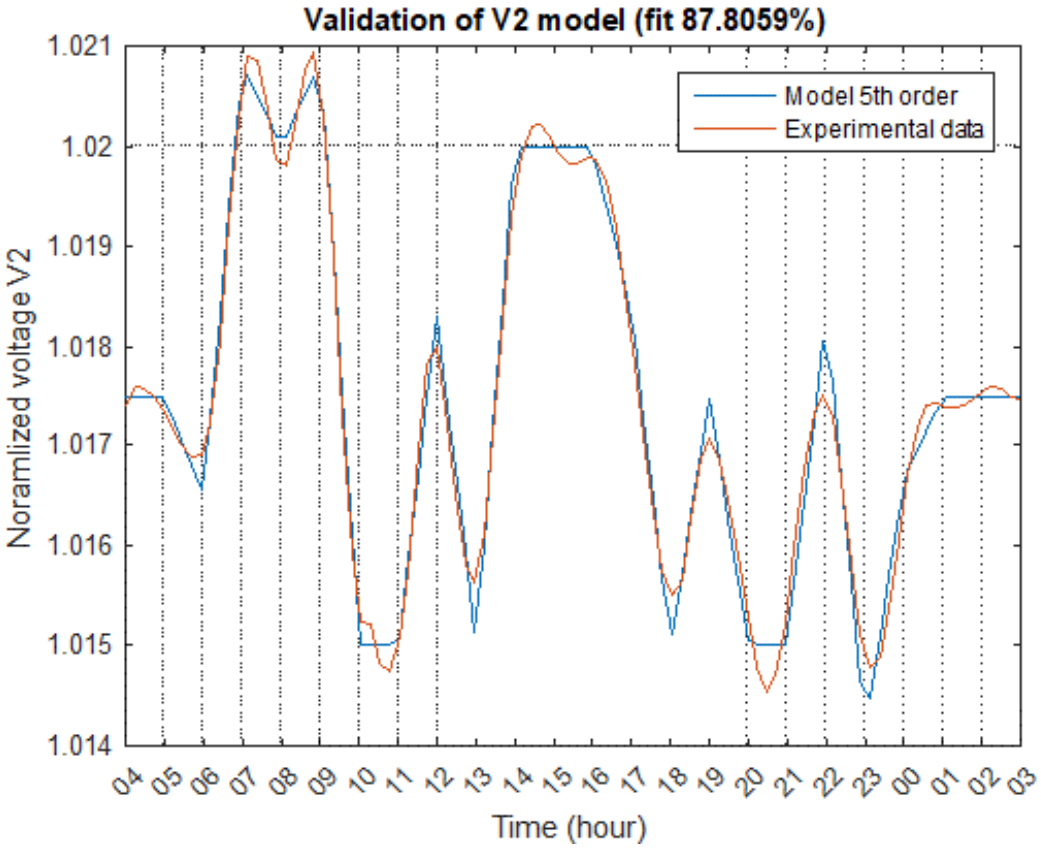

Figure 6.19: Validation of the model for V2 - 7th order

Figure 6.19 contains the validation comparison between the experimental and simulated from the model data for the V_2 signal. The achieved level of fit between the model and the data is around 87.81 % which is relatively high for models obtained from data. However in order to obtain the higher percentage of fit to experimental

data a 7th order model was employed - where in contrast to V_1 only a 5th order model was enough to have a percentage of fit above 80 %. In the figure as can be seen the experimental data is oscillatory. That may partially explain the oscillatory nature of the model itself which we demonstrated with the step and impulse responses above. The achieved 87% fit is high enough level allowing to practically employ the model for forecasting or other analysis. The observed differences between the experimental data and the model can be related to measurement time quantization (sampling) which causes discontinuity of the first derivative at some points.

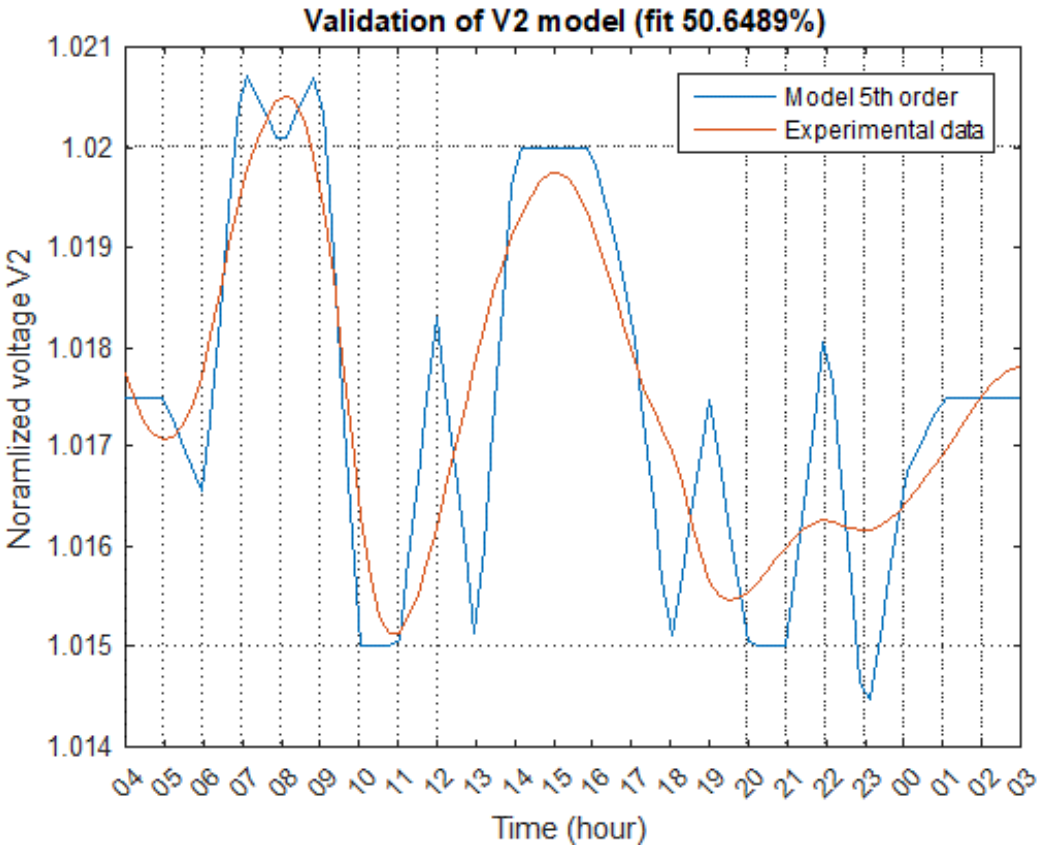

Figure 6.20: Validation of the model for V2 - 5th order

If we try a lower order model, like 5th order the level of fit decreases dramatically to 50% or less depending on the initial conditions. The simpler model captures only the oscillations with largest amplitudes and neglects the smaller oscillations. In the data there are high variations from one hour to the next which need to be modelled

with adding some faster poles. So we decided to extend the 5th order model to a 7th order with transforming 4 of its poles to complex pairs and adding another 2 complex poles.

A strong resonance region from 2 to 6 rad/hr with respect to all input variables P1,P2,P3 and PV. Magnitude plot at -40dB so no much sensitivity of V2 to power variations compared to V1. Interestingly sensitivity to P2 is really small at -80dB P3 and PV have overlapping phase responses so the response of V2 to them is with same reaction delay. Generally a lot of variation of the phase response from 0 lower to higher frequencies which indicates complex pattern of the V2 signal due to phase shifts.

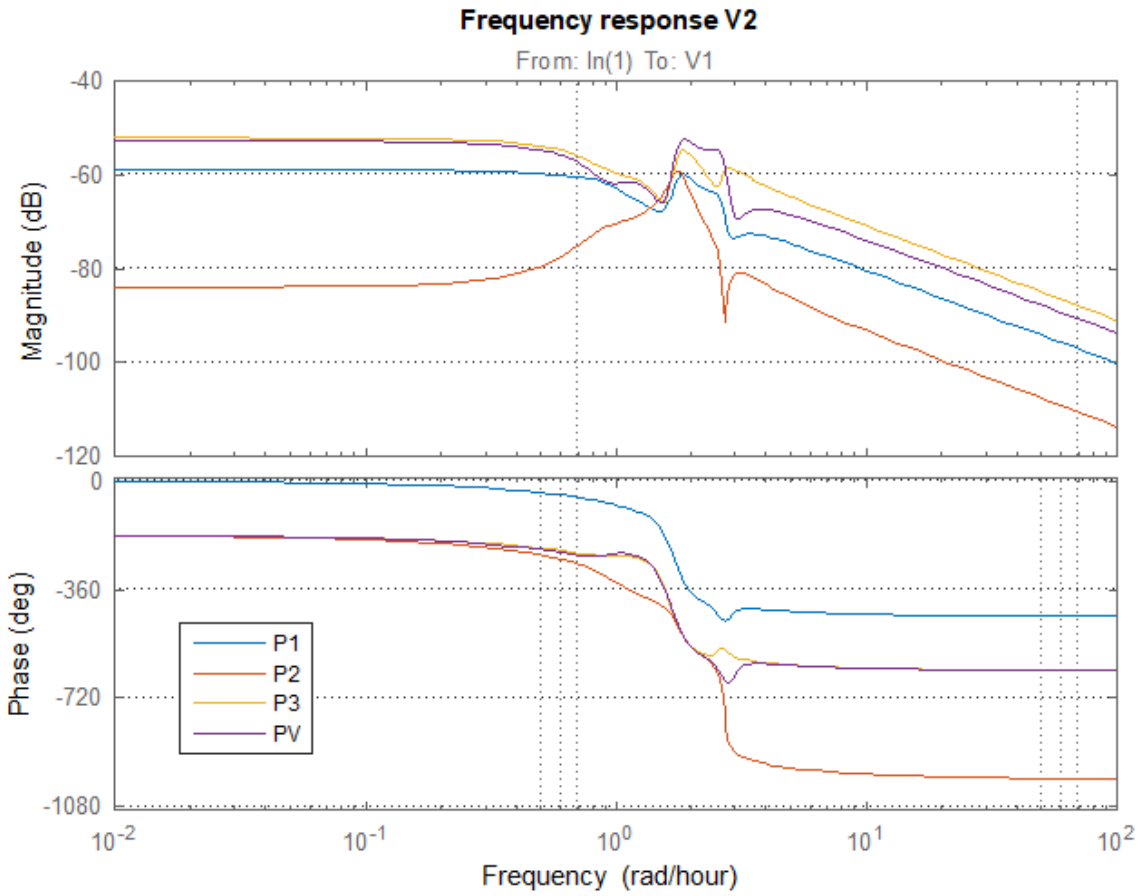

Figure 6.21: Frequency domain analysis for V2 - 7th order

The model allows different load profiles to be simulated Only have to be accounted

that the transfer functions are with respect to bias of V1,V2 or V3 from the normalized voltage of 1. This simulation is executed at continuous time so we can get a simulated value of voltage for each time instant during the day.

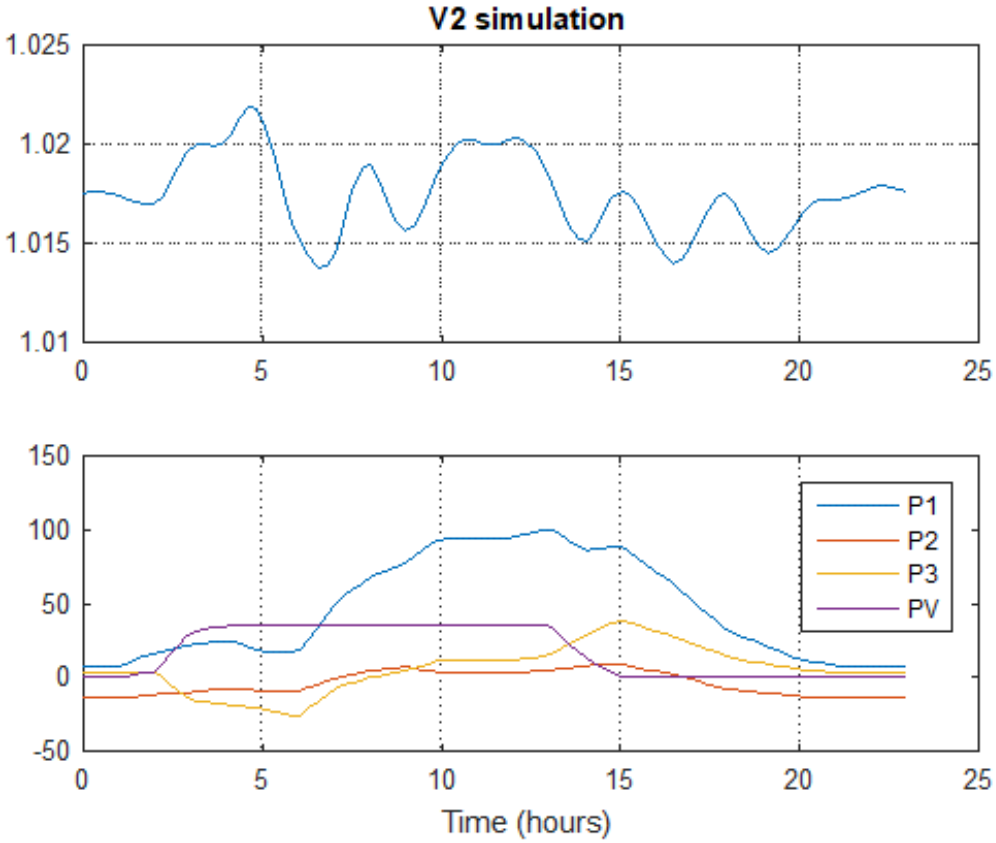

Figure 6.22: Load profile simulation for V2 - 7th order

Inputs: P1, P2, P3 and PV Output: V3 Aperiodic behavior due to real poles All poles very close to each other varying only from -0.6 to -0.8. Many of the zeros in the numerator are close to the pole locations which means that this model order is possible to be reduced further The transfer function from PV has a positive zero which makes it non-minimal phase, i.e. during transient the reaction of V3 to PV will be in initially in positive direction and the will be in the negative direction. Correlation between P3 and V3 negative with gain -0.0005. Correlation with V3 with the rest signals P1 and P2 positive however the sensitivity to P2 is very small. Correlation with PV is negative with highest gain of -0.002

$$V_3 = \frac{10^{-4}}{(s+0.8)(s+0.6)^2}[5.2(s+2.4)(s+0.6)P_1 + 0.1(s+32)(s-0.4)P_2 - 4.8(s+6)(s+0.6)P_3 + 15(s-1.9)(s+0.6)P_{pv}] \quad (6.26)$$

Aperiodic responses with delayed start of increase due to multiple poses at a same location You can see the effect of non-minimal phase zero at PV to V3 channel - the reaction first goes up for some time before heading down. V3 reacts in positive direction to constant increase in P1, but acts in negative direction to constant increase in P3 and PV. Sensitivity to P2 is not much however a non-minimal phase again.

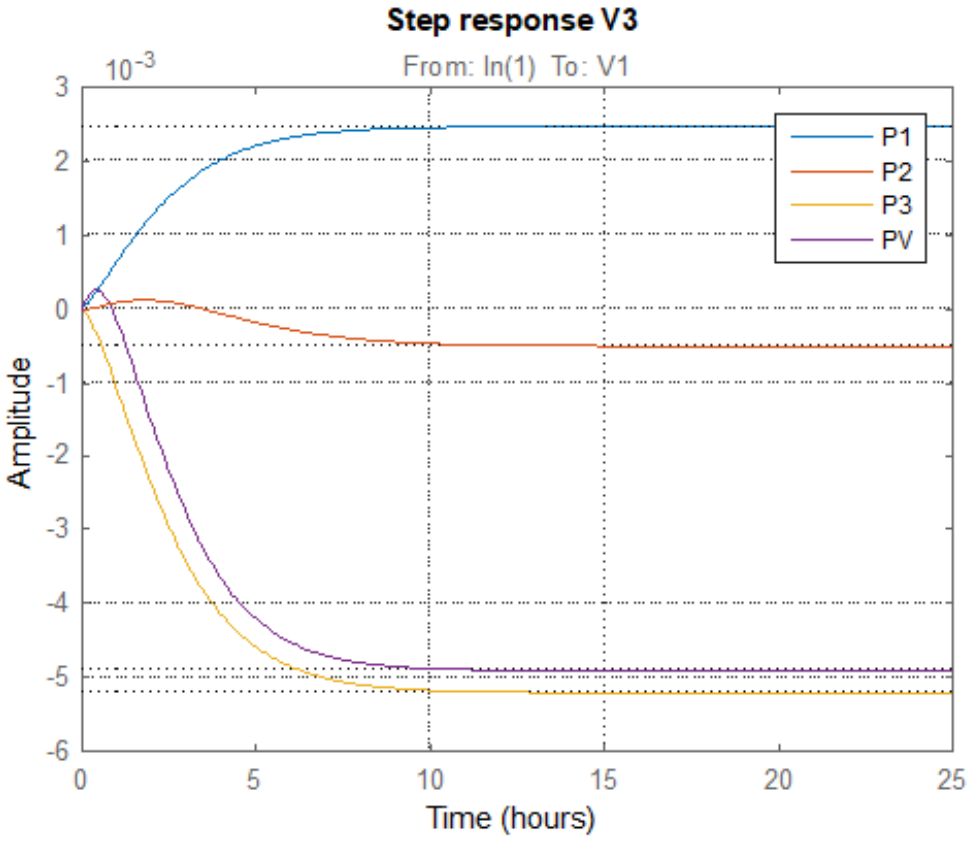

Figure 6.23: Temporal analysis for V3

Well pronounced aperiodic behavior Settling time around 10 hours Similar phases

between P3 and PV

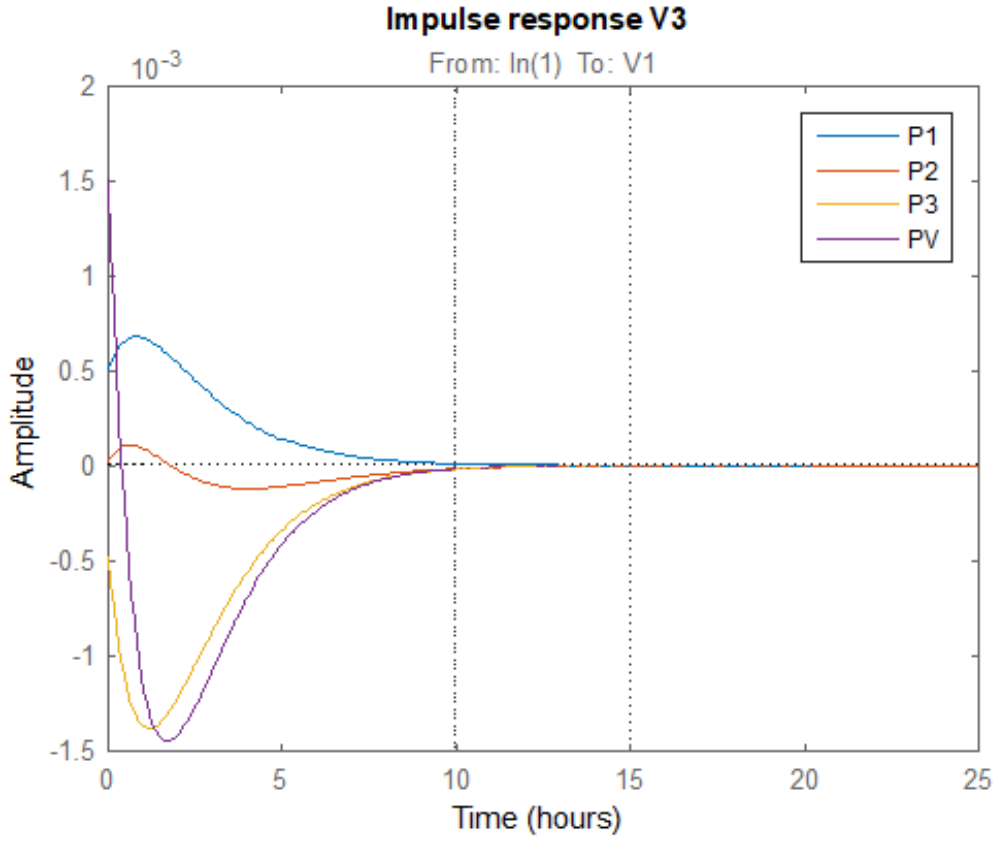

Figure 6.24: Temporal analysis for V3

Comparison with experimental data shows good fit of around 76%. Differences bigger between 9am to 5pm. That can be improved with increase of the model order. The error is in higher frequencies when the changes in V3 are faster than 1 hour and in lower frequencies the model is more accurate. Magnitude response pretty close on all channels, except for P2. The passband is around 1 rad/hr. Phase response more complex due to positive zeros at P3 and P2 channels. P3 phase response ranges from 180 at 0 rad/hr to -100 at 10 rad/hr. This makes the response of V3 with respect to P2 more complex with strongly shifter harmonics.

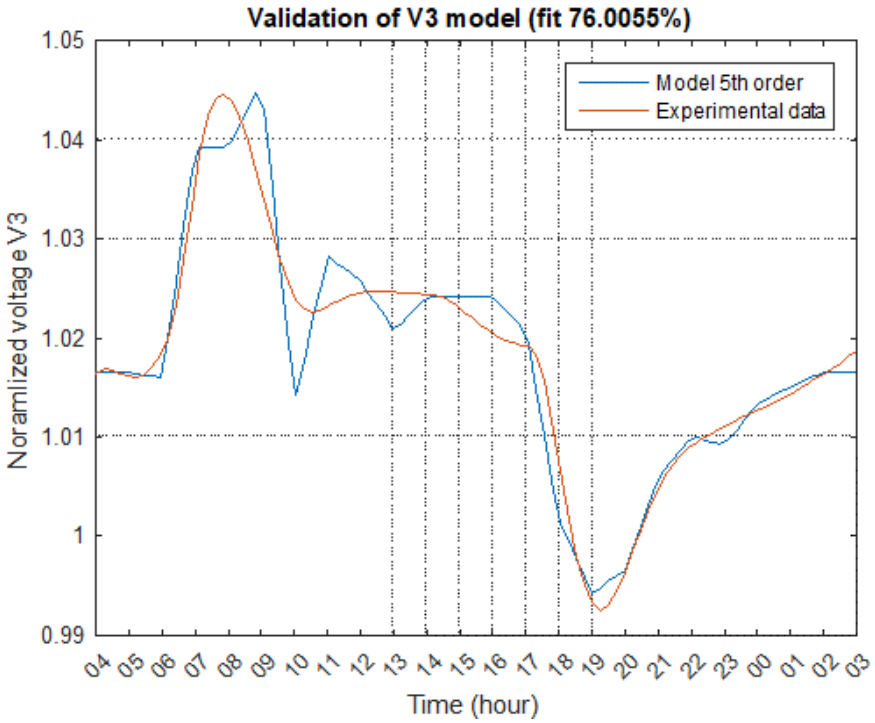

Figure 6.25: Validation of the model for V3

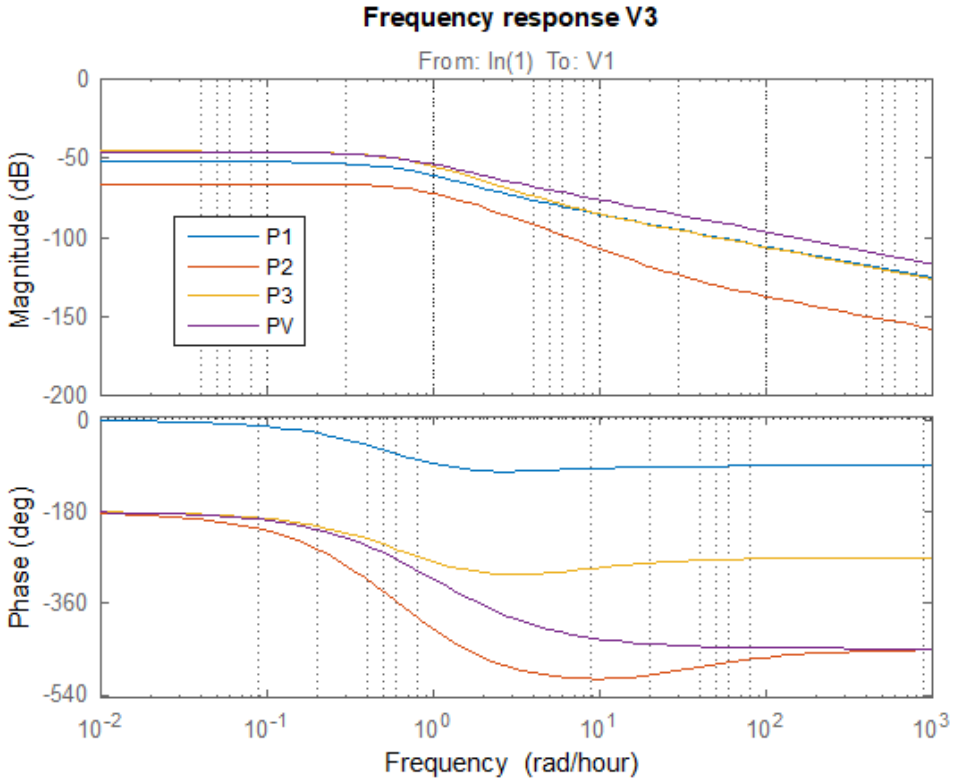

Figure 6.26: Frequency domain analysis for V3

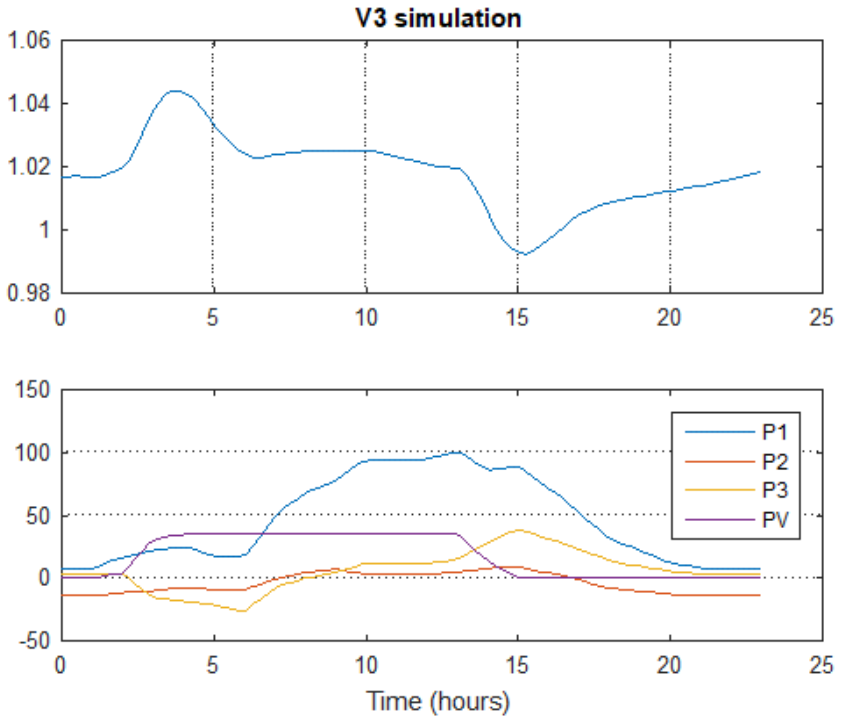

Figure 6.27: Load profile simulation for V3

The model can be used to simulate various load and PV profiles. Here we simulated the reaction to the experimental data. This simulation is executed at continuous time so we can get a simulated value of voltage for each time instant during the day.

6.5 Cloudy day analysis

Inputs are P1, P2, P3 and PV. Output is V1. The model is of 8th order. Timebase is hours.

$$
\begin{aligned}
V_1 = \frac{10^{-3}}{(s+1)(s+1.5)(s^2+0.7s+0.1)(s^2+1.3+0.7)(s^2+s+0.6)}[\\
3.1(s-1.5)(s^2+4s+4)(s^2+0.6s+0.1)(s^2+s+1)P_1 \\
-10(s-1.5)(s^2+0.8s+0.2)(s^2+1.5s+0.7)(s^2+2s+2.7)P_2 \\
+6.8(s-1)(s^2+0.7s+0.2)(s^2+1.3s+0.7)(s^2+4s+6)P_3 \\
+3.6(s-4.5)(s^2+0.9s+0.2)(s^2+0.4s+0.2)(s^2+1.4s+1)P_{pv}] \quad (6.27)
\end{aligned}
$$

We see that the dominant pole is at -1 which gives a dominant time constant around 1hr. The steady state gain between P1 and V1 is -0.003, between P2 and V1 is 0.01, between P3 and V1 is -0.007, between PV and V1 is 0.004.

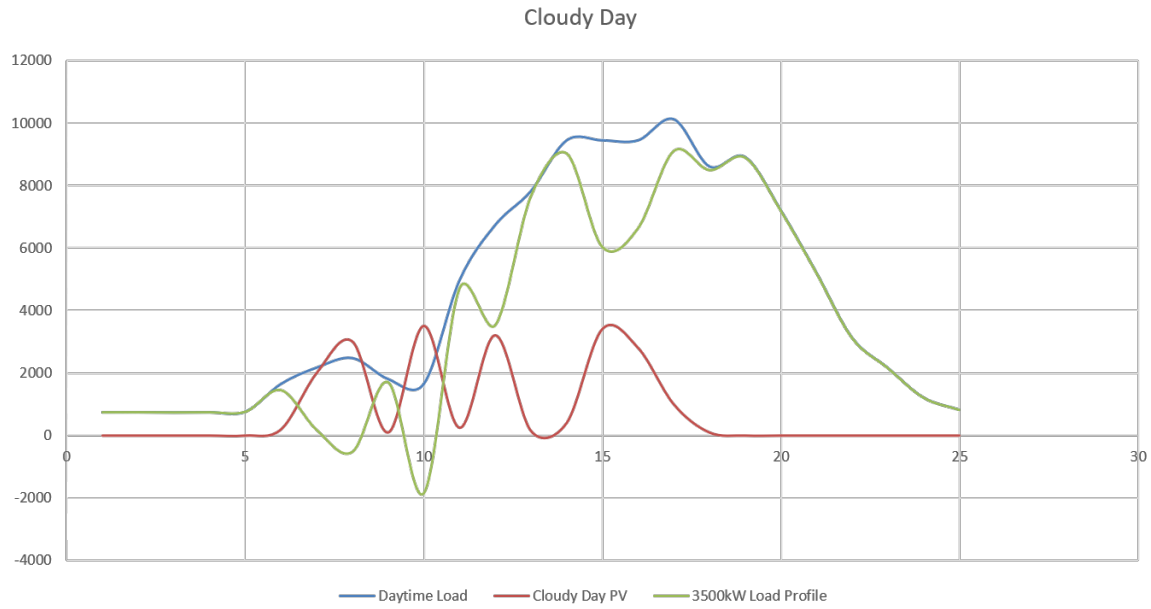

Figure 6.28: Cloudy day analysis

Figure 6.29 compares the measured data about V1 with the simulated output from the model given the input data for P1,P2,P3 and PV. The value of fit 90% is very high, as we can see the model captures well enough the data variation. The difference between experimental data and the model is due to unobservable signals which are not included in this particular model like Q1, Q2 and Q3. The other reason is reduced model order which I investigated is not big contribution on that difference and the third factor is possibly presence of some nonlinear effects acting on the data from the physical nature of the components in the system. We can see that the approximation is better when the V1 changes and the error is bigger when V1 is at steady state.

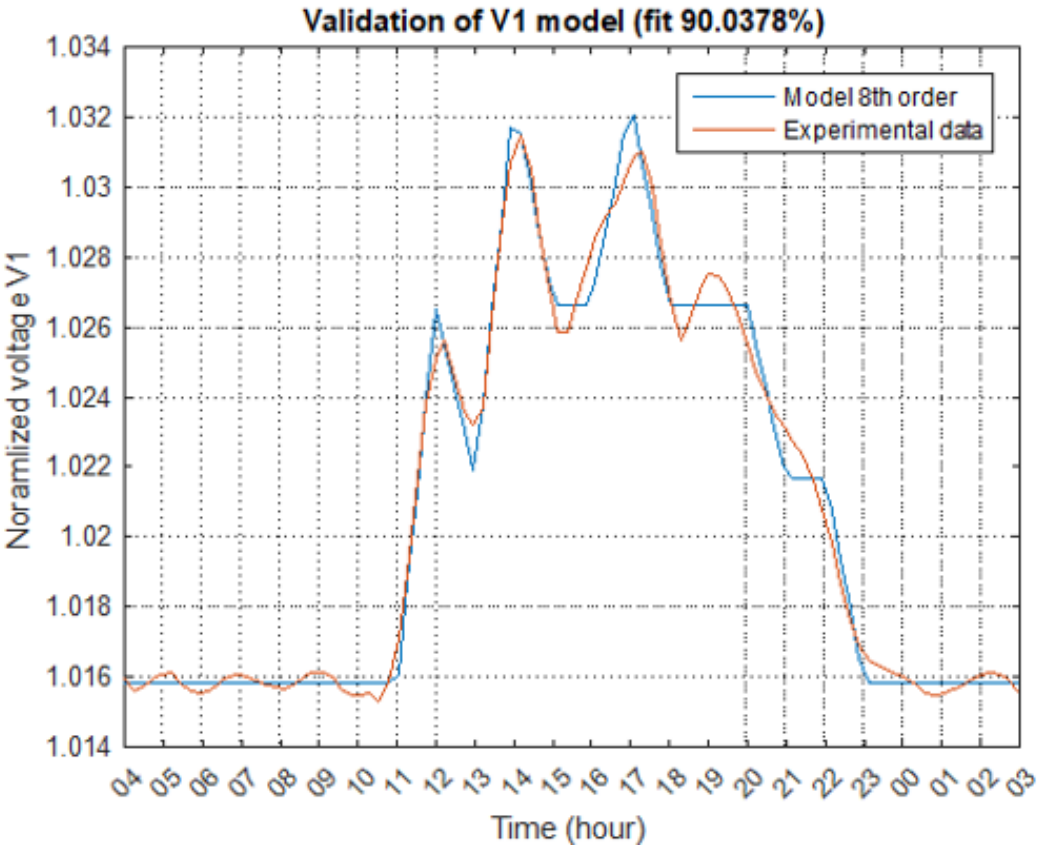

Figure 6.29: Validation with the experimental data V1

Step response of the V1 model with respect to P1, P2, P3 and PV have similar time constant. Reaction of V1 with respect to P2 and P3 show clear nonminimal phase behavior because then first go into reverse direction for a while before settle to the steady state values. This non-minimal phase also can be interpreted as a delay of the response on these channels. So the response on P1 is delayed around 1hr and on P3 is delayed around 2hrs. Also note positive correlation of V1 to PV and P2 and negative correlation of V1 to P1 and P3. Negative correlation means that V1 will be dropping when the power consumption in P1 and P3 nodes is increasing. Positive correlation means that V1 will be increasing when PV power is increasing or P2 power consumption is increasing.

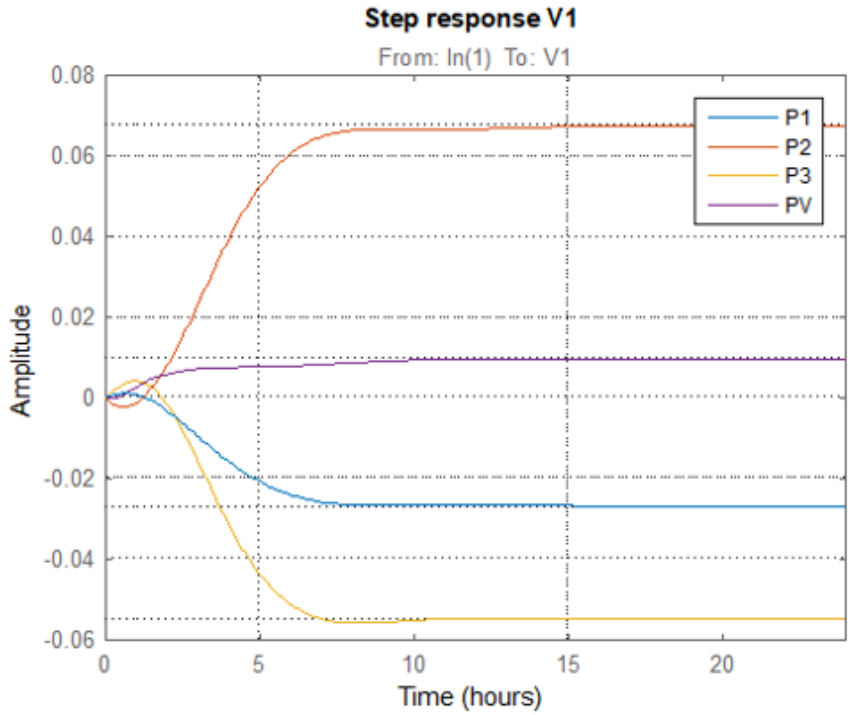

Figure 6.30: Temporal analysis V1 model

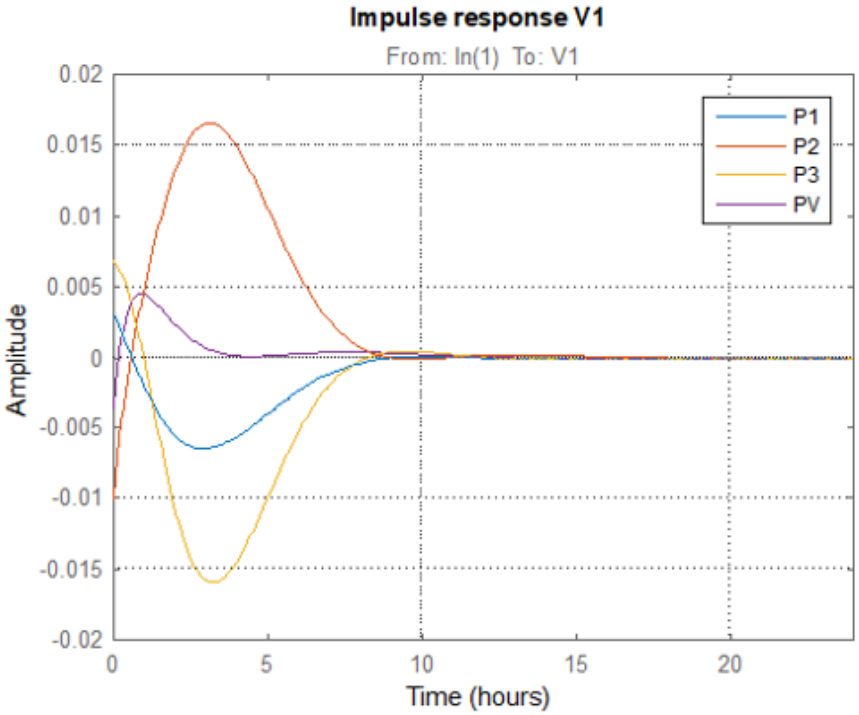

Figure 6.31: Temporal analysis V1 model

In the impulse response you can see how the past values of P1,P2,P3 and PV are weighted to amount to the current value of V1 (due to Duhamel integral formula). So the current value of V1 reflects to a greater extent the values of P2 before 4 hours (the maximal value in the plot). Also V1 reflects the past values of P3 before 3 hours, the past values of P1 before 2.5 hours and the past values of PV less than an 1 hour. Also there is an immediate reaction of V1 to the P1,P2,P3 and PV inputs due to non-negative values at time 0.

The model can be used for simulation of V1 (the upper part of the figure) given the variations in P1, P2, P3 and PV (the lower part of the figure). If you examine the PV signal you can see the variations of the delivered photovoltaic power during the day due to clouds. These variations also are translated in the P2 and P3 signals. Also you can observe the P1 loading profile and the reaction of V1 to all these signals.

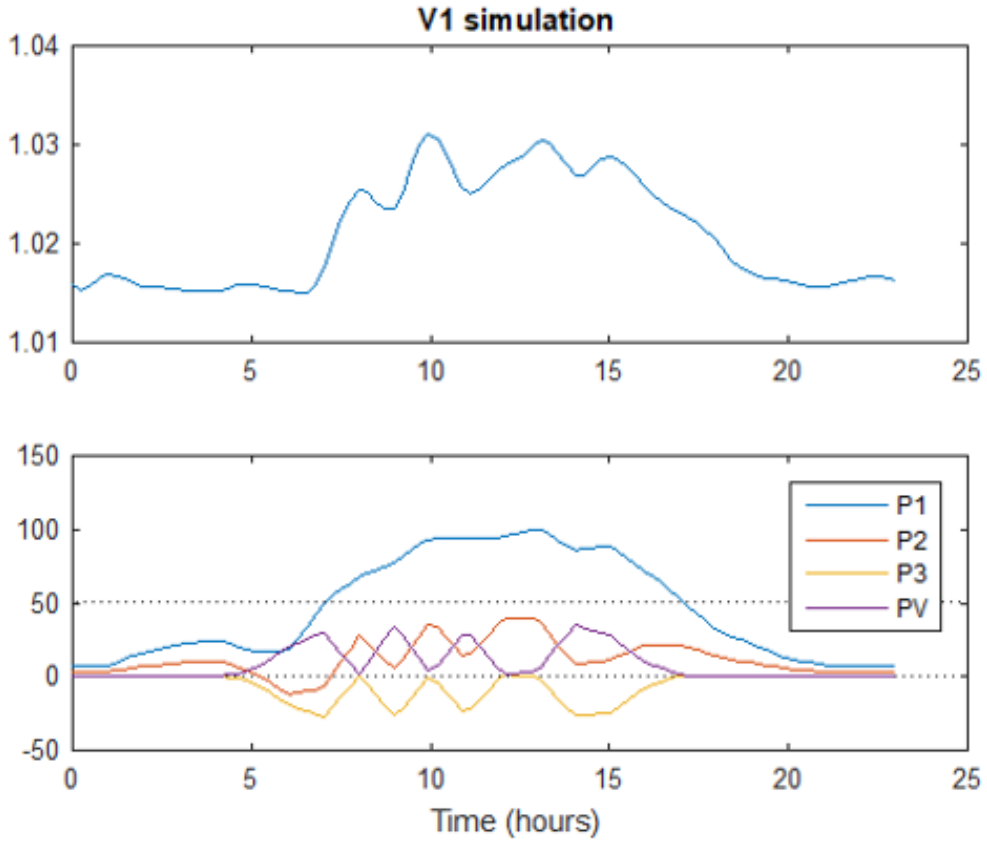

Figure 6.32: Temporal analysis V1 model

From the magnitude response we see that the bandwidth of the system is around 1 rad/hr where the sharp drop of the characteristic begins. There are not resonances of the V1 response, except for the slight damping resonance with respect to PV at about 0.7 rad/sec. The phase response shows us that response of the V1 is in phase with two of the channels P3 and PV and with 180deg delay (which means negative correlation) for P1 and P3 channels.

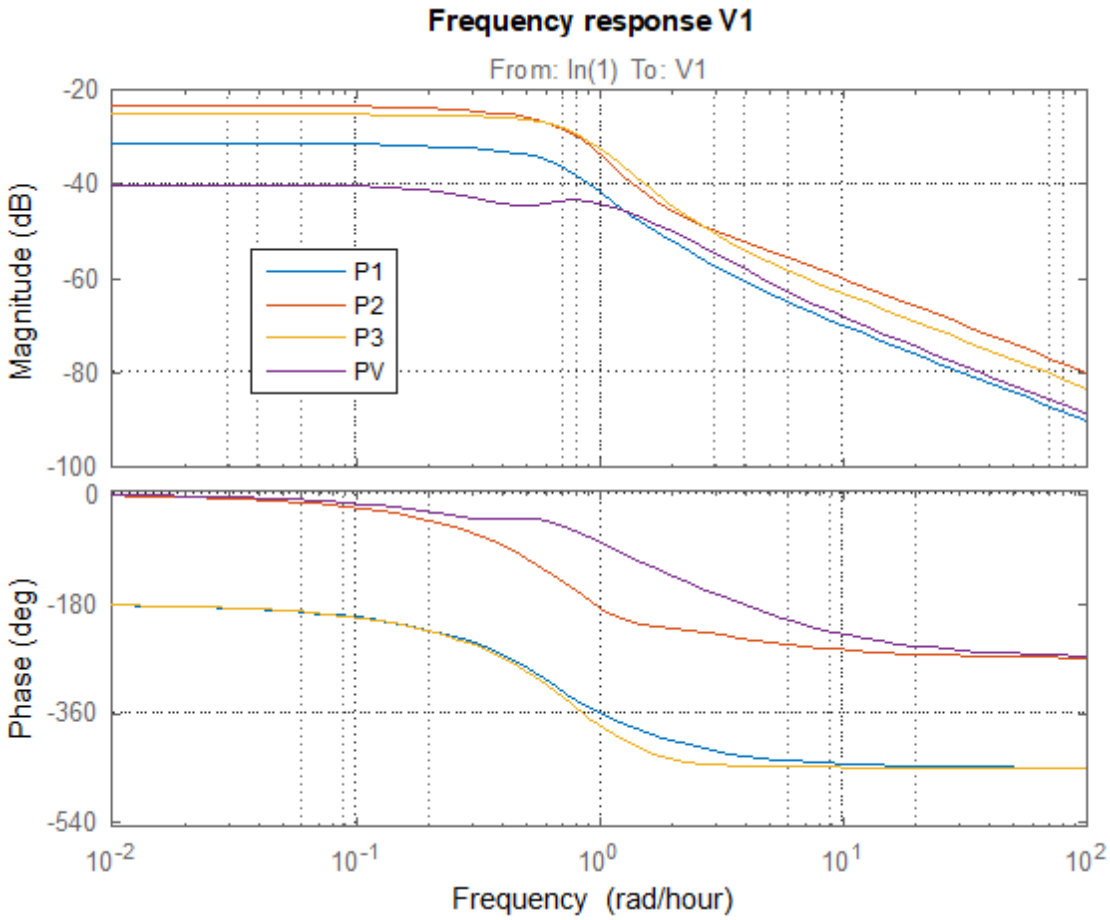

Figure 6.33: Frequency domain analysis of V1 model

There is a nonminimal zero (right hand side 'o') in all of the channels. That positive zero is closest to the imaginary axis for P3 channel so the non-minimal (delayed) response of the system will be most strongly pronounce there. In all the graphs you can observer that some zeros 'o' and poles 'x' are pretty close which means that their

effects counteract each other. This is an indication that it is possible to make model reduction of the model order without considerably degrading its performance. Also you can check the poles ('x') which are not on the real axis - they introduce oscillatory modes in the response. However in all the cases there are zeros around these complex pole pairs which neglects their effect. There are also complementary complex zeros in P2 response which cause the observed damping resonance in that channel.

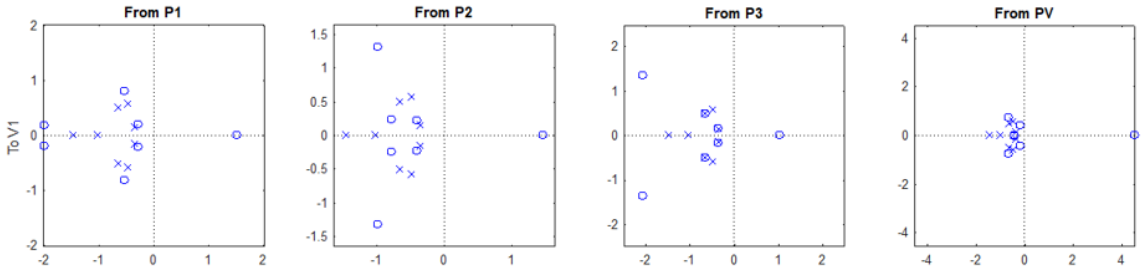

Figure 6.34: Zeros and poles of V1 model

Inputs are P1, P2, P3 and PV. Output is V2. The model is of 8th order. Timebase is hours. We see that the dominant pole is at -1.4 which gives a dominant time constant around 40 min. The steady state gain between P1 and V2 is -0.01, between P2 and V2 is 0.025, between P3 and V2 is -0.019, between PV and V2 is 0.006.

$$V_2 = \frac{10^{-3}}{(s+1.5)(s+1.4)(s^2+0.6s+2.3)(s^2+0.7s+3.7)(s^2+10)}[$$
$$-10(s+1.5)(s^2+0.7s+1.9)(s^2+0.5s+4.7)(s^2+0.1s+10)P_1$$
$$+25(s+1.4)(s^2+0.5s+2)(s^2+0.9s+5)(s^2+0.02s+10)P_2$$
$$-19(s+1.6)(s^2+s+2.5)(s^-0.4s+4)(s^2-0.2s+10)P_3$$
$$+5.9(s+0.5)(s^2+0.8s+1.4)(s^2+0.1s+9)(s^2+3.4s+13)P_{pv}] \quad (6.28)$$

This figure compares the measured data about V2 with the simulated output from the model given the input data for P1,P2,P3 and PV The value of fit 85% is very

high, as we can see the model captures well enough the data variation. The difference between experimental data and the model is due to unobservable signals which are not included in this particular model like Q1, Q2 and Q3. The other reason is reduced model order which I investigated is not big contribution on that difference and the third factor is possibly presence of some nonlinear effects acting on the data from the physical nature of the components in the system. We can see that the approximation is better when the V2 changes and the error is bigger when V2 is fastly changing its direction.

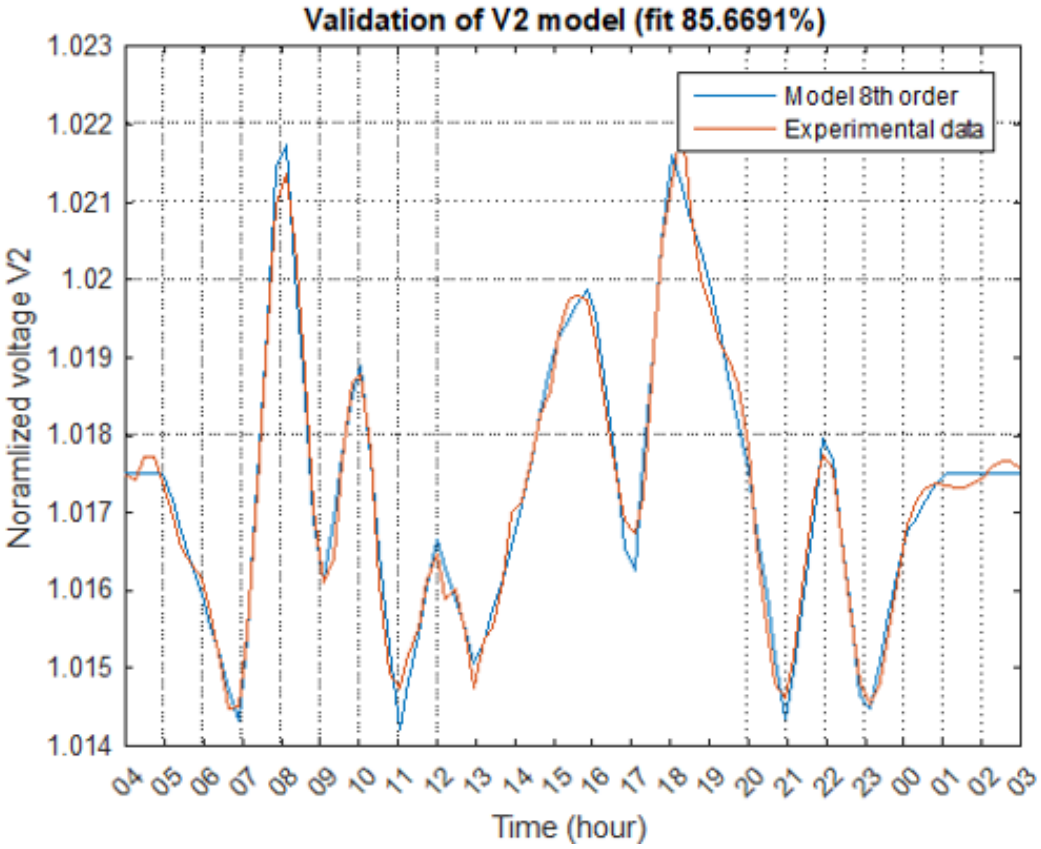

Figure 6.35: Validation with the experimental data V2

Step response of the V2 model with respect to P2 and PV are faster than response to P1 and P3. All reactions present an oscillatory behaviour. The oscillations are highest in the PV channel followed by P3, P2 and P1. Also note positive correlation of V2 to PV and P2 and negative correlation of V2 to P1 and P3. Negative correlation

means that V2 will be dropping when the power consumption in P1 and P3 nodes is increasing. Positive correlation means that V2 will be increasing when PV power is increasing or P2 power consumption is increasing.

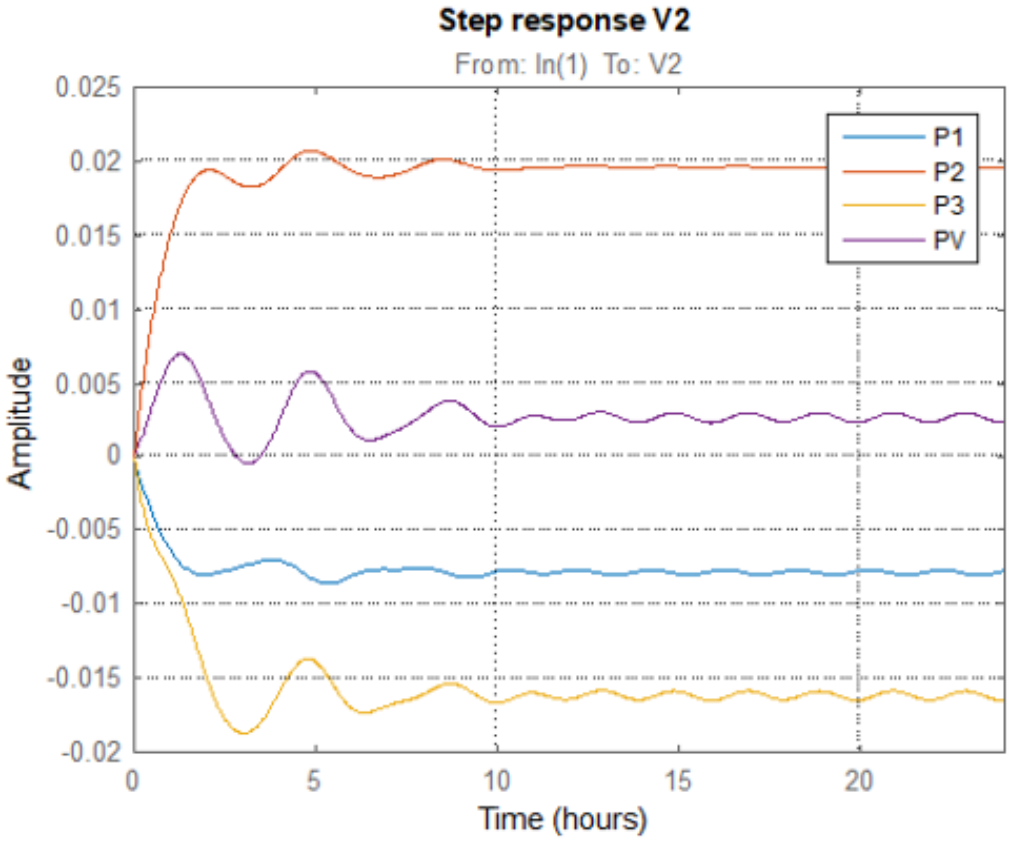

Figure 6.36: Temporal analysis V2 model

There is large immediate reaction of V2 to the P1,P2,P3 and PV inputs due to non-negative values at time 0. The period of the oscillations are quite similar for PV, P3 and P2 channels. Their phase delay is similar, too. The oscillations for the P1 channels are more dampened and more delayed. Generally the response of V2 is quite fast because it depends most heavily mostly on the less than an hour past values of the input channels.

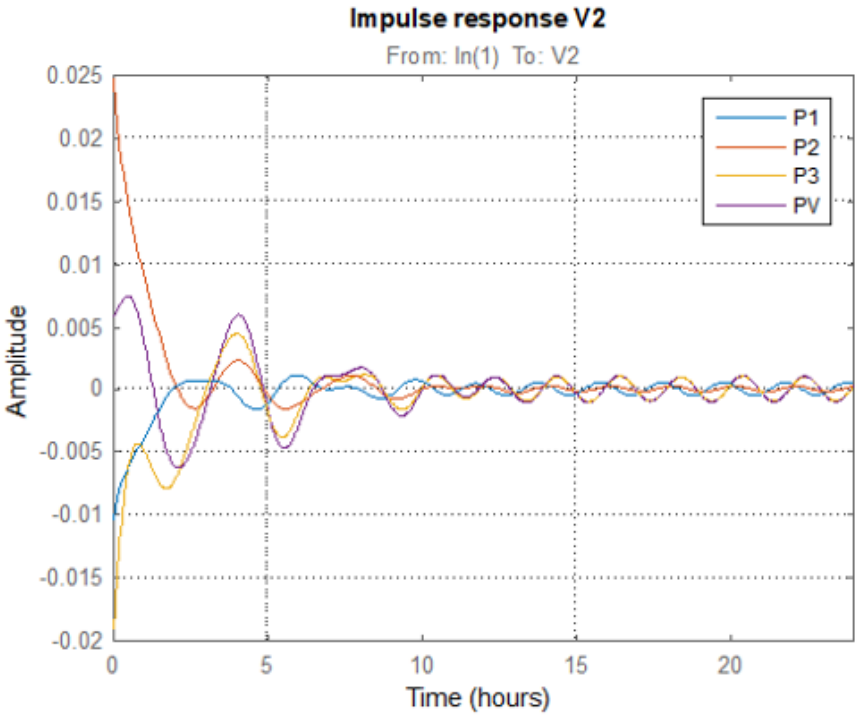

Figure 6.37: Temporal analysis V2 model

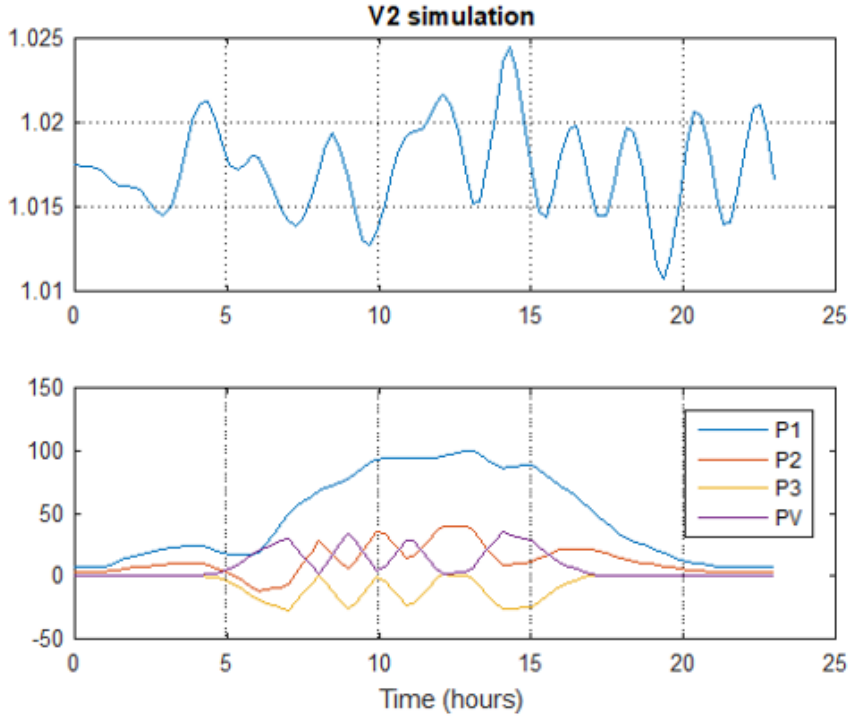

Figure 6.38: Temporal analysis V2 model

The model can be used for simulation of V2 (the upper part of the figure) given the variations in P1, P2, P3 and PV (the lower part of the figure). If you examine the PV signal you can see the variations of the delivered photovoltaic power during the day due to clouds. These variations also are translated in the P2 and P3 signals. Also you can observe the P1 loading profile and the reaction of V2 to all these signals. From the magnitude response we see that the bandwidth of the system is around 10 rad/hr where the sharp drop of the characteristic begins. This makes the V2 channel like 10 times faster than the V1 channel. There are strong resonance of the V2 response at 7 rad/hr as high as 80dB. And there is second smaller resonance at 4 rad/hr. These two resonances predict that the system will be highly oscillatory. The phase response experience large shift around the resonance frequency which means that this resonance is highly localized around a particular frequency.

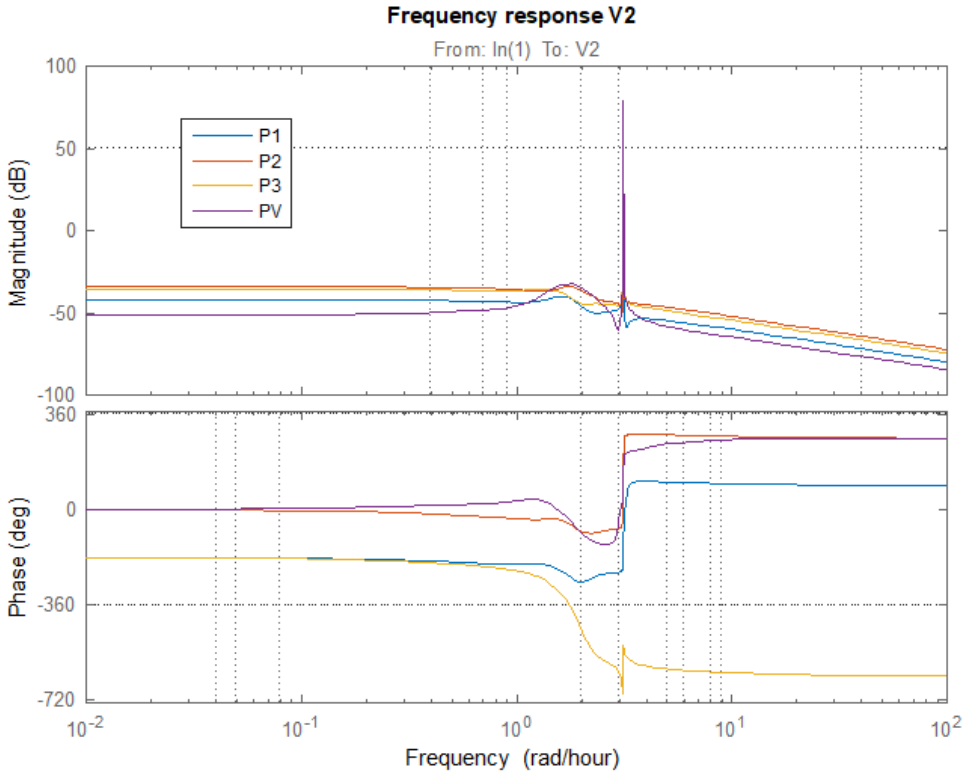

Figure 6.39: Frequency domain analysis of V2 model

All poles and zeros are with negative real parts which means that the system is

exponentially converging and with minimal delay. This is not true only for the P3 channel where there are two zeros in the right side of the imaginary axis but they are very close to it and their effect is compensated by the complementary pair of poles in the left side In all the graphs you can observer that some zeros 'o' and poles 'x' are pretty close which means that their effects counteract each other. This is an indication that it is possible to make model reduction of the model order without considerably degrading its performance. There are uncompensated complementary pair of poles in the PV response which shows that the reaction of V2 to PV will be highly oscillatory which was observed in the impulse and step responses too.

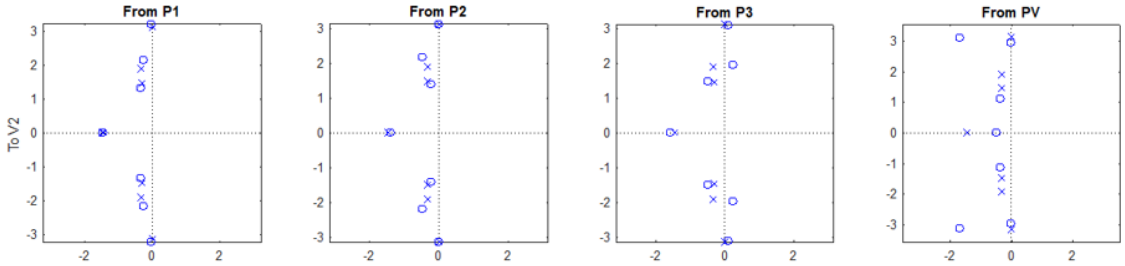

Figure 6.40: Zeros and poles of V2 model

Inputs are P1, P2, P3 and PV. Output is V3. The model is of 8th order. Timebase is hours. The systems have poles close to 0 so it will exhibit integrator-like behavior. The steady state gain between P1 and V3 is -0.04, between P2 and V3 is -0.08, between P3 and V13 is 0.083, between PV and V3 is -0.0005.

$$V_3 = \frac{10^{-3}}{s(s^2+1.3s+1)(s^2+5s+7)(s^2+3s+4)}[$$
$$-40(s+0.9)(s-1.3)(s^2+2s+3)(s^2+3s+14)P_1$$
$$+76(s+1.2)(s-1.3)(s^2+3s+4)(s^2+3s+10)P_2$$
$$-83(s+0.8)(s-1.1)(s^2+3s+4)(s^+3s+13)P_3$$
$$0.5(s-76)(s+1.6)(s^2-0.6s+1.5)(s^2+5s+16)P_{pv}] \quad (6.29)$$

The figure below compares the measured data about V3 with the simulated output from the model given the input data for P1,P2,P3 and PV The value of fit 83% is very high, as we can see the model captures well enough the data variation. The difference between experimental data and the model is due to unobservable signals which are not included in this particular model like Q1, Q2 and Q3. The other reason is reduced model order which I investigated is not big contribution on that difference and the third factor is possibly presence of some nonlinear effects acting on the data from the physical nature of the components in the system. We can see that the approximation is better when the V3 changes and the error is bigger when V3 is trending slowly to a new value.

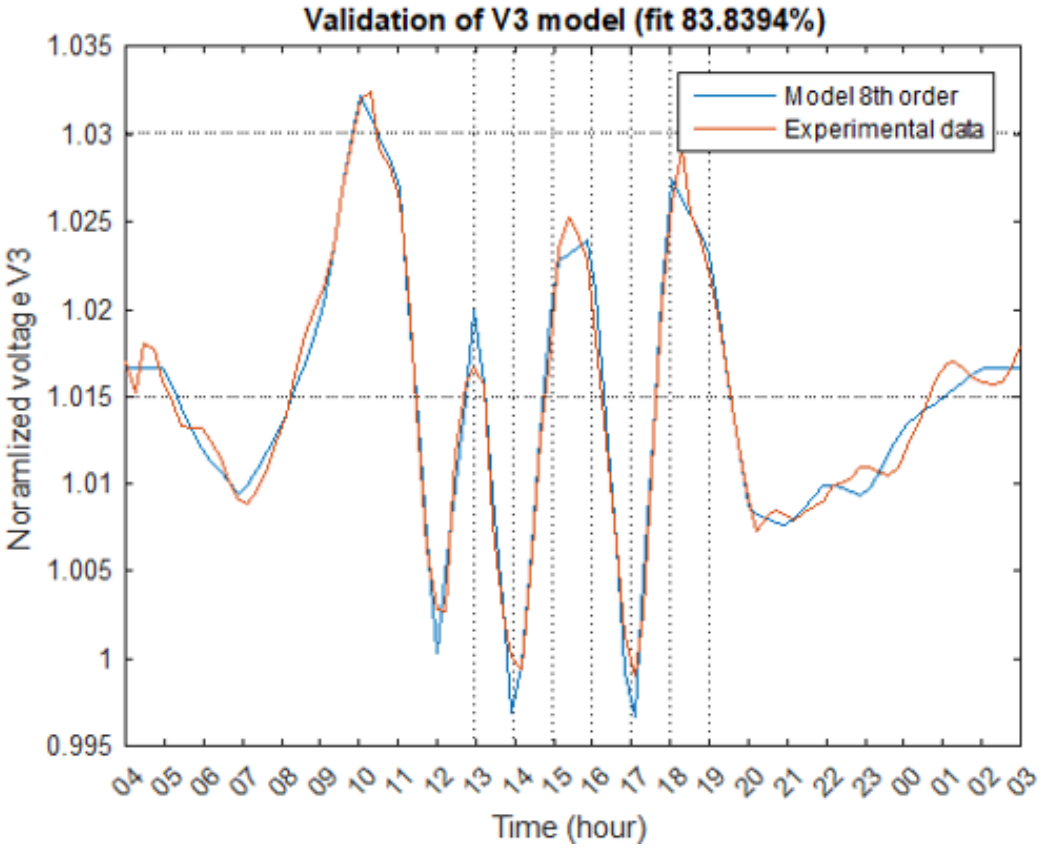

Figure 6.41: Validation with the experimental data V3

Step response of the V3 model with respect to P1, P2, P3 and PV is very slow because of the integrator-like behavior, indicating long term effects in the V3 due to

change in P1,P2,P3 and PV. However this effect might be just an artifact from the model and have to be more investigated. Also note positive correlation of V3 to P1 and P3 and negative correlation of V1 to P2 and PV. Negative correlation means that V1 will be dropping when the power consumption in P2 and PV nodes is increasing. Positive correlation means that V1 will be increasing when PV power is increasing or P2 power consumption is increasing.

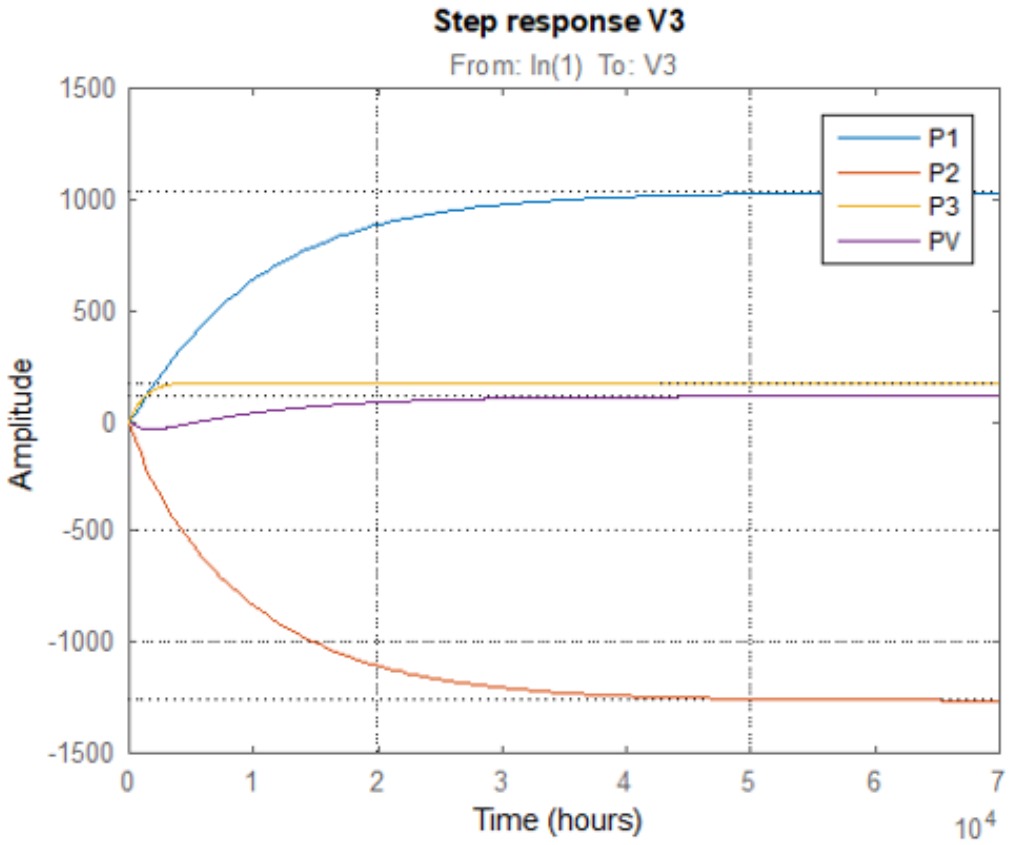

Figure 6.42: Temporal analysis V3 model

There is large immediate reaction of V3 to the P1,P2,P3 and PV inputs due to non-negative values at time 0. The reaction of the V3 is aperiodic without oscillations. Interesting to note that V3 is strongly dependent on all of its inputs P1,P2,P3 and PV.

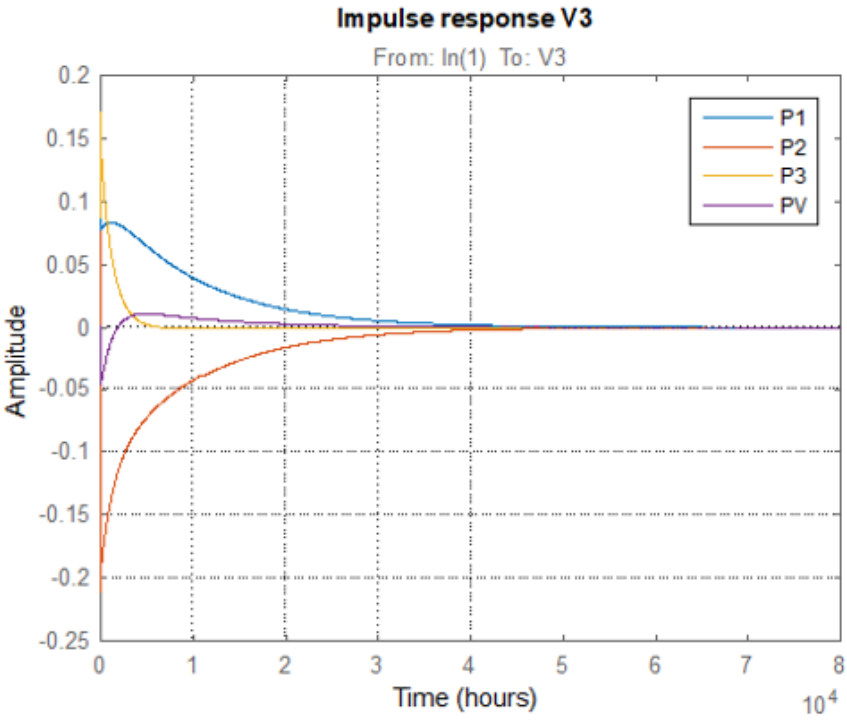

Figure 6.43: Temporal analysis V3 model

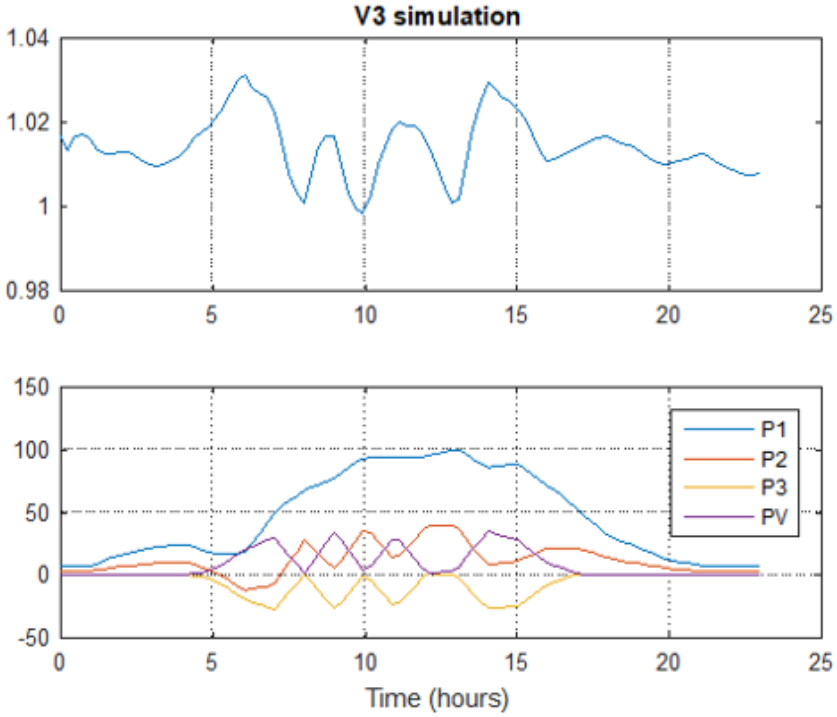

Figure 6.44: Temporal analysis V3 model

The model can be used for simulation of V3 (the upper part of the figure) given the variations in P1, P2, P3 and PV (the lower part of the figure). If you examine the PV signal you can see the variations of the delivered photovoltaic power during the day due to clouds. These variations also are translated in the P2 and P3 signals. Also you can observe the P1 loading profile and the reaction of V3 to all these signals.

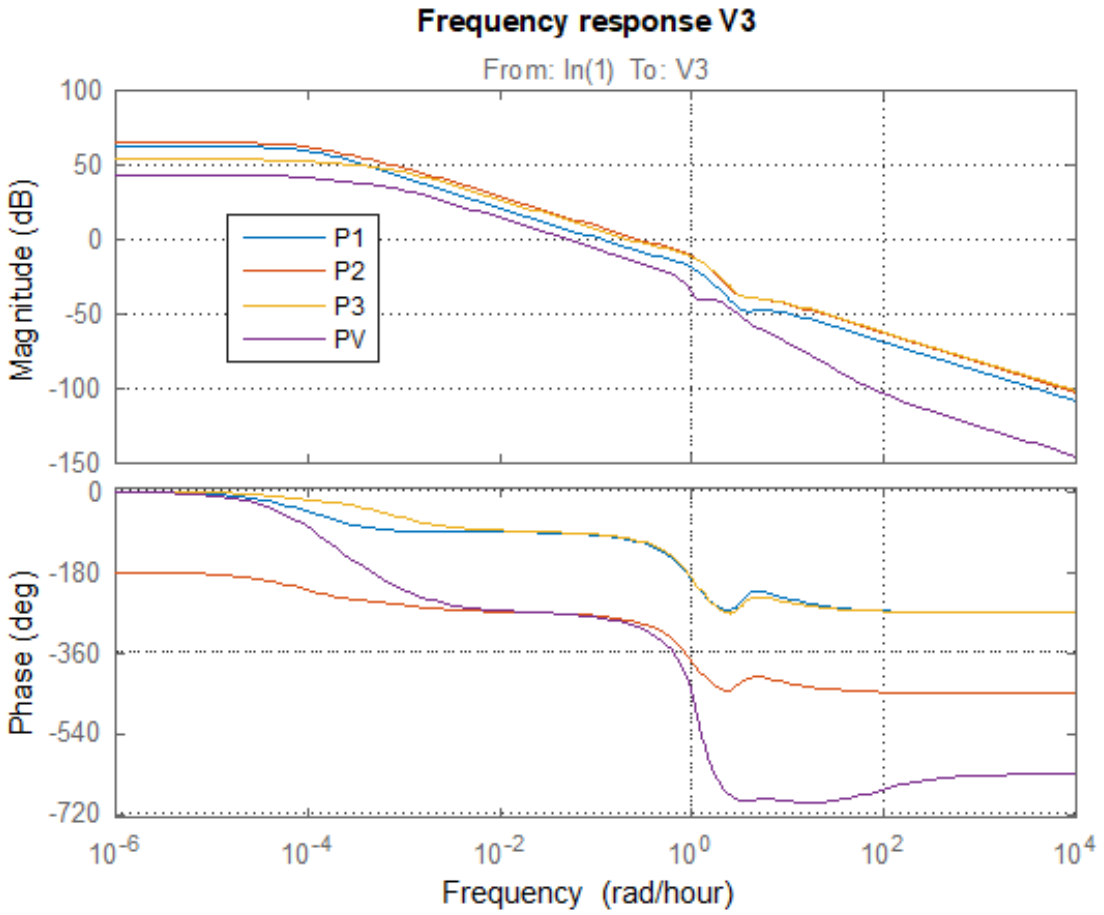

Figure 6.45: Frequency domain analysis of V3 model

From the magnitude response we see that the system has integral behavior with logarithmic responses descending at fixed rate measured in decibels per decade. The response of V3 with respect to PV falls somehow faster than other channels after 1 rad/hr. There are not resonances of the V3 response, except for the slight damping resonance with respect to P1 at about 2 rad/sec. The phase response shows us that

response of the V3 is in phase with three of the channels P1, P3 and PV and with 180deg delay (which means negative correlation) for P2 channel. There is a nonminimal zero (right hand side 'o') in all of the channels. That positive zero is farthest from the imaginary axis for PV channel so the non-minimal (delayed) response of the system will be less strongly pronounced there and even can be neglected. In all the graphs you can observer that some zeros 'o' and poles 'x' are pretty close in P2 and P3 channels which means that their effects counteract each other. There are located poles near the location 0+j0 which is the reason for the integrator like behavior.

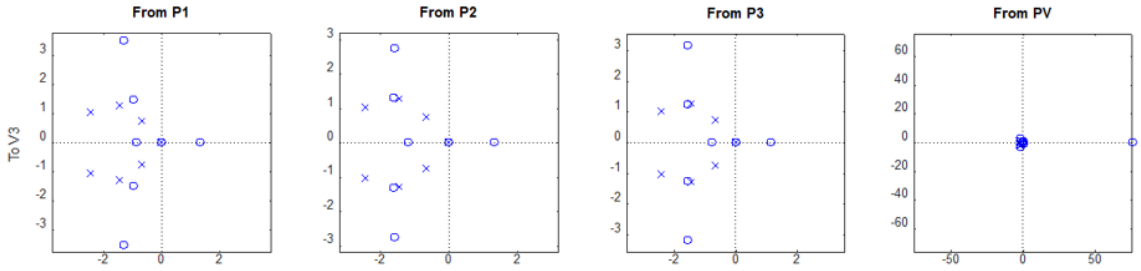

Figure 6.46: Zeros and poles of V3 model

6.6 Symmetric sensitivity model

The vector matrix equation can be represented as

$$V_r(s) = \frac{\sum_{i=1}^{3} B_{r,i}(s)P_i(s) + \sum_{i=1}^{3} C_{r,i}(s)Q_i(s)}{A(s)}, \quad r = 1 \dots 3 \tag{6.30}$$

where the denominator $A(s) = (s + 0.48)(s^2 + 14s + 53)(s^2 + 14s + 55)(s^2 + 15s + 65)$ is a stable fifth order polynomial with one aperiodic and two oscillatory modes. In the numerator with respect to active power we have polynomials $B_{r,i}$ with first index specifying the voltage channel and second index specifying the active power channel. The correlation between V_1 and P_1 is $B_{1,1}(s) = -0.02(s + 0.2)(s + 6)(s^2 + 21s + 115)(s^2 + 1.7s + 5)$, containing two real zeros and two complex zero pairs and having negative static gain. The effect of P_2 upon V_1 is expressed with $B_{1,2}(s) = 0.01(s + 9)(s + 0.8)(s^2 + 0.3s + 2.3)(s^2 + 7.5s + 47)$ with positive static gain. And the

influence of P_3 on V_1 is characterized with $B_{1,3}(s) = 0.07(s+9)(s+0.4)(s^2+0.9s+5.3)(s^2+13s+59)$, which has almost the same zeros as the $B_{1,2}$ but higher static gain. $B_{2,1}(s) = -0.02(s+0.4)(s+6)(s^2+21s+114)(s^2+4s+10)$, representing correlation between V_2 and P_1 which has negative value. Similarly we have other terms:

$$B_{2,2}(s) = 0.01(s+9)(s+1.2)(s^2-0.44s+0.35)(s^2+7.5s+41),$$
$$B_{2,3}(s) = 0.3(s+0.5)(s+0.6)(s^2+4.2s+7.2)(s^2+13s+58),$$
$$B_{3,1}(s) = -0.1(s+6)(s+0.5)(s^2+21s+115)(s^2+5.4s+10),$$
$$B_{3,2}(s) = 0.03(s+9)(s+1.9)(s-0.7)(s+0.3)(s^2+6.7s+31),$$
$$B_{3,3}(s) = 0.3(s+0.5)(s+9)(s^2+4.2s+7.2)(s^2+13s+58),$$
$$C_{1,1}(s) = -0.004(s+55)(s+9)(s^2+0.7s+0.7)(s^2+6.9s+47),$$
$$C_{1,2}(s) = -0.04(s+13)(s+9)(s+4)(s+0.7)(s^2-2.4s+9.6),$$
$$C_{1,3}(s) = -0.06(s-17)(s+13)(s-3)(s+0.5)(s^2+14s+53),$$
$$C_{2,1}(s) = -0.01(s+47)(s+9)(s^2+s+0.7)(s^2+7s+40),$$
$$C_{2,2}(s) = -0.06(s+13)(s+9)(s+4)(s+0.6)(s^2+1.2s+8.6),$$
$$C_{2,3}(s) = -0.7(s+12)(s+0.5)(s^2+14s+53)(s^2-6.7s+13),$$
$$C_{3,1}(s) = -0.01(s+78)(s+9)(s^2+s+0.5)(s^2+5.5s+26),$$
$$C_{3,2}(s) = -0.25(s+13)(s+8.6)(s+3.8)(s+0.5)(s^2+3.9s+6.8),$$
$$C_{3,3}(s) = -0.7(s+12)(s+0.5)(s^2+14s+53)(s^2-0.4s+1.2).$$

6.7 Steady state analysis

Lets examine one of the identified models which has the form

$$\begin{cases} \dot{x} = Ax(t) + Bu(t) \\ y = Cx(t) + Du(t) \end{cases} \tag{6.31}$$

where $y = (\Delta V_1, \Delta V_2, \Delta V_3)^T$ with $\Delta V_i(t) = V_i(t) - V_{i,0}$ with $V_{i,0}$ being the respective bias used to normalize data to obtain better fit during identification ($V_{1,0} = 1.0158$, $V_{2,0} = 1.0175$ and $V_{3,0} = 1.0167$). Also $u = (P_1, P_2, P_3, Q_1, Q_2, Q_3)^T$ with $P_1 =$

$P_{1,load} - P_{pv}$ and $Q_1 = Q_{1,load} - Q_{pv}$. The transfer matrix of the system can be calculated from the state space representation as

$$W(s) = C(sI - A)^{-1}B + D \tag{6.32}$$

In order to obtain the steady state response of the system denoted as K_{ss} we set $t \to \infty$ which is equivalent to setting $s \to 0$. Hence we have steady state gain matrix of the system

$$K_{ss} = \begin{pmatrix} -1.2 & 0.8 & 7.7 & -6.9 & -13.6 & -85.6 \\ -7.4 & 0.2 & 19 & -7.8 & -17.3 & -65 \\ -26.5 & -0.5 & 59.7 & -8.4 & -40.7 & -30.5 \end{pmatrix} \times 10^{-4} \tag{6.33}$$

or equivalently

$$\begin{cases} 10^4 \Delta V_1 = -1.2P_1 + 0.8P_2 + 7.7P_3 - 6.9Q_1 - 13.6Q_2 - 85.6Q_3 \\ 10^4 \Delta V_2 = -7.4P_1 + 0.2P_2 + 19P_3 - 7.8Q_1 - 17.3Q_2 - 65Q_3 \\ 10^4 \Delta V_2 = -26.5P_1 - 0.5P_2 + 59.7P_3 - 8.4Q_1 - 40.7Q_2 - 30.5Q_4 \end{cases} \tag{6.34}$$

In order to calculate the effect on increase of V_i on generated photovoltaic power $P_{pv}(V_i)$ and $Q_{pv}(V_i)$ we may take two approaches - componentwise or matrix which would give different estimates. If we work component wise we have $P_{pv}(V_1) = -10^4(V_1 - V_{1,0})/(-1.2)$ and $Q_{pv}(V_1) = -10^4(V_1 - V_{1,0})/(-6.9)$. Results from these calculations are presented in Table 6.5. Alternative we can find Moore-Penrose generalized inverse of K_{ss} as $L_{ss} = (K_{ss}^T K_{ss})^{-1} K_{ss}^T$ which however for the particular model $(K_{ss}^T K_{ss})^{-1}$ is with not full rank or poor conditioned. One way to solve this is to add a random regularization $\epsilon \in R^{6\times 6}$ or $L_{ss}^*(\epsilon) = (K_{ss}^T K_{ss} + \epsilon)^{-1} K_{ss}^T$.

Table 6.5: PV power with respect to node voltage V_i

V_i	$P_{pv}(V_1)$	$Q_{pv}(V_1)$	$P_{pv}(V_2)$	$Q_{pv}(V_2)$	$P_{pv}(V_3)$	$Q_{pv}(V_3)$
1.00	-134	-23	-24	-22	-6	-20
1.01	-49	-8	-10	-10	-3	-8
1.02	35	6	3	3	1	4
1.03	120	20	17	16	5	16
1.04	204	35	30	29	9	28
1.05	288	49	44	41	13	40

Table 6.6: PV active power with respect to reactive component for $V_i = 1.05$

$Q_{pv}(V_i)$	$P_{pv}(V_1)$	$P_{pv}(V_2)$	$P_{pv}(V_3)$	$Q_{pv}(V_i)$	$P_{pv}(V_1)$	$P_{pv}(V_2)$	$P_{pv}(V_3)$
0	342	46	123	-60	762	115	301
-10	412	58	153	-70	832	126	331
-20	482	69	183	-80	902	138	360
-30	552	81	212	-90	972	149	390
-40	622	92	242	-100	1042	161	420
-50	692	104	272				

The random regularization variable ϵ can be selected to produce L^*_{ss} to give which gives similar magnitudes for $P_{pv}(V_1)$. If we take $|\epsilon| \leq 10^{-10}$ we have

$$L^*_{ss} = \begin{pmatrix} 0.8527 & -1.1111 & 0.2409 \\ -0.6220 & 0.7633 & -0.1697 \\ -0.0090 & 0.0228 & 0.0115 \\ -0.2533 & 0.2841 & -0.0532 \\ -0.5714 & 0.7837 & -0.1730 \\ 0.0814 & -0.1232 & 0.0280 \end{pmatrix} \times 10^4 \tag{6.35}$$

And if we take $V_1 = 1.05$, assuming $V_2 = V_{2,0}$ and $V_3 = V_{3,0}$ we have $L^*_{ss}(V_1 - V_{1,0}, 0, 0)^T$ or $P_{pv}(V_1) = 291$.

Another interesting calculation is to find how PV active power P_{pv} varies when reactive power Q_{pv} is decreased when voltage V_i at node i is elevated. Again we can use componentwise or matrix approach. When using componentwise approach for fixed $V_1 = 1.05$ we have $P_{pv}(V_1) = (10^4 \Delta V_1 - 6.9 Q_{pv})/1.2$. Similarly we can calculate what will be $P_{pv}(V_2) = (10^4 \Delta V_2 - 7.8 Q_{pv})/7.4$ and $P_{pv}(V_3) = (10^4 \Delta V_3 - 8.4 Q_{pv})/26.5$. The results for P_{pv} when Q_{pv} changes from 0 to -100 are presented in Table 6.6 and in Figure 6.47.

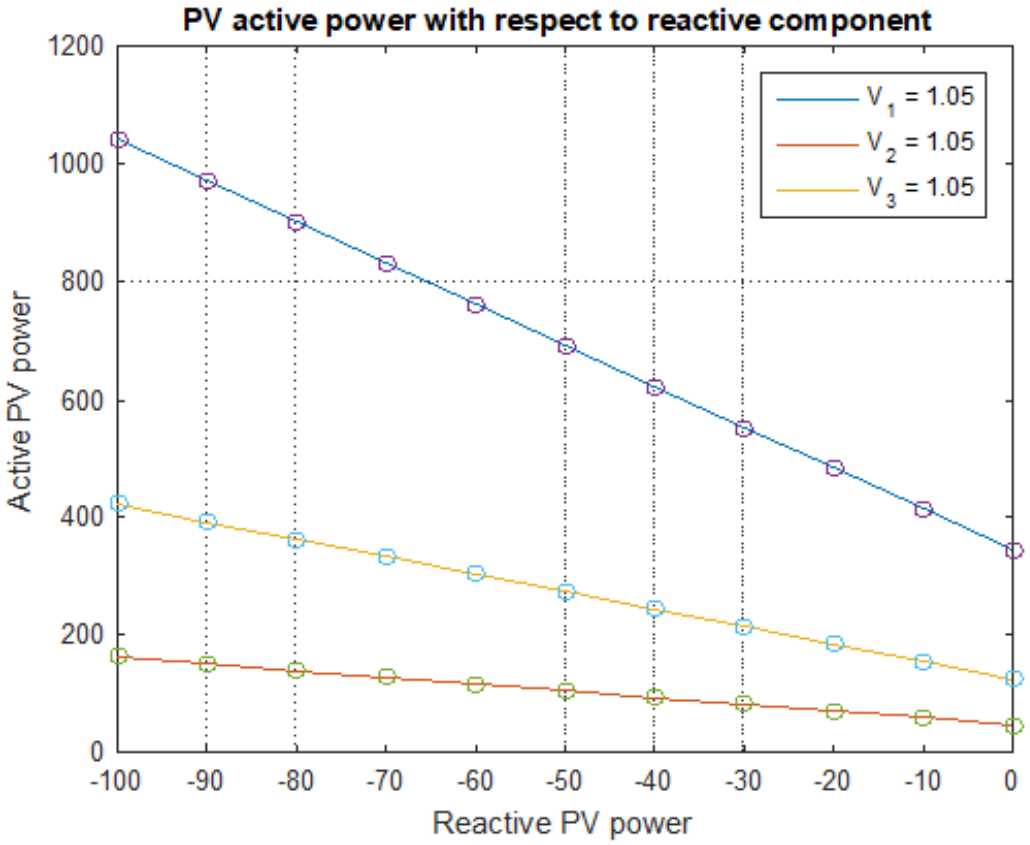

Figure 6.47: PV active power for elevated node voltage

6.8 Summary

In this Chapter a framework for developing parametric models was applied to a complex distribution power grid with DERs and dynamic loads. The eleven step System Identification methodology developed in chapter 5 was used to developed models of a real and much larger distribution system. The static gain model of the system was determined and investigated to obtain a practical understanding of the system under study. These models developed using system identification provided simplified relationships between inputs and outputs. After determining the static gain model auto-regression was used to obtain the dynamic model to fit the changing dynamics of the input and out put data of system. Static gain and auto-regression techniques were used to derive parametric models that allowed the researcher to closely analyze steady-state voltages across the system when collecting measured active and reactive powers. Both step and impulse responses were analyzed to understand system dynamics in the time domain for temporal analysis for changes in load. Model validation and at different model orders were evaluated to determine the optimal order for each section of the feeder.Experimental data from the power flow was used to compare and validate the system responses against transfer function models in a MIMO model comparison.

A critical finding in chapter 6 is the fact that the MIMO transfer function models can be used to simulate any load profile from measured system data. For a given feeder a measured load profile or a constructed load profile can be used to predict the behavior of the system at different DER penetration levels. To further analyze the novel frame work of developing MIMO parametric models a more complex solar generation profile was evaluated. Under this experiment the same system was perturbed by a cloudy day or sporadic solar output.

Lastly, in chapter 6 the state space parametric models calculate the impact of voltage stability from generated photovoltaic active and reactive powers. Holding

voltage steady from 1.00 through 1.05 per unit the models were used to determine the amount of PV that could be added to the system in specific areas of the system. In this case up to 372 kW of active power PV could be added to the system. However, the models were further used to optimize active and reactive power settings to determine the PV that could be added if the plants were allowed to absorb reactive power to keep the voltage rise effect down. Under these condition the more reactive power absorbed by the plnats the more active power could be deployed across the system. At reactive power absorption levels of 100 kvAR, the system deploy over 1600 kW. This framework and model development methodology is an enhancement to current distribution planning methods that allows the planning engineer to maximize the DER penetration levels while maintaining voltage stability at any an all load levels for a given feeder.

CHAPTER 7: CONCLUSIONS AND FUTURE WORK

In this dissertation the researcher has proposed, proven and applied frameworks that enhance distribution planning method using state of the art System Identification modeling techniques that facilitate high growth DERs. The literature review revealed an antiquated distribution planning process with limited methods for the planning engineer to assess the optimal DER penetration levels. Literature review also found that around the USA many DER interconnection requests are denied due to outdated planning methods. New and enhanced distribution planning methods are necessary to meet the coming climate challenges. System identification has rarely been used in the planning space. The one artifact uncovered dealt with rudimentary irradiance and production and did not pose any realizable solution to This work also developed a dynamic impedance modeling and validation of a power network where it was proved that equivalent circuits of power networks can be derived when using a six step procedure is valid for all load levels using classic power flow n that power networks can be analyzed. In addition, this research effort coupled circuit analysis with the Newton Raphson power flow iterative technique to derive the Bus Admittance Matrix to analyze and dynamically model radial power distribution systems. The power flow equations were explicitly used to uncover and highlight the issue of voltage stability created by active power injections on a radial system.

Moreover, this work performed sensitivities about power system response to perturbations caused by DER active power injections. The grey box system identification process was used to develop approximate models of a small random power system to identify the observability and controllability of the system. These dynamical models were constructed from observed input and output data. The step by step method-

ology for System Identification was successful in creating approximate parametric models used to predict system response. Lastly and more importantly the System Identification process was scaled up and applied to a larger and real power system. The parametric models identified using the new System Identification framework were validated under varying load levels and system conditions from sunny days with maximum output to cloudy days with variable output. Furthermore, these models were used to find the optimal DER deployment on a real power network at varied levels and combinations of active and reactive power. These unprecedented findings provide the planning engineer the with a tool to identify optimal DER deployment levels and settings on any distribution network. This work make the following contributions to the planning of electric power distribution systems:

- A dynamic impedance modeling and validation framework for an electric power distribution network
- Framework to develop and validate parametric models of power networks on a large scale for use in the distribution planning process
- Demonstrate that aggregate transfer functions for larger power networks can be derived using system identification
- Proven framework that can be leveraged and trusted to understand the effects of DERs on power system voltage and various operating states and load levels.

The above contributions are valuable in that up until now changes in how the electric distribution system in planned and designed have been slow. Most conservative deterministic planning methods have been used. This work proffers an enhancement that leverages the proven traditional deterministic planning methods and pares them with new modeling techniques used in other fields such as aviation. The application of System Identification techniques in distribution planning will help electric

utility companies deploy an increased amount of carbon free DERs without risking system reliability or voltage instability. With the use of parametric models or Grey Box Modeling, this work proves that planning of the electric distribution system can evolve from deterministic planning to more probabilistic planning methods based on validated parametric models based on System identification.

While the contributions of this work are novel and impactful there is considerable work that can be done in the future to improve upon these efforts. For example, this work is based on the assumption of a three-phase balanced system. The framework developed here can be applied to single phase or double phase parts of the system. More detailed parametric models can be developed and aggregated to study any part or parts of the system. More granularity can be developed at the head, middle and ends of the system. For example, boundaries can be drawn around any part of the system the framework can be re-applied to a smaller sub-section for planning purposes to determine the need for DERs, feeder upgrades or microgrid considerations. Secondly, this framework can be used to identify possible microgrid applications or further used to analyze microgrids under steady state conditions based on actual or constructed load profiles. The possibility of microgrid applications became evident when the parametric models were used to optimize DER deployment at different voltage levels. Holding the voltage steady limited reverse power flow and required that reactive power be supplied locally. In essence and ideally, distributions systems could be studied and designed to operate as mini balancing authorities (MBAs), theoretically with both scheduled and inadvertent power exchanges between the MBAs. Thirdly, future work could involve using the parametric models to analyze the impact of DER deployments on the transmissions systems. There may be a way to use aggregate transfer function models to determine the optimal amount of back-flow or reactive power resources necessary to maintain transmission system reliability under high penetrations scenarios. Lastly, this work can be used to uncover a or possi-

bly design a distribution market for primary or ancillary services. Given that the parametric models developed and validated here are principled on the physics that changes in voltage are accompanied by changes in active and reactive powers based on location, positive or negative cost values can be assigned to changes in voltages or powers. For example, if a part of the distribution system has a low and unstable voltage say below 0.95 per unit, theoretically a dollar value could be assigned to a DER that has the ability to regulate voltage up. The same holds true for a high voltage scenario, a DER capable of lowering the voltage by absorbing vars can also be compensated for each system or locational per unit increment.

The contributions made here are both impactful and achievable, and represent an enhancement to existing and outdated distribution planning processes that currently exist. In order to make a carbon free future more than just aspirational, adopting these enhancements into the day-to-day distribution planning process is necessary for realizing a modern grid. In addition to the contributions of this research being achievable in the near term, the work is foundational in that future work in the power systems space can be based on the state of the art modeling principles of system identification.

REFERENCES

[1] D. Manz, R. Walling, N. Miller, B. LaRose, R. D\textquotesingleAquila, and B. Daryanian, "The Grid of the Future: Ten Trends That Will Shape the Grid Over the Next Decade," *{IEEE} Power and Energy Magazine*, vol. 12, pp. 26–36, may 2014.

[2] R. Messenger and A. Abtahi, *Photovoltaic Systems Engineering, Third Edition*. 2010.

[3] "Solar industry research data." http://www.seia.org/research-resources/solar-industry-data. Accessed: 2020-11-11.

[4] E. Tnne, J. A. Foosns, and T. Pynten, "Power system planning in distribution networks today and in the future with smart grids," in *22nd International Conference and Exhibition on Electricity Distribution ({CIRED} 2013)*, Institution of Engineering and Technology, 2013.

[5] J. A. Momoh, "Smart grid design for efficient and flexible power networks operation and control," in *2009 IEEE/PES Power Systems Conference and Exposition, PSCE 2009*, 2009.

[6] R. E. Brown and H. L. Willis, "The economics of aging infrastructure," *{IEEE} Power and Energy Magazine*, vol. 4, pp. 36–43, may 2006.

[7] P. S. C. O. T. D. O. COLUMBIA, "Formal Case No. 1119, The Merger Application of Exelon Corporation, Pepco Holdings, Inc., Potomac Electric Power Company, Exelon Energy Delivery Company, LLC and New Special Purpose Entity, LLC,," 2015.

[8] B. Wojszczyk and M. Brandao, "High penetration of distributed generation and its impact on electric grid performance - utility perspective," in *2011 {IEEE} {PES} Innovative Smart Grid Technologies*, IEEE, nov 2011.

[9] M. O. W. Grond, J. Morren, and J. G. Slootweg, "Integrating smart grid solutions into distribution network planning," in *2013 {IEEE} Grenoble Conference*, IEEE, jun 2013.

[10] T. M. Taylor, "New considerations for distribution network planning and design," in *14th International Conference and Exhibition on Electricity Distribution ({CIRED} 1997 - Distributing Power for the Millennium)*, IEE, 1997.

[11] H. L. Willis, *Power Distribution Planning Reference Book, Second Edition*. {CRC} Press, mar 2004.

[12] I. Ziari, G. Ledwich, A. Ghosh, and G. Platt, "Integrated Distribution Systems Planning to Improve Reliability Under Load Growth," *{IEEE} Transactions on Power Delivery*, vol. 27, pp. 757–765, apr 2012.

[13] Y. Zhou and J. H. Spare, "Optimizing Reliability Project Portfolios for Electric Distribution Companies," in *2007 {IEEE} Power Engineering Society General Meeting*, IEEE, jun 2007.

[14] Regulatory Assistance Project, "Electricity Regulation in the US: A Guide," *Regulatory Assistance Project*, p. 130, 2011.

[15] J. P. Tomain, "The Past and Future of Electricity Regulation," *Environmental Law*, vol. 32, no. 2, pp. 435–474, 2002.

[16] U.S. Environmental Protection Agency Combined Heat and Power Partnership, "Catalog of CHP Technologies: Sectopm 6. Technology Characterization - Fuel Cells," tech. rep., 2015.

[17] U. D. of Energy, "Grid Energy Storage," tech. rep., 2013.

[18] "Fuel Cells | U.S. Department of Energy." https://www.energy.gov/eere/fuelcells/fuel-cells. Accessed: 2020-09-23.

[19] Fan Zhang and C. S. Cheng, "A modified newton method for radial distribution system power flow analysis," *IEEE Transactions on Power Systems*, vol. 12, no. 1, pp. 389–397, 1997.

[20] R. A. Messenger and A. Abtahi, *Photovoltaic systems engineering*. CRC press, 2017.

[21] E. Ikonen and K. Najim, *Advanced Process Identification and Control*. Marcel Dekker, Inc., 2002.

[22] N. Pettit, *Analysis of piecewise linear dynamical systems*. UMIST Control Systems Centre series, Research Studies Press, 1995.

[23] Y. Lin, *General Systems Theory: A Mathematical Approach*. IFSR International Series on Systems Science and Engineering, Springer US, 2006.

[24] R. Isermann and M. Munchhof, *Identification of Dynamic Systems*. Springer, 2011. An Introduction with Applications.

[25] R. Isermann, *Mechatronic Systems*. Springer, 2005.

[26] T. Kailath, *Linear Systems*. Prentice-Hill,Inc., 1980.

[27] L. Ljung, *System Identification: Theory for the User*. Prentice-Hall, 1999.

[28] G. Goodwin, S. Graebe, and M. Salgado, *Control System Design*. Upper Saddle River, NJ: Prentice Hall, 2001.

[29] A. Kolmogorov and S. Fomin, *Elements of the Theory of Functions and Functional Analysis*. Graylock Press, 1961.

[30] N. Bhatia and G. Szegö, *Stability Theory of Dynamical Systems*. Classics in Mathematics, Springer Berlin Heidelberg, 2002.

[31] K. Moudgalya, *Digital Control*. John Wiley & Sons, Ltd, 2007.

[32] S. K. Khator and L. C. Leung, "Power distribution planning: a review of models and issues," *{IEEE} Transactions on Power Systems*, vol. 12, no. 3, pp. 1151–1159, 1997.

[33] T. Basso, "{IEEE} 1547 and 2030 Standards for Distributed Energy Resources Interconnection and Interoperability with the Electricity Grid," tech. rep., dec 2014.

[34] M. Amirabadi, H. T. . I. E. Conversion, and undefined 2012, "A new class of PV inverters: Series partial resonant converters," *ieeexplore.ieee.org*.

[35] District of Columbia Public Service Commission, "Distribution planning and design criteria for pepco holdings inc. district of columbia, distribution planning department," tech. rep., 2014.

[36] LLC, "Formal case no. 1119, the merger application of exelon corporation, pepco holdings, inc., potomac electric power company, exelon energy delivery company, llc and new special purpose entity," tech. rep., 2016.

[37] B. Boulet and Y. Duan, "The Fundamental Tradeoff Between Performance and Robustness," *IEEE Control Systems Magazine*, 2007. A new perspective on loop shaping.

[38] D. Warne, *Newnes Electrical Power Engineer's Handbook*. Elsevier Science, 2005.

[39] H. Pender, *Electricity and Magnetism for Engineers: Electric and magnetic circuits*. Electricity and Magnetism for Engineers, McGraw-Hill book Company, Incorporated, 1918.

[40] H. Kwatny and G. Blankenship, *Nonlinear Control and Analytical Mechanics: A Computational Approach*. No. v. 1 in Control Engineering - Birkhäuser, Birkhäuser Boston, 2000.

[41] W. Greiner, *Quantum Mechanics: An Introduction*. Physics and Astronomy, World Books Publishing Corporation, 2001.

[42] C. Isham, *Modern Differential Geometry for Physicists*. Allied Publ., 2002.

[43] S. Wiggins, *Introduction to Applied Nonlinear Dynamical Systems and Chaos*. Texts in Applied Mathematics, Springer New York, 2013.

[44] J. Webster and H. Eren, *Measurement, Instrumentation, and Sensors Handbook, Second Edition: Spatial, Mechanical, Thermal, and Radiation Measurement*. Measurement, instrumentation, and sensors handbook, Taylor & Francis, 2014.

[45] C. Chen, *Analog and Digital Control System Design.* Saunders College Publishing, 2000. Transfer-Function, State-Space, and Algebraic Methods.

[46] N. Wiener, *Cybernetics Or Control and Communication in the Animal and the Machine.* The MIT paperback series: Massachusetts Institute of Technology, M.I.T. Press, 1961.

[47] G. Chartrand, *Introductory Graph Theory.* Dover Books on Mathematics, Dover Publications, 2012.

[48] H. Simon, "The Architecture of Complexity," *Proceedings of the Americal Philosophical Society*, vol. 106,6, pp. 467–482, 1962.

[49] K. Aström and R. Murray, *Feedback Systems: An Introduction for Scientists and Engineers.* Princeton University Press, 2010.

[50] S. Ingram and A. Attoui, *Real-Time and Multi-Agent Systems.* Practitioner Series, Springer London, 2012.

[51] IEEE, *Standard for Binary Floating-Point Arithmetic*, 1987. Reprinted in SIGPLAN 22, 2, 9-25.

[52] R. Hartley, "Transmission of information," *Time and Identity: Topics in Contemporary Philosophy*, vol. 6, 2008.

[53] NASA Headquarters, *Systems Engineering Handbook.* NASA, 2007. SP-2007-6105 Rev1.

[54] B. Goldberg, K. Everhart, and R. Stevens, *System Engineering Ťoolboxf́or Design-Oriented Engineers.* NASA, 1994.

[55] W. Greblicki and M. Pawlak, *Nonparametric System Identification.* Cambridge University Press, 2008.

[56] M. Grewal and A. Andrews, *Kalman Filtering: Theory and Practice, 2ed.* John Wiley Sons, Inc., 2001. Using MATLAB.

[57] O. Staffans, *Well-Posed Linear Systems.* Cambridge University Press, 2005.

[58] A. Papoulis, *Probability, Random Variable, and Stochastic Processes.* McGraw-Hill, 1991.

[59] B. Sklar, *Digital Communications, 2nd ed.* Prentice-Hall, Englewood Cliffs, 2001.

[60] U.S. Department of Energy, *Instrumentation and Control.* DOE, 1992. DOE Fundamentals Handbook.

[61] N. Anderson, *Instrumentation for process measurement and control 3 ed.* CRC Press, 1998.

[62] C. Kilian, *Modern Control Technology: Components and Systems 3ed.* Delmar/Thomson Learning, 2006.

[63] J. Anderson, *Digital Transmission Engineering.* Wiley-IEEE Press, 2005.

[64] E. Sontag, *Mathematical Control Theory 2ed.* Springer, 1998. Deterministic Finite Dimensional Systems.

[65] J. Lunze and F. Lamnabhi-Lagarri, *Handbook of Hybrid Systems Control.* Cambridge University Press, 2009.

[66] R. Dorf and R. Bishop, *Modern Control Systems 11ed.* Prentice Hall, 2008.

[67] R. Ash, *Information Theory.* Courier Corporation, 1965.

[68] P. Antsaklis and A. Michel, *Linear Systems.* Birkhauser, 2006.

[69] D. S. Naidu, *Optimal Control Systems.* Electrical Engineering Textbook Series, CRC Press, 2003.

APPENDIX A: MATLAB codes

A.1 Analysis of daily profile in sunny day

First load the data as MATLAB array and then interpolate for 15 min sample time. The data are provided from the excel sheet as normalized values with the nominal voltage and power. The P_1 term is divided into generating $P_{1,load}$ and load $P_{1,pv}$ terms.

```
% V1 V2 V3 P1_load P1_pv P1 P2 P3 Q1 Q2 Q3
data = [
1.0158 1.0175 1.0167 7.38 0 7.43 -14.22 3.22 -0.19 0.27 0.02
...
1.0158  1.0175 1.0167 7.38 0 7.43 -14.22 3.22 -0.19 0.27 0.02];

Ts_base = 1; % one hour sample time
Ts = 0.25; % 15 min sample time
N = size(data,1)/Ts*Ts_base; % interpolation length
t = (0:Ts_base:size(data,1)*Ts_base-Ts_base)';
t1 = (linspace(0,size(data,1)*Ts_base-Ts_base,N))';
V1_ = interp1(t,data(:,1),t1);
V2_ = interp1(t,data(:,2),t1);
V3_ = interp1(t,data(:,3),t1);
P1_load_ = interp1(t,data(:,4),t1);
P1_pv_ = interp1(t,data(:,5),t1);
P1_ = interp1(t,data(:,6),t1);
P2_ = interp1(t,data(:,7),t1);
P3_ = interp1(t,data(:,8),t1);
Q1_ = interp1(t,data(:,9),t1);
Q2_ = interp1(t,data(:,10),t1);
Q3_ = interp1(t,data(:,11),t1);
```

Listing A.1: Loading data and interpolation

As you can see here we subtract the initial voltage which acts as a bias for the model operating point.

```
dati_1 = iddata([P2_],[P1_load_ V1_ P1_pv_],Ts,'TimeUnit','hours');
dati_1.InputName = {'P1','V1','PV'};
dati_1.OutputName = {'P2'};

dati_2 = iddata([V2_-V2_(1)],[P1_load_ P2_ P3_ P1_pv_],Ts,'TimeUnit'
    ,'hours');
dati_2.InputName = {'P1','P2','P3','PV'};
dati_2.OutputName = {'V1'};

dati_3 = iddata([V3_-V3_(1)],[P1_load_ P2_ P3_ P1_pv_],Ts,'TimeUnit'
    ,'hours');
dati_3.InputName = {'P1','P2','P3','PV'};
dati_3.OutputName = {'V1'};
```

Listing A.2: Create MATLAB data objects and name their ports

```
opt = greyestOptions;
opt.SearchMethod = 'lm';
opt.InitialState = 'zero';
opt.Focus = 'simulation';
opt.SearchOption.MaxIter = 100; % can change this
opt.Display = 'on';

a_vec = -ones(1,5)*0.1;
b_vec = ones(1,15)*0.1;
c_vec = ones(1,5)*0.1;
model_ss_1 = idgrey('power_sys_v2_p1v1pv',{a_vec,b_vec,c_vec},'c'
    ,{},0);
model_ss_1.TimeUnit = 'hours';
model_ss_1 = greyest(dati_1,model_ss_1,opt);

compare(model_ss_1,dati_1);
```

Listing A.3: Estimate graybox model for V_1

```
a_vec = -(1:7)*0.2; %-ones(1,7)*1e-3;
b_vec = (1:28)*0.1; %ones(1,28)*1e-3;
c_vec = (1:7)*0.1; %ones(1,7)*1e-3;
model_ss_2 = idgrey('power_sys_v3_mimo',{a_vec,b_vec,c_vec},'c'
    ,{},0);
model_ss_2.TimeUnit = 'hours';
model_ss_2 = greyest(dati_2,model_ss_2,opt);
```

Listing A.4: Estimate graybox model for V_2

```
a_vec = -ones(1,5)*0.1;
b_vec = ones(1,20)*0.1;
c_vec = ones(1,5)*0.1;
model_ss_3 = idgrey('power_sys_v2_mimo',{a_vec,b_vec,c_vec},'c'
    ,{},0);
model_ss_3.TimeUnit = 'hours';
model_ss_3 = greyest(dati_3,model_ss_3,opt);
```

Listing A.5: Estimate graybox model for V_3

```
xlabels = {'04','05','06','07','08','09','10','11',...
           '12','13','14','15','16','17','18','19',...
           '20','21','22','23','00','01','02','03'};
xticks = 0:23; % 24 hour ticks
[yh,yfit,~] = compare(model_ss_1,dati_1);
figure(1);
plot(t1,V1_,t1,yh.y+V1_(1));
set(gca,'XTick',xticks,'XTickLabel',xlabels,'XTickMode','manual','
    XTickLabelRotation',45,'XLimMode','manual','XLim',[0,23]);
grid;
title(['Validation of V1 model (fit ',num2str(yfit),'%)']);
legend('Model 5th order','Experimental data');
xlabel('Time (hour)');
```

```
ylabel('Noramlized voltage V1');
```

Listing A.6: Plot comparison between experimental and model data for V_1

```
figure(2);
step(model_tf_1(1,1),model_tf_1(1,2),model_tf_1(1,3),model_tf_1(1,4)
    ,24);
title('Step response V1');
legend('P1','P2','P3','PV');
grid;
```

Listing A.7: Plot the step responses of V_1 with respect to inputs

```
figure(3);
impulse(model_tf_1(1,1),model_tf_1(1,2),model_tf_1(1,3),model_tf_1
    (1,4),24);
title('Impulse response V1');
legend('P1','P2','P3','PV');
grid;
```

Listing A.8: Plot the impulse responses of V_1 with respect to inputs

```
figure(4);
bode(model_tf_1(1,1),model_tf_1(1,2),model_tf_1(1,3),model_tf_1(1,4)
    );
title('Frequency response V1');
legend('P1','P2','P3','PV');
grid;
```

Listing A.9: Plot magnitude and phase frequency responses of V_1 with respect to inputs

```
% six hours simulation
v1_sim = lsim(model_ss_1,[P1_load_ P2_ P3_ P1_pv_],t1);


figure(5);
```

```
subplot(2,1,1);
plot(t1,v1_sim+V1_(1));
grid;
title('V1 simulation');
subplot(2,1,2);
plot(t1,[P1_load_ P2_ P3_ P1_pv_]);
legend('P1','P2','P3','PV');
grid;
xlabel('Time (hours)');

eig(model_ss_1)
```

Listing A.10: Plot simulated response of V_1 with respect to custom inputs

Figures for V_2 and V_3 are plotted with analogical commands.

A.1.1 Graybox model structures described as MATLAB functions

A general state space structure in continuous time is given with the following equation. The state space model is most universal structure in linear control system theory, because can describe any system of ordinary differential equations in a vector matrix form.

$$\begin{cases} \dot{x}(t) = Ax(t) + Bu(t) \\ y(t) = Cx(t) + Du(t) \end{cases}, \tag{A.1}$$

where $A \in \mathbf{R}^{N \times N}$, $B \in \mathbf{R}^{N \times N_u}$, $C \in \mathbf{R}^{N_y \times N}$ and $D \in \mathbf{R}^{N_y \times N_u}$ are matrices with proper dimensions.The N is number of hidden states, N_y is the number of output signals which for example can be the node voltages V_1, V_2 and V_3, and N_u is the number of input signals which for example can be the note power magnitudes P_1, P_2 and P_3. Of course the inputs and outputs can be different quantities depending on the purpose of the analysis.

```
function [A,B,C,D] = power_sys_v2_p1v1pv(a_vec,b_vec,c_vec,Ts)
A = [a_vec(1) 0         0         0         0
```

```
     0         a_vec(2) 0         0         0
     0         0         a_vec(3) 0         0
     0         0         0         a_vec(4) 0
     0         0         0         0         a_vec(5)];
B = reshape(b_vec,5,3);
C = reshape(c_vec,1,5);
D = zeros(1,3);
```

Listing A.11: Fifth order model with real poles

```
function [A,B,C,D] = power_sys_v4_mimo(a_vec,b_vec,c_vec,Ts)
A = [a_vec(1) 0 0 0 0 0 0 0
     0 a_vec(2) 0 0 0 0 0 0
     0 0 a_vec(3) -a_vec(4) 0 0 0 0
     0 0 a_vec(4) a_vec(3) 0 0 0 0
     0 0 0 0 a_vec(5) -a_vec(6) 0 0
     0 0 0 0 a_vec(6) a_vec(5) 0 0
     0 0 0 0 0 0 a_vec(7) -a_vec(8)
     0 0 0 0 0 0 a_vec(8) a_vec(7)];
B = reshape(b_vec,8,4);
C = reshape(c_vec,1,8);
D = zeros(1,4);
```

Listing A.12: Eight order model with two real poles and three complex pole pairs

```
function [A,B,C,D] = power_sys_v3_mimo(a_vec,b_vec,c_vec,Ts)
A = [a_vec(1) 0 0 0 0 0 0
     0 a_vec(2) -a_vec(3) 0 0 0 0
     0 a_vec(3) a_vec(2) 0 0 0 0
     0 0 0 a_vec(4) -a_vec(5) 0 0
     0 0 0 a_vec(5) a_vec(4) 0 0
     0 0 0 0 0 a_vec(6) -a_vec(7)
     0 0 0 0 0 a_vec(7) a_vec(6)];
B = reshape(b_vec,7,4);
C = reshape(c_vec,1,7);
```

```
D = zeros(1,4);
```

Listing A.13: Seventh order model with one real pole and three complex pole pairs

```
function [A,B,C,D] = power_sys1(a_vec,b_vec,c_vec,Ts)
A = [a_vec(1) a_vec(2) 0         0         0
     a_vec(3) a_vec(4) 0         0         0
     0        0        a_vec(5) 0         0
     0        0        0        a_vec(6) 0
     0        0        0        0         a_vec(7)];
B = reshape(b_vec,5,6);
C = reshape(c_vec,3,5);
D = zeros(3,6);
```

Listing A.14: Fifth order model with three real poles and one complex pole pair

```
function [A,B,C,D] = power_sys(a_vec,b_vec,c_vec,d_vec,Ts)
A = a_vec;
B = b_vec*ones(1,6);
C = reshape(c_vec,3,1);
D = reshape(d_vec,3,6);
```

Listing A.15: Sixth order model with free parametrization

A.2 Matlab Code for Error Calculation at Varying Load Levels

```
close all
clear all
load percent = [];
error_percent = [];
prompt={'%Load level','S1:','S2:','S3','V1','V2','V3'};
name='Input for parameters';
numlines=1;
defaultanswer={'50', '436 - 473j','174 - 267j','90 + 41j',...
'4.4e3','4.4e3', '4.5e3'};
answer=inputdlg(prompt,name,numlines,defaultanswer);
```

```
temp = str2num(answer{1});
load_percent = [load_percent temp];
S1 = str2num(answer{2});
S2 = str2num(answer{3});
S3 = str2num(answer{4});
V1 = str2num(answer{5});
V2 = str2num(answer{6});
V3 = str2num(answer{7});
error = error_calculation(S1, S2, S3, V1, V2, V3);
error_percent = [error_percent error];
prompt={'%Load level','S1:','S2:','S3','V1','V2','V3'};
name='Input for parameters';
numlines=1;
defaultanswer={'75' '650 - 343j','259 - 215j','90 + 41j',...
'4.4e3','4.3e3', '4.4e3'};
answer=inputdlg(prompt,name,numlines,defaultanswer);
temp = str2num(answer{1});
load_percent = [load_percent temp];
S1 = str2num(answer{2});
S2 = str2num(answer{3});
S3 = str2num(answer{4});
V1 = str2num(answer{5});
V2 = str2num(answer{6});
V3 = str2num(answer{7});
error = error_calculation(S1, S2, S3, V1, V2, V3);
error_percent = [error_percent error];
prompt={'%Load level','S1:','S2:','S3','V1','V2','V3'};
name='Input for parameters';
numlines=1;
defaultanswer={'100' '869 - 200j','345 - 160j','120 + 55j',...
'4.4e3','4.3e3', '4.3e3'};
answer=inputdlg(prompt,name,numlines,defaultanswer);
temp = str2num(answer{1});
```

```
load_percent = [load_percent temp];
S1 = str2num(answer{2});
S2 = str2num(answer{3});
S3 = str2num(answer{4});
V1 = str2num(answer{5});
V2 = str2num(answer{6});
V3 = str2num(answer{7});
error = error_calculation(S1, S2, S3, V1, V2, V3);
error_percent = [error_percent error];
prompt={'%Load level','S1:','S2:','S3','V1','V2','V3'};
name='Input for parameters';
numlines=1;
defaultanswer={'105' '914 - 171j','363 - 149j','126 + 57j',...
'4.4e3','4.2e3', '4.2e3'};
answer=inputdlg(prompt,name,numlines,defaultanswer);
temp = str2num(answer{1});
load_percent = [load_percent temp];
S1 = str2num(answer{2});
S2 = str2num(answer{3});
S3 = str2num(answer{4});
V1 = str2num(answer{5});
V2 = str2num(answer{6});
V3 = str2num(answer{7});
error = error_calculation(S1, S2, S3, V1, V2, V3);
error_percent = [error_percent error];
prompt={'%Load level','S1:','S2:','S3','V1','V2','V3'};
name='Input for parameters';
numlines=1;
defaultanswer={'110' '959 - 140j','380 - 138j','132+ 60j',...
'4.4e3','4.2e3', '4.2e3'};
answer=inputdlg(prompt,name,numlines,defaultanswer);
temp = str2num(answer{1});
load_percent = [load_percent temp];
```

```
S1 = str2num(answer{2});
S2 = str2num(answer{3});
S3 = str2num(answer{4});
V1 = str2num(answer{5});
V2 = str2num(answer{6});
V3 = str2num(answer{7});
error = error_calculation(S1, S2, S3, V1, V2, V3);
error_percent = [error_percent error];
figure('Name','DelError')
plot(load_percent, error_percent, 'bo-')
grid on
xlabel('Load Level percentage'
```

APPENDIX B: Additional figures and analysis

B.1 Supplementary figures for Chapter 2

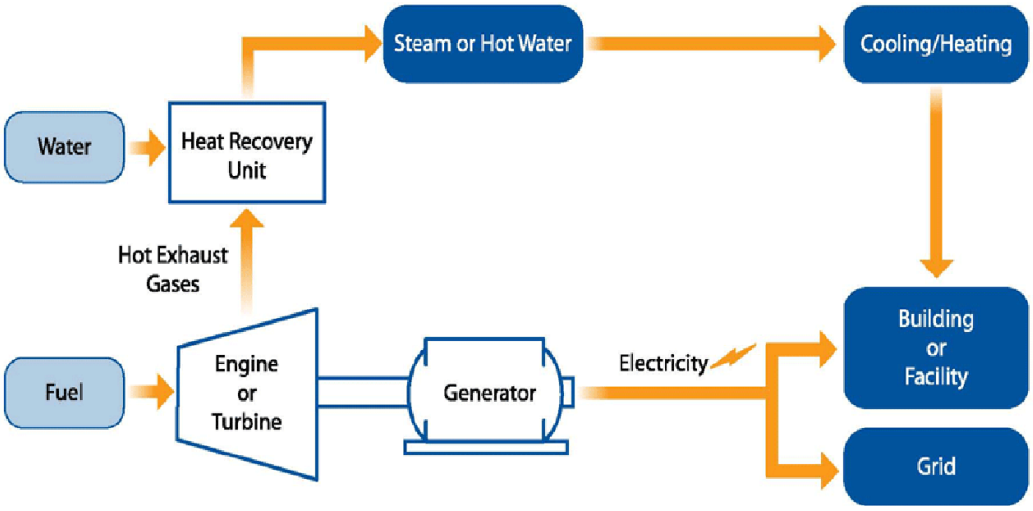

Figure B.1: Combined Heat and Power (CHP) source: EPA.gov

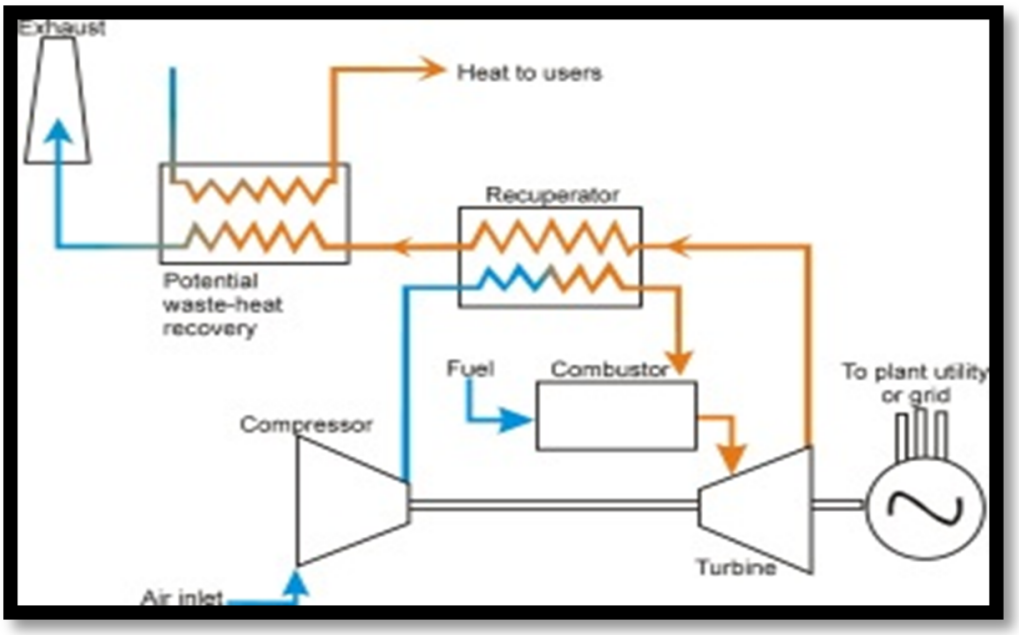

Figure B.2: Microturbine Diagram

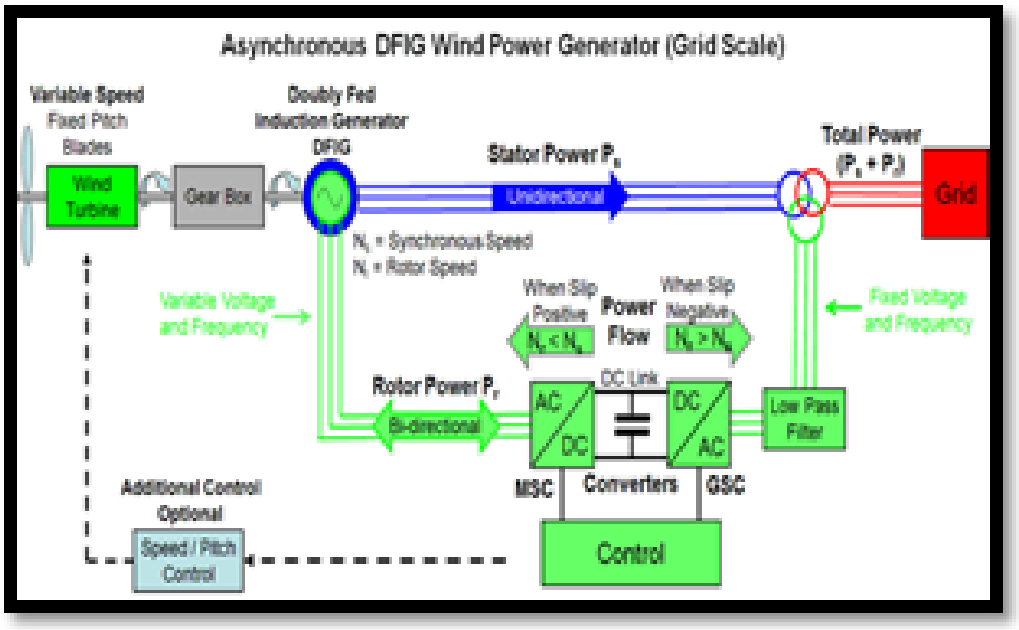

Figure B.3: DFIG Wind Generator

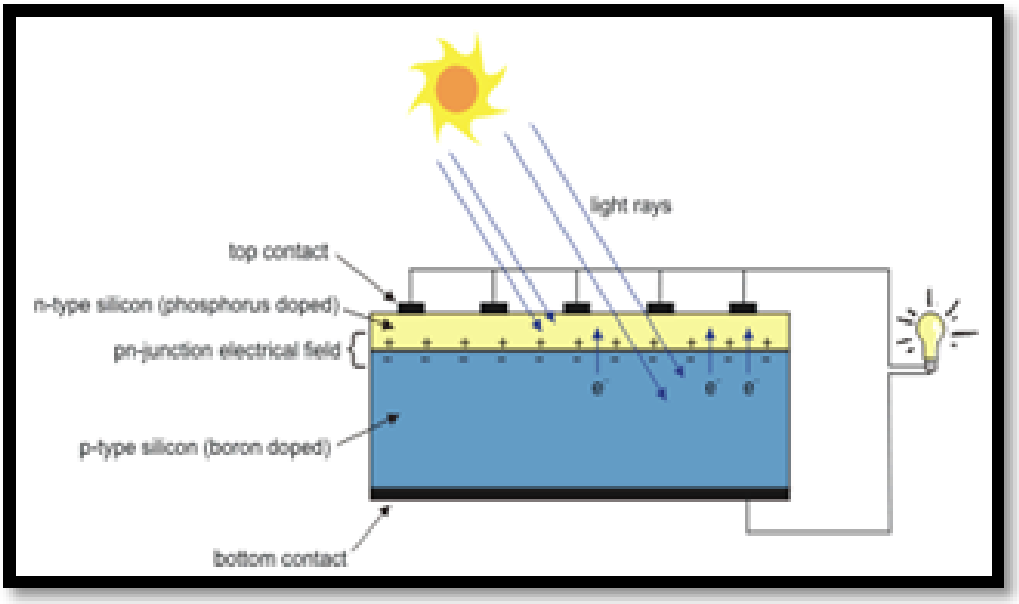

Figure B.4: Induction Machine Operating as a Wind Turbine Generator

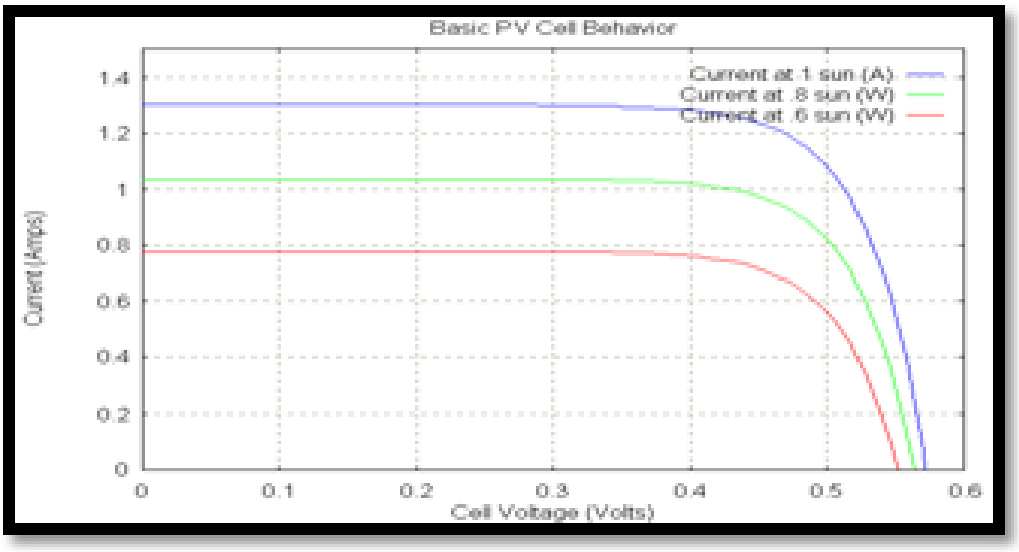

Figure B.5: 9 I-V Curves at Different Angles of the Sun[2]

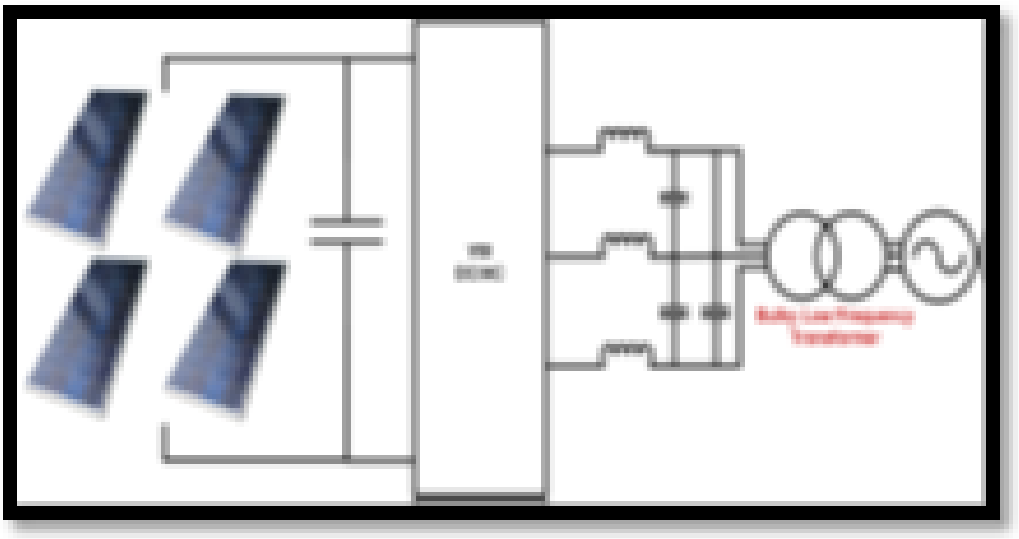

Figure B.6: Conventional Inverter for PV Generation

B.2 Supplementary figures for chapter 3

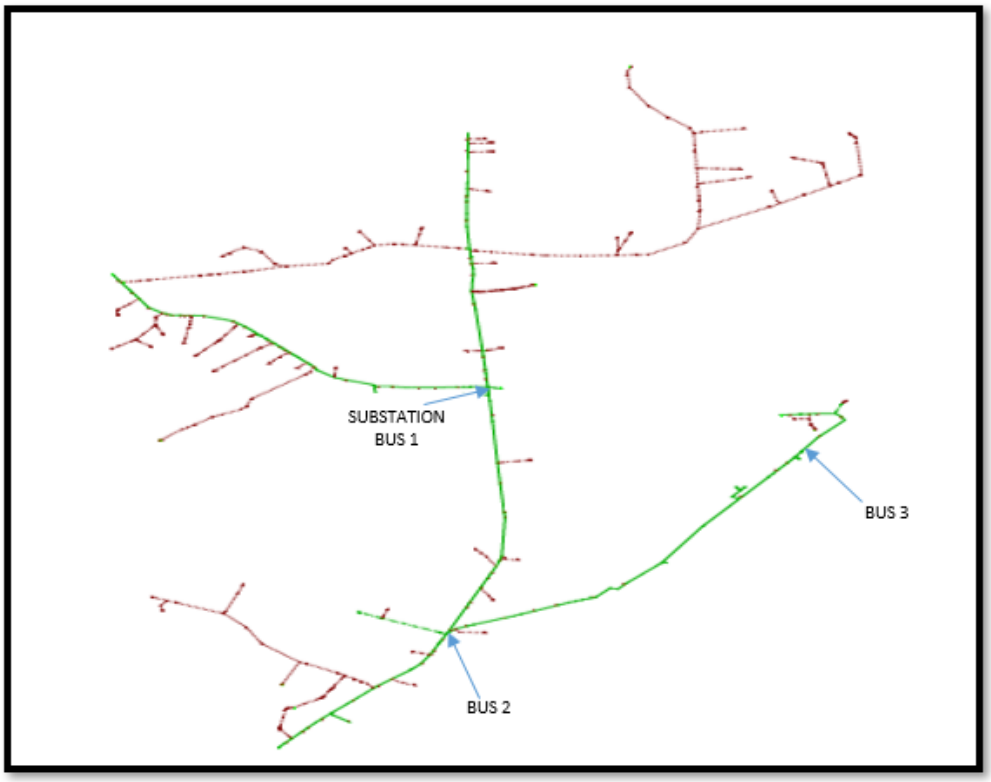

Figure B.7: Power Flow Geographical Layout of Feeder RC103

B.3 Supplementary material for chapter 5

$$W_{bus,1} = \frac{\sum_{i=1}^{29} b_{i,1}}{s^{30} + \sum_{i=1}^{29} a_{i,1}},\ W_{bus,2} = \frac{\sum_{i=1}^{29} b_{i,2}}{s^{30} + \sum_{i=2}^{29} a_{i,2}},\ W_{bus,3} = \frac{\sum_{i=1}^{29} b_{i,3}}{s^{30} + \sum_{i=1}^{29} a_{i,3}} \quad \text{(B.1)}$$

TFbus1 =

$$\frac{29.68\,s^{29}+315.9\,s^{28}+2176\,s^{27}+1.078e04\,s^{26}+4.301e04\,s^{25}+1.427e05\,s^{24}+4.043e05\,s^{23}+9.955e05\,s^{22}+2.147e06\,s^{21}+4.086e06\,s^{20}+6.875e06\,s^{19}+1.023e07\,s^{18}+1.343e07\,s^{17}+1.548e07\,s^{}+1.554e07\,s^{15}+1.347e07\,s^{14}+9.911e06\,s^{13}+6.103e06\,s^{12}+3.084e06\,s^{11}+1.25e06\,s^{10}+3.984e05\,s^{9}+9.611e04\,s^{8}+1.645e04\,s^{7}+1684\,s^{6}+9.166\,s^{5}-23.09\,s^{4}-2.218\,s^{3}-0.03419\,s^{2}-7.019e-06\,s-7.507e-15}{s^{30}+9.094\,s^{29}+57.48\,s^{28}+271.1\,s^{27}+1038\,s^{26}+3364\,s^{25}+9390\,s^{24}+2.298e04\,s^{23}+4.966e04\,s^{22}+9.53e04\,s^{21}+1.629e05\,s^{20}+2.479e05\,s^{19}+3.353e05\,s^{18}+4.013e05\,s^{17}+4.219e05\,s^{16}+3.86e05\,s^{15}+3.033e05\,s^{14}+2.011e05\,s^{13}+1.104e05\,s^{12}+4.939e04\,s^{11}+1.785e04\,s^{10}+5157\,s^{9}+1175\,s^{8}+205.8\,s^{7}+26.38\,s^{6}+2.264\,s^{5}+0.1156\,s^{4}+0.00288\,s^{3}+5.369e-07\,s^{2}+1.821e-15\,s+1.478e-24}$$

TFbus2 =

$$\frac{29.68\,s^{29}+315.9\,s^{28}+2176\,s^{27}+1.078e04\,s^{26}+4.301e04\,s^{25}+1.427e05\,s^{24}+4.043e05\,s^{23}+9.955e05\,s^{22}+2.147e06\,s^{21}+4.086e06\,s^{20}+6.875e06\,s^{19}+1.023e07\,s^{18}+1.343e07\,s^{17}+1.548e07\,s^{}+1.554e07\,s^{15}+1.347e07\,s^{14}+9.911e06\,s^{13}+6.103e06\,s^{12}+3.084e06\,s^{11}+1.25e06\,s^{10}+3.984e05\,s^{9}+9.611e04\,s^{8}+1.645e04\,s^{7}+1684\,s^{6}+9.166\,s^{5}-23.09\,s^{4}-2.218\,s^{3}-0.03419\,s^{2}-7.019e-06\,s-7.507e-15}{s^{30}+9.094\,s^{29}+57.48\,s^{28}+271.1\,s^{27}+1038\,s^{26}+3364\,s^{25}+9390\,s^{24}+2.298e04\,s^{23}+4.966e04\,s^{22}+9.53e04\,s^{21}+1.629e05\,s^{20}+2.479e05\,s^{19}+3.353e05\,s^{18}+4.013e05\,s^{17}+4.219e05\,s^{16}+3.86e05\,s^{15}+3.033e05\,s^{14}+2.011e05\,s^{13}+1.104e05\,s^{12}+4.939e04\,s^{11}+1.785e04\,s^{10}+5157\,s^{9}+1175\,s^{8}+205.8\,s^{7}+26.38\,s^{6}+2.264\,s^{5}+0.1156\,s^{4}+0.00288\,s^{3}+5.369e-07\,s^{2}+1.821e-15\,s+1.478e-24}$$

TFbus3 =

$$\frac{29.68\,s^{29}+315.9\,s^{28}+2176\,s^{27}+1.078e04\,s^{26}+4.301e04\,s^{25}+1.427e05\,s^{24}+4.043e05\,s^{23}+9.955e05\,s^{22}+2.147e06\,s^{21}+4.086e06\,s^{20}+6.875e06\,s^{19}+1.023e07\,s^{18}+1.343e07\,s^{17}+1.548e07\,s^{}+1.554e07\,s^{15}+1.347e07\,s^{14}+9.911e06\,s^{13}+6.103e06\,s^{12}+3.084e06\,s^{11}+1.25e06\,s^{10}+3.984e05\,s^{9}+9.611e04\,s^{8}+1.645e04\,s^{7}+1684\,s^{6}+9.166\,s^{5}-23.09\,s^{4}-2.218\,s^{3}-0.03419\,s^{2}-7.019e-06\,s-7.507e-15}{s^{30}+9.094\,s^{29}+57.48\,s^{28}+271.1\,s^{27}+1038\,s^{26}+3364\,s^{25}+9390\,s^{24}+2.298e04\,s^{23}+4.966e04\,s^{22}+9.53e04\,s^{21}+1.629e05\,s^{20}+2.479e05\,s^{19}+3.353e05\,s^{18}+4.013e05\,s^{17}+4.219e05\,s^{16}+3.86e05\,s^{15}+3.033e05\,s^{14}+2.011e05\,s^{13}+1.104e05\,s^{12}+4.939e04\,s^{11}+1.785e04\,s^{10}+5157\,s^{9}+1175\,s^{8}+205.8\,s^{7}+26.38\,s^{6}+2.264\,s^{5}+0.1156\,s^{4}+0.00288\,s^{3}+5.369e-07\,s^{2}+1.821e-15\,s+1.478e-24}$$

Figure B.8: Bus Transfer function

B.4 Supplementary figures for Chapter 6

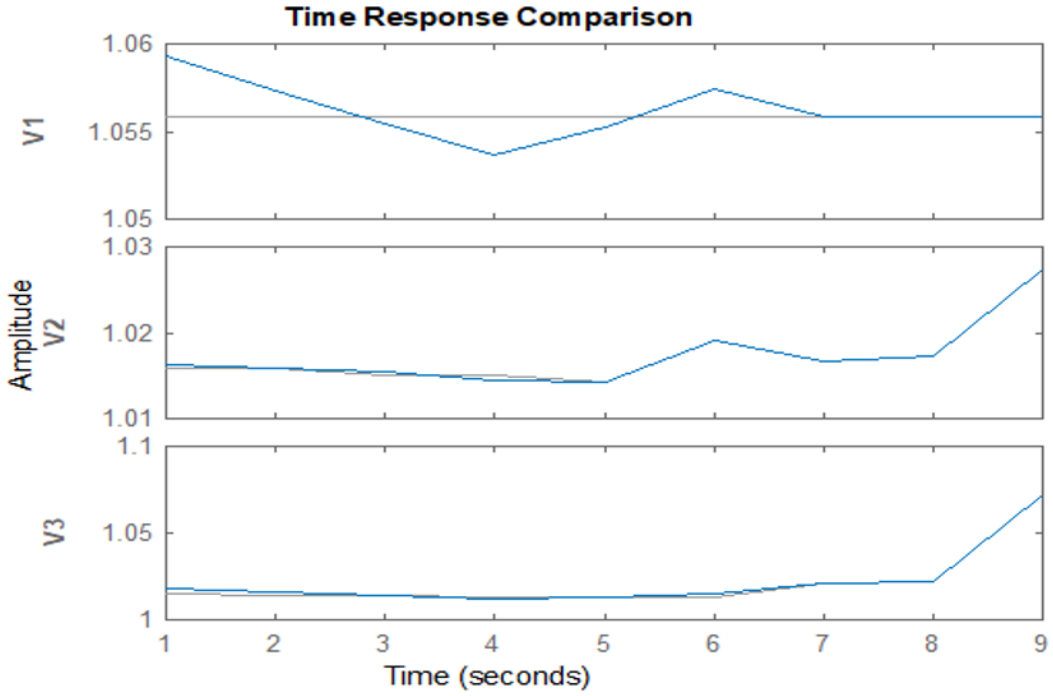

Figure B.9: Time response comparison between the model and identification data-set for V_1, V_2 and V_3

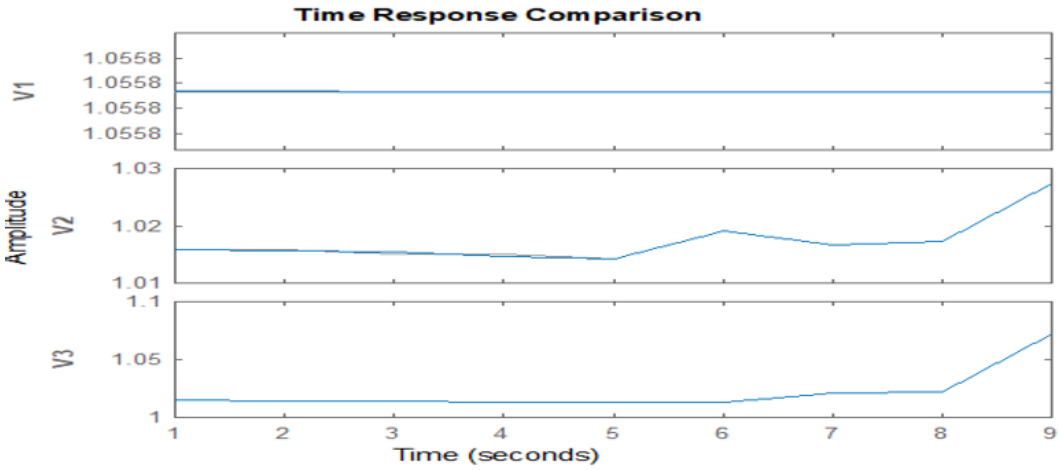

Figure B.10: ARX Model

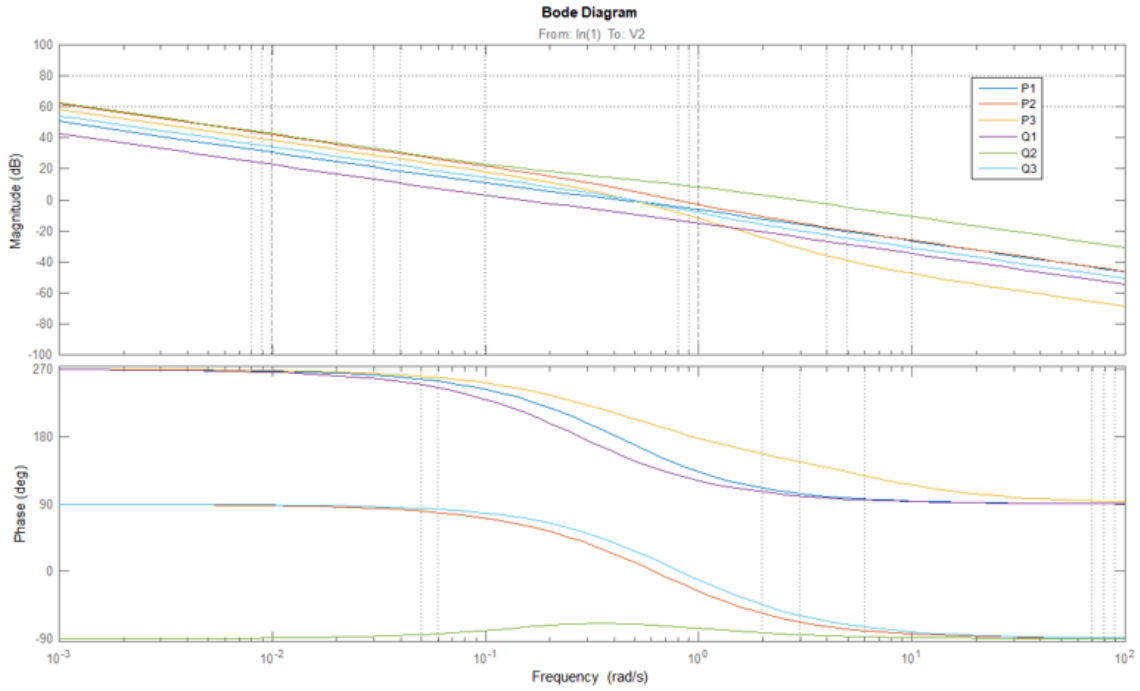

Figure B.11: Magnitude and Phase Plot for V_2

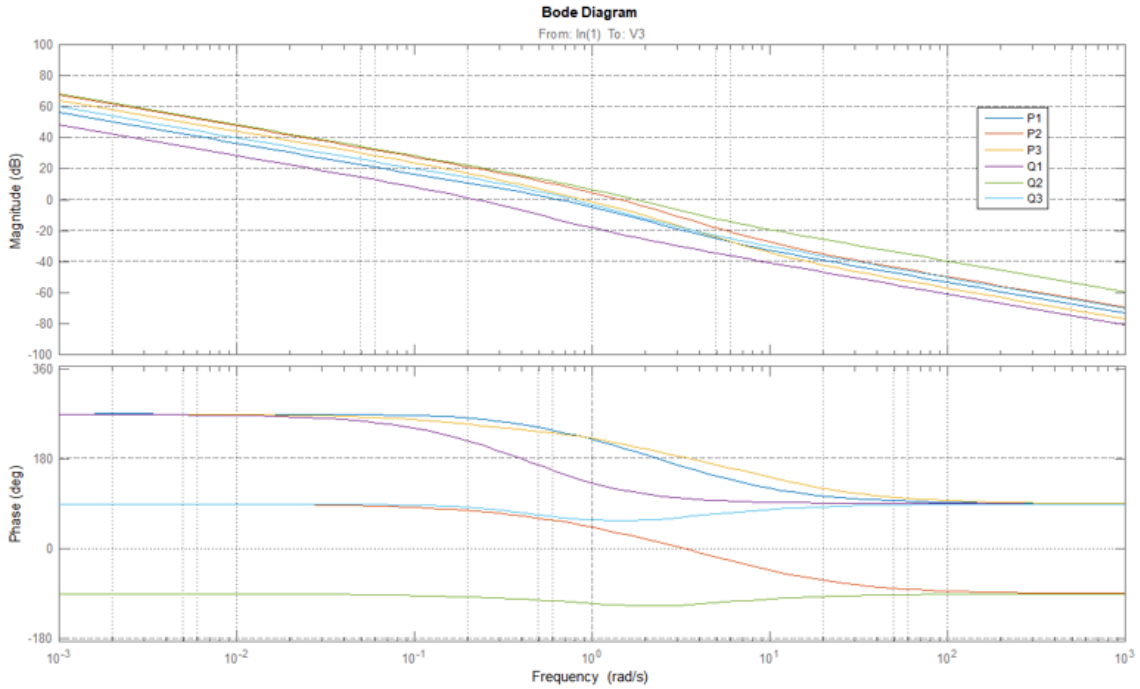

Figure B.12: Magnitude and Phase Plot for V_3

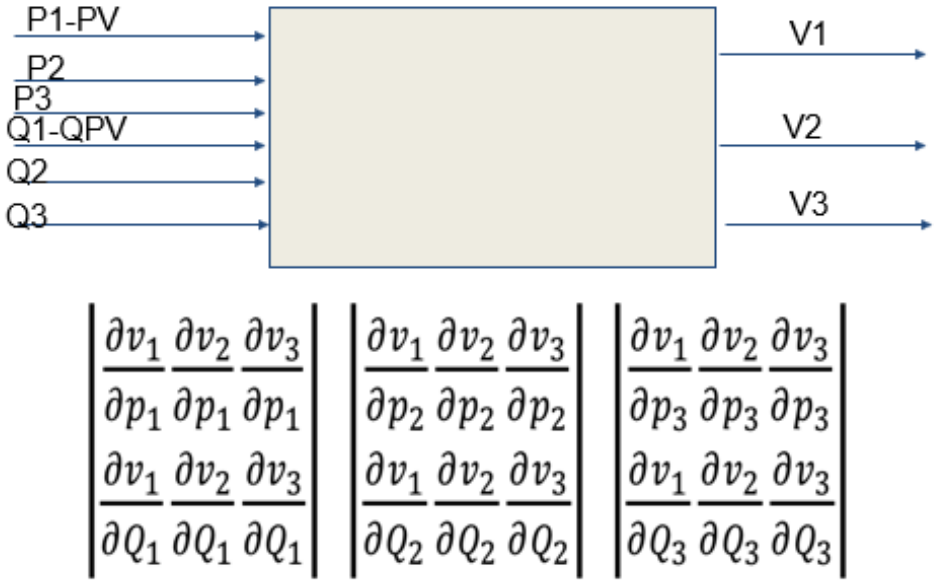

$$\begin{vmatrix} \frac{\partial v_1}{\partial p_1} & \frac{\partial v_2}{\partial p_1} & \frac{\partial v_3}{\partial p_1} \\ \frac{\partial v_1}{\partial Q_1} & \frac{\partial v_2}{\partial Q_1} & \frac{\partial v_3}{\partial Q_1} \end{vmatrix} \quad \begin{vmatrix} \frac{\partial v_1}{\partial p_2} & \frac{\partial v_2}{\partial p_2} & \frac{\partial v_3}{\partial p_2} \\ \frac{\partial v_1}{\partial Q_2} & \frac{\partial v_2}{\partial Q_2} & \frac{\partial v_3}{\partial Q_2} \end{vmatrix} \quad \begin{vmatrix} \frac{\partial v_1}{\partial p_3} & \frac{\partial v_2}{\partial p_3} & \frac{\partial v_3}{\partial p_3} \\ \frac{\partial v_1}{\partial Q_3} & \frac{\partial v_2}{\partial Q_3} & \frac{\partial v_3}{\partial Q_3} \end{vmatrix}$$

Figure B.13: Matrix of MIMO Transfer function

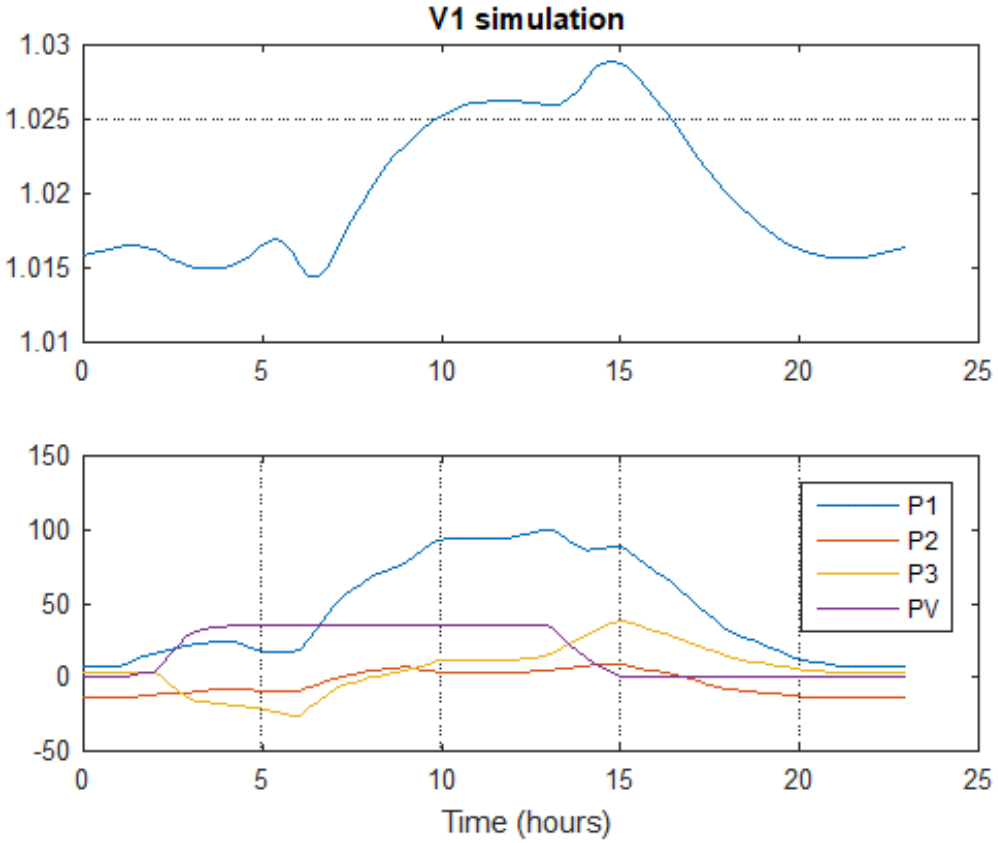

Figure B.14: Change the load profile